TIME-DOMAIN SIMULATION OF MULTIBODY FLOATING SYSTEMS BASED ON STATE-SPACE MODELING TECHNOLOGY

A Dissertation

by

XIAOCHUAN YU

Submitted to the Office of Graduate Studies of
Texas A&M University
in partial fulfillment of the requirements for the degree of

DOCTOR OF PHILOSOPHY

August 2011

Major Subject: Ocean Engineering

TIME-DOMAIN SIMULATION OF MULTIBODY FLOATING SYSTEMS BASED ON STATE-SPACE MODELING TECHNOLOGY

A Dissertation

by

XIAOCHUAN YU

Submitted to the Office of Graduate Studies of
Texas A&M University
in partial fulfillment of the requirements for the degree of

DOCTOR OF PHILOSOPHY

Approved by:

Chair of Committee,	Jeffrey M. Falzarano
Committee Members,	Shankar P. Bhattacharyya
	Moo-Hyun Kim
	Richard S. Mercier
Head of Department,	John Niedzwecki

August 2011

Major Subject: Ocean Engineering

ABSTRACT

Time-domain Simulation of Multibody Floating Systems Based on State-space Modeling Technology. (August 2011)

Xiaochuan Yu, B.S.; B.S., Shanghai Jiao Tong University;

M.S., Shanghai Jiao Tong University;

M.S., University of Hawaii at Manoa

Chair of Advisory Committee: Dr. Jeffrey M. Falzarano

A numerical scheme to simulate time-domain motion responses of multibody floating systems has been successfully proposed. This scheme is integrated into a time-domain simulation tool, with fully coupled hydrodynamic coefficients obtained from the hydrodynamic software - WAMIT which solves the Boundary Value Problem. The equations of motion are transformed into standard state-space format, using the constant coefficient approximation and the impulse response function method. Thus the Ordinary Differential Equation solvers in MATLAB can be directly employed. The time-domain responses of a single spar at sea are initially obtained. The optimal Linear Quadratic Regulator controller is further applied to this single spar, by assuming that the Dynamic Positioning (DP) system can provide the optimized thruster forces. Various factors that affect the controlling efficiency, e.g., the time steps $\Delta\tau$ and Δt, the weighting factors (Q, R), are further investigated in detail. Next, a two-body floating system is studied. The response amplitude operators of each body are calculated and compared

with the single body case. Then the effects of the body-to-body interaction coefficients on the time-domain responses are further investigated. Moreover, the mean drift force is incorporated in the DP system to further mitigate the motion responses of each body. Finally, this tool is extended to a three-body floating system, with the relative motions between them derived.

in memory of my dear grandmother, Ms.Yang, Cuihua

ACKNOWLEDGEMENTS

It is a pleasure for me to express my sincere gratitude to my advisor, Prof. Jeffrey M. Falzarano, for his continuous support and encouragement in the past three years. His guidance during our numerous discussions gave me a strong motivation to finish this work.

I wish to thank Prof. Richard S. Mercier, Prof. Moo-Hyun Kim, and Prof. Shankar P. Bhattacharyya. The discussions with them have been particularly helpful for this work. I would also like to thank Mike Hughes of the David Taylor Model Basin for providing us with various reports and several grid files.

I am particularly grateful to Dr. Yusong Cao and Dr. Xiaobo Chen for their kind help and valuable comments on my dissertation topic. I deeply appreciate the help from my classmates and other group members, including Liqing Huang, Maopeng Fang, John Bandas, Zhiyong Su and Amitava Guha, during my Ph.D. study at TAMU.

My gratitude also goes to my parents, my sister and my brother, who continuously encouraged and supported me.

Financial support for this work was provided by the Office of Naval Research, Grant N00014-07-1-1067

TABLE OF CONTENTS

LIST OF FIGURES

FIGURE Page

FIGURE Page

LIST OF TABLES

CHAPTER I

INTRODUCTION

1.1 Literature Review

The coupled hydrodynamics and dynamics of multibody systems in the oil and gas industry has been an important topic for years. Significant hydrodynamic interactions occur when floating bodies on the ocean surface are located in close proximity. Newman (2001) presented a brief historical review of wave effects on multiple bodies, with special attention given to the seminal works of Professor Makoto Ohkusu (1969). He further summarized the extensive analytical and numerical accomplishments in this field. New computations were included to illustrate first and second-order interaction effects. Two examples of drift forces on multiple bodies were given: one is the slow oscillations of two independent bodies and the other is the drift force on individual elements of a large array. Chakrabarti (2000) reviewed the developments of the multiple scattering technique since the 1970/s and described an analytical/numerical approach that determines the wave forces on multiple structures located in the vicinity of one another. The proposed method involved the consideration of multiple body interaction and scattering in waves. The analysis was an extension of the semi-analytical multiple vertical cylinder analysis and similar to the one proposed by

---

This dissertation follows the style of Ocean Engineering.

Kagemoto and Yue (1986) for the axisymmetric bodies. This analysis was accomplished by combining the direct method with a semi-closed analytical method of multiple scattering developed for an array composed of vertical cylindrical structures. This analytical method had a limitation owing to the geometry of many offshore structures including, e.g., the Mobile Offshore Base (MOB). The limitation of the geometry of the vertical cylinder group in the multiple-module scattering of waves may be remedied by combining the technique of multiple-cylinder scattering with the linear diffraction analysis already described for a general structure shape. Thus it was successfully extended to an arbitrary geometry. In this method, the direct matrix method of the diffraction problem was applied to an isolated module and then extended to structures with the multiple-scattering technique to account for the interaction of multiple structures. Finally, comparisons were made within the results from the analytical and conventional numerical diffraction theory with those of the semi-analytical tool using the above-mentioned analysis. Kashiwagi, et al. (2005) computed the second-order wave drift forces on each ship using the near-field method based on the direct pressure integration, and the results were validated by the far-field method. Further, experiments were also conducted in beam waves for the side-by-side arrangement of a Wigley model and a rectangular barge model. Both measured results and computed results showed good agreement not only for the first-order hydrodynamic forces, but also for the second-order mean forces in sway and heave. Some other overviews of the hydrodynamics of two floating bodies can be found in Chakrabarti (1987) and Kim (2008).

The significant hydrodynamic interaction between multiple bodies in close proximity exists in many applications of practical importance, which require rational engineering analyses. Koo and Kim (2005) studied hydrodynamic interactions and relative motions of two floating platforms with mooring lines in a side-by-side offloading operation. Hong, et al. (2005) applied the Higher-Order Boundary Element Method (HOBEM) to analyze the motions and drift force of side-by-side moored multiple vessels, such as Floating Production Storage and Offloading (FPSO) unit for Liquid Natural Gas (LNG) and the shuttle tankers. Jacobsen and Clauss (2006) studied the lifting operation of a semisubmersible crane and a transport barge by transforming the frequency-domain results into the time-domain. Lewandowski (2008) studied the motions of two vessels in close proximity using traditional 2D and 3D boundary element methods. Naciri, et al. (2007) performed a benchmark study with three programs: AQWA, LIFSIM and aNySIM for side-by-side offloading from an LNG Carrier to a turret-moored Floating Storage and Regasification Unit (FSRU). This study resulted in an improved understanding of the complex dynamic behavior of two side-by-side vessels. Xiang, et al. (2007) presented the numerical results of coupled motion RAOs of two side-by-side ships in waves by using the China Ship Scientific Research Center (CSSRC) in-house program CSR-INT and the results showed good agreement with those from HydroSTAR, the state-of-the-art hydrodynamic software developed by Bureau Veritas.

Extensive model tests were carried out to study the hydrodynamic interaction and dynamic behavior of multibody floating systems. The Offshore Technology Research

Center (OTRC) at Texas A & M University (TAMU) conducted model tests to investigate hydrodynamic effects associated with the small gap between two barges, which is fundamental for understanding FPSO-shuttle tanker interactions during side-by-side offloading. The test results and comparisons with numerical model predictions were used to optimize future test plans involving side-by-side FPSO-shuttle tanker configurations. The Maritime Research Institute Netherlands (MARIN) has also accumulated a great deal of experience in the testing and numerical modeling of side-by-side loading operations for oil and LNG. The staff has developed tools that take into account the observed interactions, and these tools have been validated based on in-house research and can be used to optimize the side-by-side operations in close proximity (MARIN, 2010). McTaggart, et al. (2003) numerically and experimentally explored the hydrodynamic interactions when two ships travel in close proximity at moderate forward speed.

The numerical simulation of the free surface waves in the gap between multiple bodies is very important. Newman (2001) used generalized modes to represent this phenomenon, and this method was later applied in the commercial hydrodynamic software WAMIT. Buncher, et al. (2001) proposed an assumed free surface with a lid to suppress the numerical anomalies observed using standard linear hydrodynamic calculations of the pressure distribution for two bodies in close proximity. Chen (2004) applied the authentic equations of the fairly perfect fluid involving the energy dissipation by introducing a damping parameter between the two bodies to deal with the resonance. Pauw, et al. (2007) concluded that tuning the damping value of the lid should be done

only on the second order wave drift force and not the first order quantities, like the wave height and the motion RAO.

Different time-domain programs have been developed to simulate motion responses of Dynamically Positioned (DP) vessel or multibody floating systems. Nienhuis (1986) validated a time-domain simulation program - DPSIM by comparing the measured and simulated results. This program was capable of adequately predicting the low-frequency motions of a dynamically positioned vessel. Srinvasan and Sen (2002) discussed a truly dynamic time-domain simulation method for a fully DP assisted semisubmersible. The computational algorithm for the simulation was based on the concept of a numerical wave tank. Ryu and Kim (2003) investigated the performance of a thruster-assisted turret-moored FPSO in terms of surge, sway, yaw motions and mooring tension time series by using a fully coupled time domain program. Tannuri and Morishita (2006) developed a computational dynamic simulator to analyze the performance of DPS in a typical offshore oil industry scenario, and scale model tests of the system were also carried out in a laboratory tank. Yu, et al. (2009, 2010a) developed a time-domain simulation tool to perform the dynamic analysis of multiple bodies in close proximity based on the state-space modeling technology. SIMO is a time domain simulation program for study of motions and station keeping of multibody systems, owned, developed and maintained by MARINTEK. Flexible modeling of station keeping forces and connecting force mechanisms (anchor lines, ropes, thrusters, fenders, bumpers, docking guide piles) are included. The results from the coupled program are presented as time traces, statistics and spectral analysis of all forces and motions of all

bodies in the analyzed system. Currently, SIMO is a modular and interactive computer program with batch processing options, and is also available as part of SESAM's DeepC package for the coupled analysis of floating vessels including station keeping systems.

Traditionally the study of ship dynamics has been separated into two main areas: (1) maneuvering or controllability in calm water; and (2) seakeeping or vessel motion in a seaway (Perez et al., 2004). Manoeuvring is associated with course keeping, course changes, turning, stopping, etc. These operations are often performed in open or restricted calm waters (i.e., in calm open seas, in sheltered waters or in harbors). Seakeeping, on the other hand, is associated with motion in a seaway while the vessel keeps its course and its speed constant. Perez (2005) further comprehensively discussed the shortcomings of the traditional seakeeping model and maneuvering model, as shown in Figure 1.1. The first shortcoming is that the model may not be used for multibody system interactions. The second one is that the maneuvering part does not incorporate fluid memory effects associated with the wave-frequency induced motion.

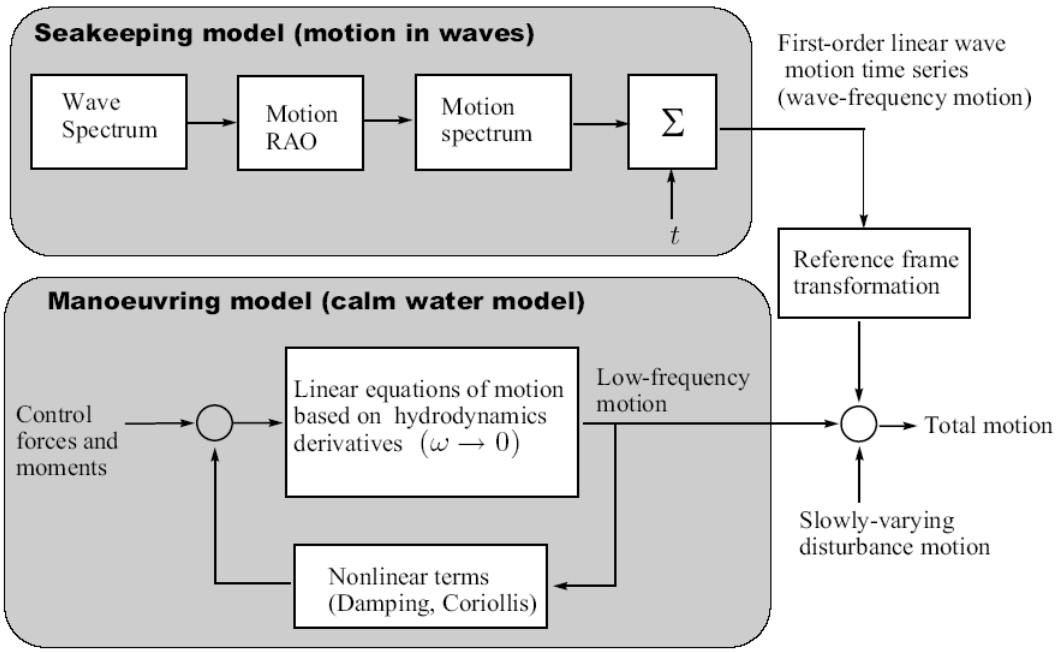

Figure 1.1 Motion superposition model of a marine vessel (Perez, 2005)

The model shown in Figure 1.2 is well known in marine technology and it is part of state-of-the-art time-domain ship motion simulators. However, its use for control system design has not yet been widely adopted. Kristansen and Egeland (2003) proposed a new method that generates a low-order state-space model from frequency-dependent added mass and potential damping as obtained from identification experiments or numerical computations. The resulting model gave an accurate and computationally efficient representation of the convolution term.

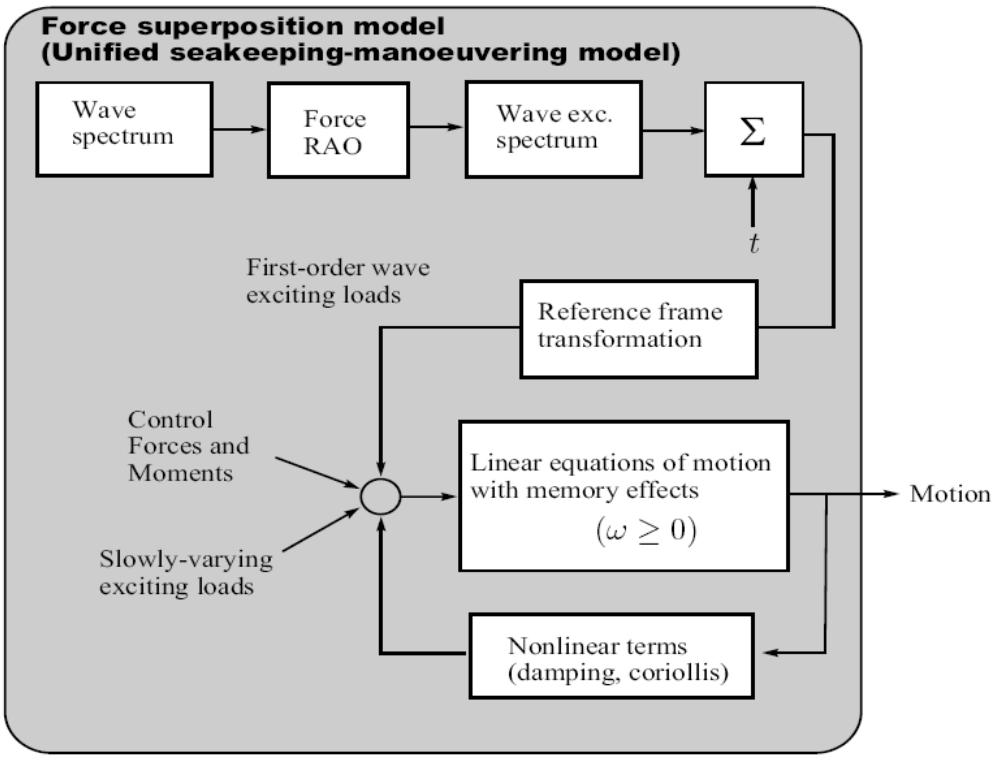

Figure 1.2 Force superposition model of a marine vessel (Perez, 2005)

A Dynamic Positioning (DP) system can be defined as a system which automatically controls a vessel's position and heading exclusively by means of active thrust. Usually a DP system mainly includes a power system, a thruster system and a control system. DP systems should be designed to have high reliability and a certain amount of built-in redundancy. Failure Modes and Effect Analysis (FMEA) should be conducted for floating vessels with a DP system. The American Petroleum Institute (API) recommended practice 2SK (2005) systematically summarizes the guidelines for design, testing and maintenance of a DP system.

The first vessel to fulfill the accepted definition of DP was the "Eureka" which was designed and engineered by Howard Shatto. During the 1990s there was a rapid increase in the number of vessels with dynamic positioning systems. Nowadays, many of these vessels have been designed for the DP and integrated control of engines and thrusters, but there are also a large number of conversions and upgrades. Faÿ (1990) extensively presented almost all the aspects related to the DP system, including the reasons for which the DP technique was developed, the marine environment, the principle of DP systems, the established specifications of a dynamic positioning project, leading applications, safety, costs, fuel consumption, the advantages of conventional mooring and DP systems, etc. Strand, et al. (2001) presented the state-of-art of DP system, including marine positioning systems, mathematical modeling of dynamically positioned and thruster-assisted anchored marine vessels, position and velocity observer design, design of controllers for positioning of marine vessels, weather optimal positioning control, methods for thrust control, etc.

Various control methods have been applied in the applications of DP systems in offshore engineering. Kalman Filtering techniques were applied to dynamic positioning systems by Balchen, et al. (1980), Grimble and Patton (1980), Grimble, et al. (1980), and Saelid, et al. (1983). Sørensen, et al. (1996) proposed a model-based control scheme which provides both station-keeping and tracking of ships. A Kalman-Filter-based state estimator and a Luenberger observer were used to compute the feedback and feed-forward control signals. Yamamoto and Morooka (2005) applied fuzzy control to a dynamic positioning system of a semi-submersible. The performance of the fuzzy

controller was compared with that of a classical Proportional-Integral-Derivative (PID) controller. Aamo and Fossen (1999) suggested controlling the line tensions dynamically as an additional means of station keeping. A model consisting of a rigid-body sub-model for the vessel and a finite element sub-model for the mooring system were presented and used for the simulations. Liang and Cheng (2004) studied the optimum control of a 2280-ton DP coring vessel with five rotary azimuth thruster marine positioning in detail. This method can quickly estimate the thrusts and angles of direction of all the thrusters.

1.2 Project Background

Cargo-transfer and underway replenishment are essentially important in long-term naval operations. The Office of Naval Research (ONR) initiated a technology development program in 2007 called STLVAST (Small to Large Vessel At-Sea Transfer). The goal of this program is to develop 'enabling capabilities' in the realm of logistic transfer (i.e. stores, equipment, vehicles) between a large transport vessel (e.g., the USNS Bob Hope) and a smaller T-craft ship, using a Deep Water Stable Crane (DWSC) spar between them. The DWSC spar consists of two entities, a catamaran craneship and a detachable spar. This spar can be rotated through 90 degrees, from the horizontal to the vertical, using seawater ballast. The de-ballasting can help to lift the catamaran clear of the water surface, allowing the system to operate as a spar and take advantage of the superior seakeeping afforded by the small waterplane area. Selfridge (2005) presented the development of the concept, its performance in the areas of

powering, stability, seakeeping, worldwide operability and alternative uses. This DWSC concept was further developed to the Rapidly Deployable Stable Platform (RDSP). Moreover, a 1/10th scale physical model test was performed at Florida Atlantic University (FAU). In their research, a DP and motion mitigation system for the RDSP was developed, including the validation of the mathematical simulation, development of a novel propulsion system, and implementation of a PID controller (Marikle, 2009).

Driscoll, et al. (2006) introduced state-of-the-art of at-sea cargo transfer. The concept of RDSP was developed to provide at-sea container transfer that enables sustainment logistics in sea states up to and including sea state 5 (SS5). The RDSP concept was very similar to DWSC, consisting of two elements: 1) a small catamaran crane ship and 2) a long SPAR that provides excellent seakeeping properties. Marikle (2009) further proposed a 6 Degree-Of-Freedom (DOF) numeric model and computer simulation along with the 1/10th scale physical model test fulfilled by the Ocean Engineering Undergraduate Program at FAU. This project focused on the development of a DP and motion mitigation system for the RDSP, including the validation of the mathematical simulation, development of a novel propulsion system, and implementation of a PID controller. The result was an assessment of the response characteristics of the RDSP that quantifies the performance of the propulsion system coupled with active control providing a solid basis for further controller development and operational testing.

Recently, Hughes, et al. (2009) improved the positioning of a single vessel in a seaway, based on the estimation of wave drift forces using wave height sensing and the

application of a Wave Feed Forward (WFF) control loop. This technique was also applied to the challenge of controlling two large vessels, but the performance was only improved at some headings. Hughes, et al. (2010) presented an overview of the STLVAST program and described the full scale offshore trials conducted by the US Navy that show-cased some of the potential of the Close-in Precision DP work carried out by STLVAST.

1.3 Problem Statement

The purpose of this research is to develop a time-domain simulation tool for the multiple vessels in close proximity at seas. The whole cargo transfer system is shown in Figure 1.3 and comprises the T-craft, the DWSC spar (or called 'spar' for short) and the USNS Bob Hope (or called 'ship' for short), from the left to the right. In order to develop such a tool, a new numerical scheme to simulate the time-domain motion responses of multibody floating systems has been successfully proposed. The scheme is initially applied to simulate the motion responses of this single spar and the ship. Then this simulation tool is further extended to a two-body floating system and the whole cargo transfer system, respectively.

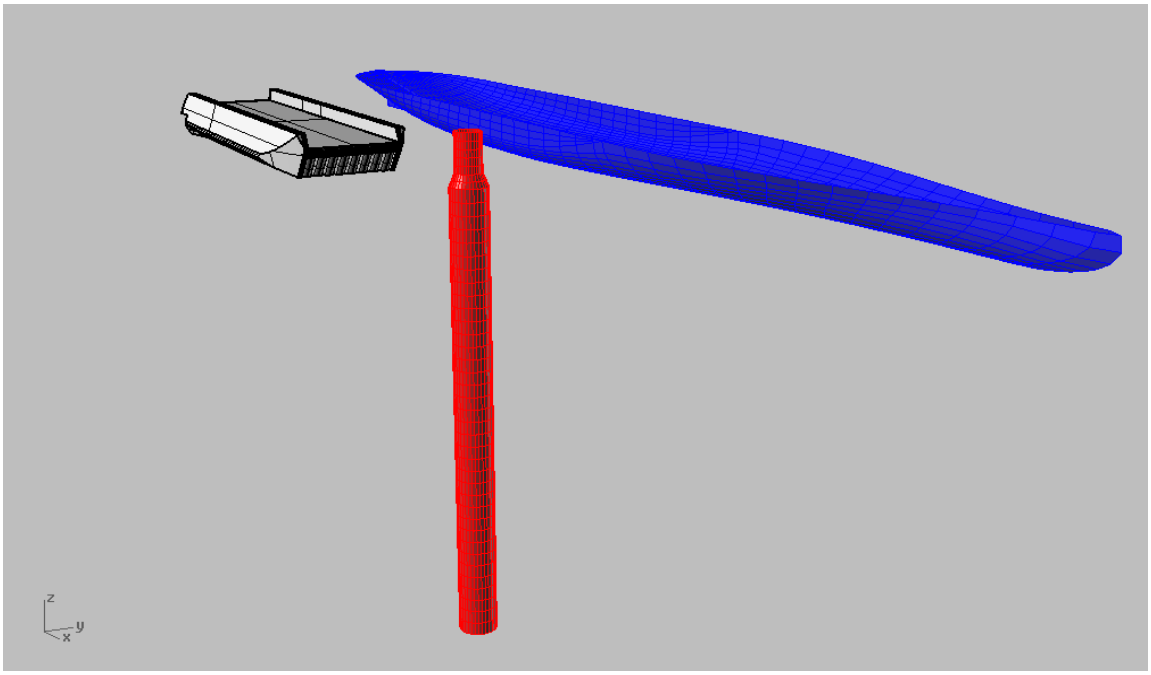

Figure 1.3 Schematic view of ship-to-ship cargo transfer using the spar

The multiple bodies in close proximity shown in Figure 1.3 can be regarded as a dynamical system as a whole, with the feedback force provided by the DP system. It is assumed that the designed DP system can maintain the relative motions between them to meet the regulated operation criteria. Herein, a single-degree-of-freedom (SDOF) system is initially analyzed.

For example, the structural control of a one-story building can be described as

$$M\ddot{x} + C\dot{x} + Kx = -M\Gamma\ddot{x}_g + \Lambda f \tag{1.1}$$

where $\ddot{x}_g$ is 1D ground acceleration or excitation; f is the vector of control forces; Γ is the vector of unit; Λ is the matrix defining how the control forces are exerted on the

structure (Yu, et al., 2010b; Yu, et al., 2011). Equation (1.1) can be written in the state-space form as

$$\dot{z} = Az + E\ddot{x}_g + +Bf \tag{1.2}$$

, and the output

$$y = Cz + Df \tag{1.3}$$

where z $= [x^T, \dot{x}^T]^T$, the state vector; $y = [\ddot{x}, x^T]^T$, the vector of measured outputs; and

$$\mathrm{A} = \begin{bmatrix} 0 & I \\ -M^{-1}K & -M^{-1}C \end{bmatrix} \tag{1.4}$$

$$B = \begin{bmatrix} 0 \\ M^{-1}\Lambda \end{bmatrix} \tag{1.5}$$

$$E = -\begin{bmatrix} 0 \\ \Gamma \end{bmatrix} \tag{1.6}$$

$$C = \begin{bmatrix} -M^{-1}K & -M^{-1}C \\ I & 0 \end{bmatrix} \tag{1.7}$$

$$D = \begin{bmatrix} M^{-1}\Lambda \\ 0 \end{bmatrix} \tag{1.8}$$

where the matrix A is called the system or plant matrix. This matrix models the dynamical behavior of the system, because it contains the inertial, damping and restoring terms, i.e., M, C and K. Matrix B is called the input matrix and it represents how the control force f is applied to the system. By analog, this state-space modeling technology can also be applied to more complicated dynamical systems with multiple DOFs.

Similar to the structural control in civil engineering, described by equations (1.1) - (1.8), the motion responses of multiple bodies in close proximity in waves can also be considered and solved this way. However, the equations of motions of the floating system considered in ocean waves are more complicated, due to the added mass and the

radiated wave damping. Two levels of approximation of hydrodynamic coefficients are considered in this study. One is the Constant Coefficient Method (CCM), including constant added mass and constant radiation damping evaluated at a specific frequency ω_0.We will discuss how to determine this frequency.

The equations of motion using the CCM can be expressed as

$$[M + a(\omega_0)]\ddot{x}(t) + b(\omega_0)\dot{x}(t) + cx(t) = f^{ext}(t) \tag{1.9}$$

where $x(t)$ denotes 6-DOF motions of a single rigid body and is a 6×1 vector; $a(\omega_0)$ is a 6×6 added mass matrix at the wave frequency ω_0; $b(\omega_0)$ is a 6×6 radiation damping matrix at the wave frequency ω_0; c is a 6×6 hydrostatic restoring coefficient matrix; $f^{ext}(t)$ is the external force vector, and it can be the sum of 1st order wave force, 2nd order wave force, the thruster force provided by the DP system, the force due to viscous damping, wind and current, or their combination, etc. Herein, $f^{ext}(t)$ is a 6×1 vector for a single body.

The alternative level of approximation is the Impulse Response Function (IRF) method, with fluid memory effects considered. The corresponding equations of motion are

$$[M + a(\infty)]\ddot{x}(t) + \int_0^t K(t-\tau)\,\dot{x}(\tau)d\tau + cx(t) = f^{ext}(t) \tag{1.10}$$

$$K(t) = \frac{2}{\pi}\int_0^\infty b(\omega)\cos(\omega t)d\omega \tag{1.11}$$

where $a(\infty)$ is the added mass at the infinite frequency and $K(t)$ is the IRF. The relationship between $K(t)$ and the radiation damping $b(\omega)$ can be correlated by equation (1.11), the so-called Ogilvie relations (Ogilvie, 1964).

Both equation (1.9) and equation (1.10) are currently employed for a single body in waves. They both can be further extended to describe the dynamics of multiple floating bodies in close proximity, as will be discussed in Chapter III in detail. The flowchart shown in Figure 1.4 describes the critical steps of the newly proposed numerical scheme (Yu and Falzarano, 2011).

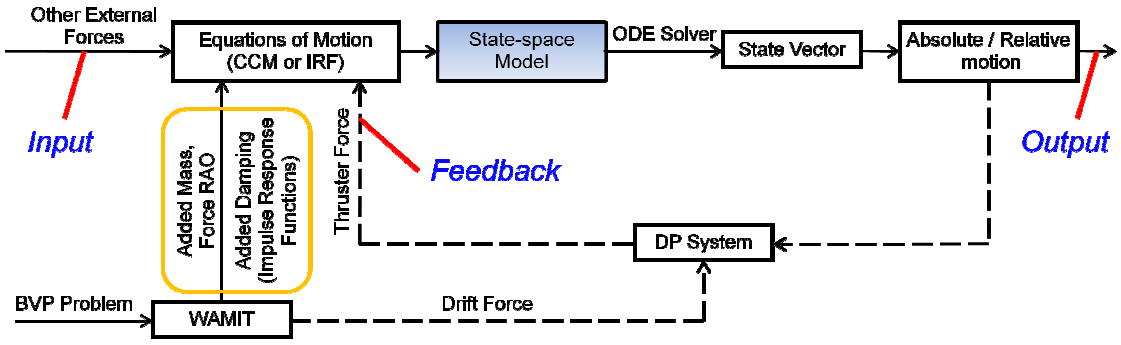

Figure 1.4 Flowchart for the time-domain multibody simulation tool

In Chapter II, the theoretical formulations can be separated into three parts: hydrodynamics, dynamics and control engineering, respectively:

1. Hydrodynamics, including the First-order Boundary Value Problem (the 1st-order BVP), the Second-order Boundary Value Problem (the 2nd-order BVP), and the first- and second- order forces. In addition, the relations between the time- and frequency-domain descriptions, i.e., the impulse response functions, are also introduced. The standard hydrodynamic software - WAMIT, developed for the linear analysis of the interaction of surface waves with offshore structures, is

employed to compute the hydrodynamic coefficients, e.g., added mass, radiation damping, RAOs, IRFs and the mean drift Quadratic Transfer Function (QTF).

2. Dynamics: the dynamic responses of floating bodies can be solved by using ODE solvers in MATLAB after the equations of motion have been transformed into standard state-space format.
3. Control engineering: the classical PID controller is briefly introduced. However, an alternative robust controller, i.e., the Linear Quadratic Regulator (LQR) method, is introduced in detail and applied in this study.

In Chapter III, the hydrodynamic coefficients of a single spar and its Response Amplitude Operators (RAOs) are calculated by solving the BVP problem using WAMIT. Moreover, the time-domain responses of the single spar in both regular and irregular waves are analyzed based on state-space models. Herein, the ideal simulation of DP systems is also performed by assuming that the DP system can produce the optimized feedback forces. The time step $\Delta\tau$ used to evaluate the IRFs determines the physical properties of the state-space model. The time-step Δt of the time-domian simulation is equal to $\Delta\tau$ for the simplicity. Thus, the effects of $\Delta\tau$ and Δt on the controlling efficiency of the LQR controller are further discussed in detail. The effects of the weighting factors (Q, R) are finally studied.

In Chapter IV, a two-body floating system is studied. The RAOs for multiple bodies are compared with those of a single body. The effects of the body-to-body hydrodynamic coefficients are also discussed. In addition, the DP system is simulated by

assuming that the thrusters can provide the optimal horizontal forces derived from the LQR controller only in x- and y- direction. Motion spectra of both cases, with control and without control, are finally obtained and discussed.

In Chapter V, the time-domain simulation code is successfully extended to a three-body case. The RAOs of the third-body, the T-craft, are obtained initially and compared with the RAOs of the single vessel. The relative vertical motions between them can be obtained after all the motion responses of the three bodies are obtained.

Finally, the conclusions and the future work are summarized in Chapter VI.

CHAPTER II

THEORETICAL FORMULATIONS

2.1 Hydrodynamics of Floating Systems

In this chapter, the linear and second-order wave theories are briefly reviewed firstly. Next, the equations of motion are discretized in state-space format based on CCM and IRF. Meanwhile, the derivation of impulse response function from the added mass and the radiation damping is also introduced. Finally, the classical PID controller and the modern LQR controller are described in detail, respectively.

2.1.1 Description of the Problem

Most contents in this section are from the WAMIT theory manual written by Lee (1995), Chakrabarti (1987) and Kim (2008). Assume that the sea water is incompressible and inviscid and the fluid motion is irrotational. The fluid velocity is given by the gradient of the velocity potential $\Phi(x, y, z, t)$

$$V(x, y, z, t) = \nabla\Phi = \frac{\partial\Phi}{\partial x}\hat{\imath} + \frac{\partial\Phi}{\partial y}\hat{\jmath} + \frac{\partial\Phi}{\partial z}\hat{k} \tag{2.1}$$

where $\hat{\imath}, \hat{\jmath}$ and $\hat{k}$ are unit vectors along the x, y, z axes, respectively; t denotes the time and $\hat{x} = (x, y, z)$ denotes the Cartesian coordinates of a point. In addition, the velocity potential satisfies Laplace's equation in the fluid domain:

$$\nabla^2\Phi = 0 \tag{2.2}$$

The pressure follows the Bernoulli's equation:

$$p(x,t) = -\rho\left(\frac{\partial\Phi}{\partial t} + \frac{1}{2}\nabla\Phi\cdot\nabla\Phi + \mathrm{gz}\right) \tag{2.3}$$

where ρ is the density of the fluid and g is the gravitational acceleration.

The velocity potential satisfies the nonlinear free-surface condition:

$$\frac{\partial^2\Phi}{\partial t^2} + g\frac{\partial\Phi}{\partial \mathrm{z}} + 2\nabla\Phi\cdot\nabla\frac{\partial\Phi}{\partial \mathrm{t}} + \frac{1}{2}\nabla\Phi\cdot\nabla(\nabla\Phi\cdot\nabla\Phi) = 0 \tag{2.4}$$

It is applied on the exact free surface

$$\zeta(x,y) = -\frac{1}{g}\left(\frac{\partial\Phi}{\partial t} + \frac{1}{2}\nabla\Phi\cdot\nabla\Phi\right)\Big|_{z=\zeta} \tag{2.5}$$

With the assumption of a perturbation solution in terms of a small wave slope of the incident waves, the velocity potential is expanded in a form

$$\Phi(x,y,z,t) = \Phi^{(1)}(x,y,z,t) + \Phi^{(2)}((x,y,z,t) + \cdots \tag{2.6}$$

When the body is not fixed, the motion amplitude of the body is also expanded in a perturbation series

$$\zeta(x,y,z) = \zeta^{(1)}(x,y,z) + \zeta^{(2)}(x,y,z) + \cdots \tag{2.7}$$

with

$$\zeta^{(1)}(x,y,z) = -\frac{1}{g}\frac{\partial\Phi^{(1)}}{\partial t} \tag{2.8}$$

$$\zeta^{(2)}(x,y,z) = -\frac{1}{g}\left(\frac{\partial\Phi^{(2)}}{\partial t} + \frac{1}{2}\nabla\Phi^{(1)}\cdot\nabla\Phi^{(1)} - \frac{1}{g}\frac{\partial\Phi^{(1)}}{\partial t}\frac{\partial^2\Phi^{(1)}}{\partial z\partial t}\right) \tag{2.9}$$

In equations (2.8) and (2.9), the right-hand sides are evaluated at the mean water level $z = 0$. Given a wave spectrum, it is customary to assume that the spectrum is

expressed as a linear superposition of the first-order incident waves of different frequencies. Thus the total first order potential for the wave-body interaction can be expressed by a sum of components with the circular frequency $\omega_j > 0$:

$$\Phi^{(1)}(x,y,z,t) = Re\sum_j \phi_j(x,y,z)e^{-i\omega_j t} \tag{2.10}$$

Here we introduce the complex velocity potential $\phi_j(x,y,z)$, which is independent of the time. In equation (2.10), $\phi_j(x,y,z)$ denotes the first-order solution in the presence of the incident wave of frequency ω_j and the wave heading β_j.

2.1.2 First-order Boundary Value Problem (1st-order BVP)

The total first-order velocity potential can be separated as follows

$$\Phi^{(1)} = \epsilon\left(\Phi_I^{(1)} + \Phi_D^{(1)} + \Phi_R^{(1)}\right) = Re[\left\{\phi_I^{(1)} + \phi_D^{(1)} + \phi_R^{(1)}\right\} \cdot e^{-i\omega t}] \tag{2.11}$$

The incident wave velocity potential is

$$\phi_I^{(1)} = Re[\frac{-igA}{\omega}\frac{\cosh k(z+d)}{\cosh kd}] \tag{2.12}$$

where k is the real root of the dispersion relation

$$k\tanh kd = \frac{\omega^2}{g} \tag{2.13}$$

The boundary conditions for the first-order potential of diffraction and radiation are

$$\nabla^2\phi^{(1)}(x,y,z) = 0 \tag{2.14}$$

$$-\omega^2\phi^{(1)} + g\frac{\partial\phi^{(1)}}{\partial z} = 0 \ , \ z = 0 \tag{2.15}$$

$$\frac{\partial \phi^{(1)}}{\partial n} = V_n, \text{ on the body surface} \tag{2.16}$$

$$\frac{\partial \phi^{(1)}}{\partial z} = 0, \quad z = -d \tag{2.17}$$

$$\lim_{R\to\infty} \sqrt{R}\left(\frac{\partial}{\partial R} \pm ik\right)\phi^{(1)} = 0 \tag{2.18}$$

where d is the water depth and R is the radial distance from the center of the structure.

2.1.3 Second-order Boundary Value Problem (2nd-order BVP)

Separate the time dependency explicitly, and write the second-order potential as

$$\Phi^{(2)} = \epsilon^2\left(\Phi_{\mathrm{I}}^{(2)} + \Phi_{\mathrm{D}}^{(2)} + \Phi_{\mathrm{R}}^{(2)}\right) \tag{2.19}$$

The second-order components ϕ_{ij} can be represented as

$$\Phi^{(2)}(x,y,z,t) = Re\sum_i\sum_j[\phi_{ij}^{+}(x,y,z)e^{i(\omega_i+\omega_j)t} + \phi_{ij}^{-}(x,y,z)e^{i(\omega_i-\omega_j)t}] \tag{2.20}$$

The second-order potentials $\phi_{ij}^{\pm}$ can be defined to satisfy the symmetry relations

$$\phi_{ij}^{+} = \phi_{ji}^{+} \tag{2.21a}$$

$$\phi_{ij}^{-} = \phi_{ji}^{-} \tag{2.21b}$$

The free-surface boundary conditions satisfied by these potentials are

$$\frac{\partial^2\Phi^{(2)}}{\partial t^2} + g\frac{\partial\Phi^{(2)}}{\partial z} = Q_F(x,y;t) \tag{2.22}$$

on $z = 0$. Here the inhomogeneous right-hand-side of the second-order free-surface condition defines the quadratic forcing function

$$Q_F = \frac{1}{\mathrm{g}}\frac{\partial\Phi^{(1)}}{\partial \mathrm{t}}\frac{\partial}{\partial \mathrm{z}}\left(\frac{\partial^2\Phi^{(1)}}{\partial \mathrm{t}^2} + \mathrm{g}\frac{\partial\Phi^{(1)}}{\partial \mathrm{z}}\right) - \frac{\partial}{\partial \mathrm{t}}(\nabla\Phi^{(1)}\cdot\nabla\Phi^{(1)}) \tag{2.23}$$

where the right-hand-side is to be evaluated on $z = 0$. In the following evaluations of the second-order products of first-order oscillatory quantities use is made of the relation

$$Re\left(Ae^{i\omega_i t}\right)Re\left(Be^{i\omega_j t}\right) = \frac{1}{2}Re\left(Ae^{i\omega_i t}\right)(Be^{i\omega_j t} + B^* e^{-i\omega_j t}) \tag{2.24}$$

where $(*)$ denotes the complex conjugate. Adopting a form for Q analogous to (2.20),

$$Q(x, y, z, t) = Re\sum_i \sum_j [Q_{ij}^+(x, y, z)e^{i(\omega_i+\omega_j)t} + Q_{ij}^-(x, y, z)e^{i(\omega_i-\omega_j)t}] \tag{2.25}$$

Consider the symmetry condition

$$Q_{ij}^+ = Q_{ji}^+ \tag{2.26a}$$

$$Q_{ij}^- = Q_{ji}^{-*} \tag{2.26b}$$

where

$$Q_{ij}^+ = \frac{i}{4g}\omega_i\phi_i\left(-\omega_j^2\frac{\partial\phi_j}{\partial z} + g\frac{\partial^2\phi_j}{\partial z^2}\right) + \frac{i}{4g}\omega_j\phi_j\left(-\omega_i^2\frac{\partial\phi_i}{\partial z} + g\frac{\partial^2\phi_i}{\partial z^2}\right) - \frac{1}{2}i(\omega_i + \omega_j)\nabla\phi_i \cdot \nabla\phi_j \tag{2.27}$$

$$Q_{ij}^- = \frac{i}{4g}\omega_i\phi_i\left(-\omega_j^2\frac{\partial\phi_j^*}{\partial z} + g\frac{\partial^2\phi_j^*}{\partial z^2}\right) + \frac{i}{4g}\omega_j\phi_j^*\left(-\omega_i^2\frac{\partial\phi_i}{\partial z} + g\frac{\partial^2\phi_i}{\partial z^2}\right) - \frac{1}{2}i(\omega_i + \omega_j)\nabla\phi_i \cdot \nabla\phi_j^* \tag{2.28}$$

The definition of the free-surface boundary condition for the second-order potential is given by

$$-(\omega_i \pm \omega_j)^2\phi_{ij}^\pm + g\frac{\partial\phi_{ij}^\pm}{\partial z} = Q_{ij}^\pm \tag{2.29}$$

2.1.4 The First-order and Second- order Forces

The expressions for the first- and second-order forces are derived from direct integration of the fluid pressure over a body boundary. From the WAMIT theory manual, the first- and second-order forces are calculated as follows

$$F^{(1)} = -\rho \iint_{SB} n\Phi_t^{(1)} dS - \rho g \iint_{SB} \left(\alpha^{(1)} \times n\right)(z + Z_0) dS - \rho g \iint_{SB} n(\xi_3^{(1)} + \alpha_1^{(1)} y - \alpha_2^{(1)} x) dS \quad (2.30)$$

$$M^{(1)} = -\rho \iint_{SB} (x \times n)\Phi_t^{(1)} dS - \rho g \iint_{SB} (x \times n)\left(\xi_3^{(1)} + \alpha^{(1)} y - \alpha_2^{(1)} x\right) dS - \rho g \iint_{SB} \left(\xi^{(1)} \times n\right)(z + Z_0) dS - \rho g \iint_{SB} [\alpha^{(1)} \times (x \times n)](z + Z_0) dS \quad (2.31)$$

The second-order force is obtained from

$$F^{(2)} = -\rho g \iint_{SB} (z + Z_0) H n dS - \rho \iint_{SB} \left(\alpha^{(1)} \times n\right)[\Phi_t^{(1)} + g(\xi_3^{(1)} + \alpha_1^{(1)} y - \alpha_2^{(1)} x)] dS - \rho \iint_{SB} [\frac{1}{2} \nabla\Phi^{(1)} \cdot \nabla\Phi^{(1)} + (\xi^{(1)} + \alpha^{(1)} \times x) \cdot \nabla\Phi_{\mathrm{t}}^{(1)}] n dS - \rho g \iint_{SB} (Hx \cdot k) n dS + \frac{1}{2} \rho g \int_{WL} [\eta^{(1)} - (\xi_3^{(1)} + \alpha_1^{(1)} y - \alpha_2^{(1)} x)]^2 \sqrt{1 - n_z^2} dl - \rho g A_{wp}\left(\xi_3^{(2)} + \alpha_1^{(2)} y_f - \alpha_2^{(2)} x_f\right) k - \rho \iint_{SB} \Phi_t^{(2)} n dS \quad (2.32)$$

The second-order force or moment due to $\Phi^{(2)}$ is decomposed into a part due to $\Phi_{\mathrm{I}}^{(2)} + \Phi_{\mathrm{S}}^{(2)}$ and the other part due to $\Phi_{\mathrm{R}}^{(2)}$. Then the force and moment take forms

$$F^{(2)} = F_q + F_p - \rho g A_{wp}\left(\xi_3^{(2)} + \alpha_1^{(2)} y_f - \alpha_2^{(2)} x_f\right) k - \rho \iint_{SB} n \frac{\partial \Phi_R^{(2)}}{\partial t} dS \quad (2.33)$$

where

$$F_q = \frac{1}{2}\rho g \int_{WL}[\eta^{(1)} - (\xi_3^{(1)} + \alpha_1^{(1)} y - \alpha_2^{(1)} x)]^2 \sqrt{1 - n_z^2} dl - \rho \iint_{SB}[\frac{1}{2}\nabla\Phi^{(1)} \cdot \nabla\Phi^{(1)} + (\xi^{(1)} + \alpha^{(1)} \times x) \cdot \nabla\Phi_{\mathrm{t}}^{(1)}]ndS + \alpha^{(1)} \times F^{(1)} - \rho g A_{wp}[\alpha_1^{(1)}\alpha_3^{(1)} x_f + \alpha_2^{(1)}\alpha_3^{(1)} y_f + \frac{1}{2}(\left(\alpha_1^{(1)}\right)^2 + \left(\alpha_2^{(1)}\right)^2) Z_0]k \quad (2.34)$$

$$F_p = -\rho \iint_{SB} \frac{\partial(\Phi_{\mathrm{I}}^{(2)} + \Phi_{\mathrm{S}}^{(2)})}{\partial \mathrm{t}} ndS \quad (2.35)$$

It should be noted that the last term in the right hand side of equation (2.33) is not evaluated in the WAMIT. Only the mean drift forces will be considered in this study, and see Chapter II, 2.6 for more details.

The second-order moment is given by

$$M^{(2)} = \frac{1}{2}\rho g \int_{WL}\left[\eta^{(1)} - \left(\xi_3^{(1)} + \alpha_1^{(1)} y - \alpha_2^{(1)} x\right)\right]^2 \sqrt{1 - n_z^2}(x \times n) dl - \rho \iint_{SB}\left[\frac{1}{2}\nabla\Phi^{(1)} \cdot \nabla\Phi^{(1)} + \left(\xi^{(1)} + \alpha^{(1)} \times x\right) \cdot \nabla\Phi_{\mathrm{t}}^{(1)}\right](x \times n) dS - \rho \int_{SB}\left(\xi^{(1)} \times n\right)[\Phi_{\mathrm{t}}^{(1)} + g\left(\xi_3^{(1)} + \alpha_1^{(1)} y - \alpha_2^{(1)} x\right)]\ dS - \rho g \iint_{SB} \xi^{(1)} \times (\alpha^{(1)} \times n)(z + Z_0) dS - \rho \iint_{SB} \alpha^{(1)} \times (x \times n)\left[\Phi_{\mathrm{t}}^{(1)} + g\left(\xi_3^{(1)} + \alpha_1^{(1)} y - \alpha_2^{(1)} x\right)\right] dS - \rho g \iint_{SB}(z + Z_0) H(x \times n) dS - \rho g \iint_{SB}(Hx \cdot k)(x \times n) dS - \rho g i[-V\xi_2^{(2)} + A_{wp} y_f \xi_3^{(2)} + (Vz_b + L_{22})\alpha_1^{(2)} - L_{12}\alpha_2^{(2)} - Vx_b\alpha_3^{(2)}] - \rho g j[V\xi_1^{(2)} - A_{wp} y_f \xi_3^{(2)} - L_{12}\alpha_1^{(2)} + (Vz_b + L_{11})\alpha_2^{(2)} - Vy_b\alpha_3^{(2)}] - \rho \iint_{SB}(x \times n)\Phi_{\mathrm{t}}^{(2)} \mathrm{dS} \quad (2.36)$$

$M^{(2)}$ in equation (2.36) can also be written as

$$M^{(2)} = M_q + M_p - \rho g i[-V\xi_2^{(2)} + A_{wp}y_f\xi_3^{(2)} + (Vz_b + L_{22})\alpha_1^{(2)} - L_{12}\alpha_2^{(2)} - Vx_b\alpha_3^{(2)}] - \rho g j\left[V\xi_1^{(2)} - A_{wp}y_f\xi_3^{(2)} - L_{12}\alpha_1^{(2)} + (Vz_b + L_{11})\alpha_2^{(2)} - Vy_b\alpha_3^{(2)}\right] - \rho \iint_{SB}(x \times n)\frac{\partial \Phi_R^{(2)}}{\partial t}dS \quad (2.37)$$

where,

$$M_q = \frac{1}{2}\rho g \int_{WL}\left[\eta^{(1)} - \left(\xi_3^{(1)} + \alpha_1^{(1)}y - \alpha_2^{(1)}x\right)\right]^2\sqrt{1-n_z^2}(x \times n)dl - \rho \iint_{sB}\left[\frac{1}{2}\nabla\Phi^{(1)} \cdot \nabla\Phi^{(1)} + \left(\xi^{(1)} + \alpha^{(1)} \times x\right) \cdot \nabla\Phi_{\mathrm{t}}^{(1)}\right](x \times n)dS + \xi^{(1)} \times F^{(1)} + \alpha^{(1)} \times M^{(1)} + \rho g i[-V\xi_1^{(1)}\alpha_3^{(1)} + V\alpha_1^{(1)}\alpha_2^{(1)}x_b - V\alpha_1^{(1)}\alpha_3^{(1)}z_b - \frac{1}{2}V\left(\left(\alpha_1^{(1)}\right)^2 - \left(\alpha_3^{(1)}\right)^2\right)y_b - \alpha_1^{(1)}\alpha_3^{(1)}L_{12} - \alpha_2^{(1)}\alpha_3^{(1)}L_{22} + \frac{1}{2}(\left(\alpha_1^{(1)}\right)^2 + \left(\alpha_2^{(1)}\right)^2)Z_0A_{wp}y_f] + \rho g j\left[-V\xi_2^{(1)}\alpha_3^{(1)} + V\alpha_1^{(1)}\alpha_3^{(1)}z_b + \frac{1}{2}V\left(\left(\alpha_2^{(1)}\right)^2 - \left(\alpha_3^{(1)}\right)^2\right)x + \alpha_1^{(1)}\alpha_3^{(1)}L_{11} + \alpha_2^{(1)}\alpha_3^{(1)}L_{12} + \frac{1}{2}\left(\left(\alpha_1^{(1)}\right)^2 + \left(\alpha_2^{(1)}\right)^2\right)Z_0A_{wp}x_f\right] + \rho g k\left[V\xi_1^{(1)}\alpha_1^{(1)} + V\xi_2^{(1)}\alpha_2^{(1)} + V\alpha_2^{(1)}\alpha_3^{(1)}x_b - V\alpha_1^{(1)}\alpha_3^{(1)}y_b\right] \quad (2.38)$$

$$M_p = -\rho \iint_{SB}(x \times n)\frac{\partial(\Phi_{\mathrm{I}}^{(2)} + \Phi_{\mathrm{S}}^{(2)})}{\partial t}ndS \quad (2.39)$$

2.1.5 Multiple Body Interaction

The linear and second-order theory described in Chapter II, 2.1.1 - Chapter II, 2.1.4 applies to a single rigid structure. Let us consider two floating bodies in close proximity.

Similar to the equations for the single body, the radiation potential for the isolated body is expressed as

$$\phi_R^I = i\omega \sum_{j=1}^{6} \zeta_j^I \phi_j^I \tag{2.40a}$$

$$\phi_R^{II} = i\omega \sum_{j=1}^{6} \zeta_j^{II} \phi_j^{II} \tag{2.40b}$$

where I and II denotes the first and second body, respectively.

The boundary condition on each independent surface can be expressed as

$$\frac{\partial \phi_j^I}{\partial n} = n_j^I \tag{2.41a}$$

$$\frac{\partial \phi_j^{II}}{\partial n} = n_j^{II} \tag{2.41b}$$

where

$$(n_1, n_2, n_3)^I = \mathbf{n}^I, (n_4, n_5, n_6)^I = \mathbf{x^I} \times \mathbf{n}^I \tag{2.42a}$$

$$(n_1, n_2, n_3)^{II} = \mathbf{n}^{II}, (n_4, n_5, n_6)^{II} = \mathbf{x^{II}} \times \mathbf{n}^{II} \tag{2.42b}$$

The diffraction potential for each body should satisfy

$$\frac{\partial \phi_D^I}{\partial n} = -\frac{\partial \phi_I^I}{\partial n} \text{, on the first body's surface } S^I \tag{2.43a}$$

$$\frac{\partial \phi_D^{II}}{\partial n} = -\frac{\partial \phi_I^{II}}{\partial n} \text{, on the second body's surface } S^{II} \tag{2.43b}$$

The above equations are for the independent body only. The boundary conditions due to the interaction between the two bodies are

$$\frac{\partial \phi_j^{I,II}}{\partial n} = n_j^I \text{, on the first body} \tag{2.44a}$$

$$\frac{\partial \phi_j^{II}}{\partial n} = 0 \text{, on the second body (fixed)} \tag{2.44b}$$

where $\phi_j^{I,II}$ is the velocity potential of the first body due to the fixed second body.

Similarly, we can also write the boundary conditions for the second body if the first body is fixed.

$$\frac{\partial \phi_j^{II,I}}{\partial n} = n_j^{II}, \text{ on the second body} \tag{2.45a}$$

$$\frac{\partial \phi_j^{I}}{\partial n} = 0, \text{ on the first body (fixed)} \tag{2.45b}$$

For more detailed discussion, see Newman (2001), Charkrabarti (1987), Kim (2008) and Kim (2003).

2.2 Equations of Motion (EOM)

As mentioned in Chapter I, two levels of approximation of hydrodynamic coefficients are considered, i.e., the CCM method and IRF method. Usually the CCM method is applicable to the regular wave case. However, the IRF used in the latter one can represent the fluids memory effects, and it is a more accurate way to approximate the impulse response of the floating body at random sea.

With the origin of the coordinate system located at the center of the waterplane area, the mass matrix M and the hydrostatic restoring coefficient matrix c in equations (1.9) and (1.10) are written as follows (Mercier, 2009)

$$M = \begin{bmatrix} m & 0 & 0 & 0 & mz_g & -my_g \\ 0 & m & 0 & -mz_g & 0 & mx_g \\ 0 & 0 & m & my_g & -mx_g & 0 \\ 0 & -mz_g & my_g & I_{YY}+I_{ZZ} & -I_{YX} & -I_{ZX} \\ mz_g & 0 & -mx_g & -I_{XY} & I_{ZZ}+I_{XX} & -I_{ZY} \\ -my_g & mx_g & 0 & -I_{XZ} & -I_{YZ} & I_{XX}+I_{YY} \end{bmatrix} \tag{2.46}$$

The products of inertia are given by

$$I_{XX} = \iiint_{V_B} x_B^2 dm \tag{2.47a}$$

$$I_{YY} = \iiint_{V_B} y_B^2 dm \tag{2.47b}$$

$$I_{ZZ} = \iiint_{V_B} z_B^2 dm \tag{2.47c}$$

$$I_{XY} = I_{YX} = \iiint_{V_B} x_B y_B dm \tag{2.47d}$$

$$I_{XZ} = I_{ZX} = \iiint_{V_B} x_B z_B dm \tag{2.47e}$$

$$I_{YZ} = I_{ZY} = \iiint_{V_B} y_B z_B dm \tag{2.47f}$$

The hydrostatic restoring coefficient matrix is

$$c = \begin{bmatrix} 0 & 0 & 0 & 0 & 0 & 0 \\ 0 & 0 & 0 & 0 & 0 & 0 \\ 0 & 0 & \rho g A^{(0)} & \rho g I_Y^A & -\rho g I_X^A & 0 \\ 0 & 0 & \rho g I_Y^A & \rho g V^{(0)} G M_T & -\rho g I_{XY}^A & 0 \\ 0 & 0 & -\rho g I_X^A & -\rho g I_{YX}^A & \rho g V^{(0)} G M_T & 0 \\ 0 & 0 & 0 & 0 & 0 & 0 \end{bmatrix} \tag{2.48}$$

where $A^{(0)}$ is the waterplane area. $V^{(0)}$ is the submerged volume.

$$I_X^A = \iint_{S_A^{(0)}} (x_0 - X_0) dxdy = \iint_{S_A^{(0)}} x_B dxdy \tag{2.49a}$$

$$I_Y^A = \iint_{S_A^{(0)}} (y_0 - Y_0) dxdy = \iint_{S_A^{(0)}} y_B dxdy \tag{2.49b}$$

$$I_{XY}^A = I_{YX}^A = \iint_{S_A^{(0)}} (x_0 - X_0)(y_0 - Y_0) dxdy \tag{2.49c}$$

$$GM_T = \frac{I_{YY}^A}{V^{(0)}} + z_b - z_g \tag{2.49d}$$

$$GM_L = \frac{I_{XX}^A}{V^{(0)}} + z_b - z_g \tag{2.49e}$$

Herein, the matrix c in equation (2.48) is for a free-floating body with no external restraints.

For an $N-$body floating system, the equations of motion can be written as (Yu, et al., 2010a; Yu and Falzarano, 2011)

$$\begin{bmatrix} M_{11}+a_{11}(\omega) & \cdots & a_{1N}(\omega) \\ \vdots & \ddots & \vdots \\ a_{N1}(\omega) & \cdots & M_{NN}+a_{NN}(\omega) \end{bmatrix} \begin{Bmatrix} \ddot{X}_1 \\ \vdots \\ \ddot{X}_N \end{Bmatrix} + \begin{bmatrix} b_{11}(\omega) & \cdots & b_{1N}(\omega) \\ \vdots & \ddots & \vdots \\ b_{N1}(\omega) & \cdots & b_{NN}(\omega) \end{bmatrix} \begin{Bmatrix} \dot{X}_1 \\ \vdots \\ \dot{X}_N \end{Bmatrix}$$

$$+ \begin{bmatrix} c_{11} & \cdots & 0 \\ \vdots & \ddots & \vdots \\ 0 & \cdots & c_{NN} \end{bmatrix} \begin{Bmatrix} X_1 \\ \vdots \\ X_N \end{Bmatrix} = \begin{Bmatrix} f_1^{ext} \\ \vdots \\ f_N^{ext} \end{Bmatrix} \tag{2.50}$$

where X_1 and X_N are the 6×1 motion vectors of the 1^{st} and the N^{th} body; M_{11} and M_{NN} are the 6×6 mass matrix of the 1^{st} and the N^{th} body; c_{11} and c_{NN} are the 6×6 hydrostatic restoring coefficient matrix of the 1^{st} and the N^{th} body; $a_{1N}(\omega_0)$ is the 6×6 added mass matrix of the 1^{st} body due to the N^{th} body; $b_{1N}(\omega)$ is the 6×6 radiation damping matrix of the 1st body due to the N^{th} body. Herein, for a two-body system, $N = 2$; for a three-body system, $N = 3$.

In terms of the convolution terms presented in Cummins equation (1962) and Ogilvie relations (1964), the equations of motion can be also written as

$$[M + a(\infty)]\ddot{x}(t) + \int_0^t K(t-\tau)\,\dot{x}(\tau)d\tau + cx(t) = f^{ext}(t) \tag{2.51}$$

$$K(t) = \frac{2}{\pi}\int_0^\infty b(\omega)\cos\omega t\, d\omega \tag{2.52}$$

Both equations are the repeat of equations (1.10) and (1.11) in Chapter I.

For a multibody system, the equations of motion using IRFs can be expressed in the following way:

$$\underbrace{\begin{bmatrix} M_{11}+a_{11}(\infty) & \cdots & a_{1N}(\infty) \\ \vdots & \ddots & \vdots \\ a_{N1}(\infty) & \cdots & M_{NN}+a_{NN}(\infty) \end{bmatrix}}_{\bar{M}} \begin{Bmatrix} \ddot{X}_1 \\ \vdots \\ \ddot{X}_N \end{Bmatrix} + \int_0^t \begin{bmatrix} K_{11}(t-\tau) & \dots & K_{11}(t-\tau) \\ \vdots & \ddots & \vdots \\ K_{N1}(t-\tau) & \dots & K_{NN}(t-\tau) \end{bmatrix} \begin{Bmatrix} \dot{X}_1 \\ \vdots \\ \dot{X}_N \end{Bmatrix} d\tau + \underbrace{\begin{bmatrix} c_{11} & \cdots & 0 \\ \vdots & \ddots & \vdots \\ 0 & \cdots & c_{NN} \end{bmatrix}}_{\bar{c}} \begin{Bmatrix} X_1 \\ \vdots \\ X_N \end{Bmatrix} = \begin{Bmatrix} f_1^{ext} \\ \vdots \\ f_N^{ext} \end{Bmatrix} \tag{2.53}$$

where X_1, $\dot{X}_1$ and $\ddot{X}_1$ are the displacement, velocity and acceleration vector of the *1*st body ; X_N, $\dot{X}_N$ and $\ddot{X}_N$ are the displacement, velocity and acceleration vector of the Nth body. For example, the state vector of the *1st* body is

$$X_1 = \begin{bmatrix} x_1^I \\ \vdots \\ x_6^I \end{bmatrix} \tag{2.54}$$

where the superscript *I* represents the first body, and the numbers $1, 2, \dots, 6$ denote the six DOFs of a single rigid body.

If we ignore the body-to-body hydrodynamic interaction coefficients in equations (2.50) and (2.53), then these two equations are mathematically simplified to represent equations of motion of N independent bodies. Moreover, for the purpose of convenience, note the whole mass matrix in equation (2.53) as $\bar{M}$, and the hydrostatic restoring coefficient matrix as $\bar{c}$, and they are both $6N \times 6N$ matrices.

In addition, the EOM of a multibody floating system can be expressed as follows if using the tensor notation

$$\sum_{j=1}^{6N} \left\{ (M_{ij} + a_{ij})\ddot{x}_j + \int_0^t K_{ij}(t-\tau)\dot{x}_j d\tau + c_{ij}x_k \right\} = f_i^{ext}(t) \quad i = 1, \dots, 6N \tag{2.55}$$

where the matrix impulse response function $K_{ij}(t)$ can be written as

$$K_{ij}(t) = \frac{2}{\pi}\int_0^\infty b_{ij}(\omega)\cos(\omega t)d\omega \tag{2.56}$$

2.3 Impulse Response Function

The matrix impulse response function $K_{ij}(t)$ in equation (2.56) is the derivative of $L_{ij}(t)$, that is

$$K_{ij}(t) = \frac{\partial}{\partial t}L_{ij}(t) \tag{2.57}$$

The fundamental relations between the time- and frequency-domain express the added mass coefficient a_{ij} and damping coefficient b_{ij} in terms of Fourier transforms of $L_{ij}(t)$

$$a_{ij}(\omega) - a(\infty) = \int_0^\infty L_{ij}(t)\ \cos\omega t \mathrm{d}t \tag{2.58}$$

$$b_{ij}(\omega) = \omega\int_0^\infty L_{ij}(t)\ \sin\omega t\ \mathrm{d}t \tag{2.59}$$

The inverse transformation of equation (2.58) and (2.59) gives the complementary relations for the impulse response function (WAMIT, 2008)

$$L_{ij}(t) = \frac{2}{\pi}\int_0^\infty (a_{ij}(\omega) - a_{ij}(\infty))\cos\omega t \mathrm{d}\omega \tag{2.60}$$

$$L_{ij}(t) = \frac{2}{\pi}\int_0^\infty (\frac{b_{ij}(\omega)}{\omega})\sin\omega t\ \mathrm{d}\omega \tag{2.61}$$

The most significant truncation error is associated with the transform of the added mass (2.60). From the partial integration of (2.58), it follows that

$$a_{ij}(\omega) - a_{ij}(\infty) = -\frac{1}{\omega}\int_0^\infty L'_{ij}\,(t)\sin\omega t \mathrm{d}t \cong -L'_{ij}(0)\omega^{-2} \tag{2.62}$$

If equation (2.60) is truncated at a finite frequency $\omega_N = \Omega$, the truncation correction is

$$\Lambda_{ij}(t) = \frac{2}{\pi}\int_{\Omega}^{\infty}[a_{ij}(\omega) - a_{ij}(\infty)]\cos\omega t \,\mathrm{d}\omega \tag{2.63}$$

However, an alternative procedure is adopted in the F2T module of WAMIT, and they are

$$L'_{ij}(0) = \frac{2}{\pi}\int_{0}^{\infty} b_{ij}(\omega)\,\mathrm{d}\omega \cong \frac{2}{\pi}\int_{0}^{\Omega} b_{ij}(\omega)\,\mathrm{d}\omega \tag{2.64}$$

For more details about how to calculate IRF numerically, see Greenhow (1986) and Lewandowski (2008).

2.4 State-space Format of EOM

The EOM of a single body based on CCM, i.e., equation (1.9), can be put into the following form

$$\dot{z} = Az + Bf^{ext} \tag{2.65}$$

where

$$A = \begin{bmatrix} 0 & I \\ -(M + a(\omega_0))^{-1}\cdot c & -(M + a(\omega_0))^{-1}\cdot b(\omega_0) \end{bmatrix} \tag{2.66}$$

$$B = \begin{bmatrix} 0 \\ (M + a(\omega_0))^{-1} \end{bmatrix} \tag{2.67}$$

In a similar way, the EOM of multibody floating systems based on CCM, i.e., equation (2.53), can be also written in state-space format. In this study, the fourth-order Runge-Kutta method is selected and the ODE45 solver of MATLAB is directly employed.

Firstly, define the state variables for a single rigid body as

$$z(t) = \begin{bmatrix} x(t) \\ \dot{x}(t) \end{bmatrix} = \begin{bmatrix} x \\ -- \\ \dot{x} \end{bmatrix} \tag{2.68}$$

For the multibody system, the state variables are

$$Z(t) = \begin{bmatrix} \bar{X}(t) \\ \dot{\bar{X}}(t) \end{bmatrix} = \begin{bmatrix} X_1 \\ \vdots \\ X_N \\ - - - \\ \dot{X}_1 \\ \vdots \\ \dot{X}_N \end{bmatrix} \tag{2.69}$$

For the multibody system, replace the mass matrix, stiffness matrix and hydrostatic restoring matrix in equations (2.65) - (2.67) with the corresponding matrices in equation (2.53), then we can obtain the state variables for the N-body system based on the CCM in a similar way.

Further, the state-space models for the IRF method are derived as following for the single body and multibody case, respectively.

Ran (2000) and Chen (2002) presented two different ways of dealing with the convolution terms when solving the EOM. Herein, the convolution term in equation (2.51) is numerically computed using the trapezoidal rule

$$\int_0^t K(t-\tau)\,\dot{x}(\tau)d\tau = \frac{1}{2}\sum_{m=0}^{n-1}[K(t-m\Delta\tau)\cdot\dot{x}(m\Delta\tau) + K(t-(m+1)\Delta\tau)\cdot\dot{x}((m+1)\Delta\tau)]\cdot\Delta\tau \tag{2.70}$$

Rearrange the terms in equation (2.70)

$$\int_0^t K(t-\tau)\,\dot{x}(\tau)d\tau = \frac{1}{2}K(0)\cdot\dot{x}(t)\cdot\Delta\tau + [\sum_{m=1}^{n-1}K(t-m\Delta\tau)\cdot\dot{x}(m\Delta\tau)\cdot\Delta t] + \frac{1}{2}K(t)\cdot\dot{x}(0)\cdot\Delta\tau \tag{2.71}$$

where n denotes the n^{th} time step, and $t = n\cdot\Delta\tau$

In the numerical calculation, the first term in equation (2.71) can be regarded as the damping term to be solved at the time t. The other two terms are the known terms and can be moved to the right-hand side.

Therefore, the state-space model for equation (2.51) can be expressed as

$$\dot{z}(t) = A_{new}z + B_{new}\left(f^{ext} - \sum_{m=1}^{n-1}[K(t-m\Delta\tau)\cdot\dot{x}(m\Delta\tau)\cdot\Delta\tau] - \frac{1}{2}K(t)\dot{x}(0)\cdot\Delta\tau\right) \tag{2.72}$$

where

$$A_{new} = \begin{bmatrix} 0 & I \\ -(M+a(\infty))^{-1}\cdot c & -(M+a(\infty))^{-1}\cdot\frac{1}{2}K(0)\cdot\Delta\tau \end{bmatrix} \tag{2.73}$$

$$B_{new} = \begin{bmatrix} 0 \\ (M+a(\infty))^{-1} \end{bmatrix} \tag{2.74}$$

The matrix A_{new} represents the physical property of this dynamical system, since the total mass term $M + a(\infty)$, the damping term $K(0)$ and the hydrostatic restoring coefficient c are all included in A_{new}. Moreover, A_{new} is dependent on the time step $\Delta\tau$ that is used to evaluate the IRFs, as indicated by equation (2.73). Therefore, how the time step $\Delta\tau$ affects the controlling efficiency will be studied in Chapter III.

For the multibody systems, all the convolution terms $\int_0^t K_{ij}(t-\tau)\dot{x}_j d\tau$ in equation (2.53) can be numerically calculated in the same way as that in equation (2.72). Therefore, the corresponding state-space model can be expressed as

$$\dot{Z} = \bar{A}_{new}Z + \bar{B}_{new}\bar{f}_{new}^{ext} \tag{2.75}$$

where

$$\bar{A}_{new} = \begin{bmatrix} 0 & I \\ -\bar{M}^{-1} \cdot \bar{c} & -\bar{M} \cdot \frac{1}{2}\bar{K}_0 \cdot \Delta\tau \end{bmatrix} \tag{2.76}$$

$$\bar{K}_0 = \begin{bmatrix} K_{11}(0) & \cdots & K_{1N}(0) \\ \vdots & \ddots & \vdots \\ K_{N1}(0) & \cdots & K_{NN}(0) \end{bmatrix} \tag{2.77}$$

$$\bar{B}_{new} = \begin{bmatrix} 0 \\ \bar{M}^{-1} \end{bmatrix} \tag{2.78}$$

$$\bar{f}_{new}^{ext} = \begin{bmatrix} {f_1}^{ext} - \sum_{j=1}^{N}\sum_{m=1}^{n-1}\left[K_{1j}(t - m\Delta\tau) \cdot \dot{X}_j(m\Delta\tau) \cdot \Delta\tau\right] - \frac{1}{2}K_{1j}(t)X_j(0) \cdot \Delta\tau \\ \vdots \\ {f_i}^{ext} - \sum_{j=1}^{N}\sum_{m=1}^{n-1}\left[K_{ij}(t - m\Delta\tau) \cdot \dot{X}_j(m\Delta\tau) \cdot \Delta\tau\right] - \frac{1}{2}K_{ij}(t)X_j(0) \cdot \Delta\tau \\ \vdots \\ {f_N}^{ext} - \sum_{j=1}^{N}\sum_{m=1}^{n-1}\left[K_{Nj}(t - m\Delta\tau) \cdot \dot{X}_j(m\Delta\tau) \cdot \Delta\tau\right] - \frac{1}{2}K_{Nj}(t)X_j(0) \cdot \Delta\tau \end{bmatrix} \tag{2.79}$$

In equation (2.75), $\bar{A}_{new}$ is $12\text{N} \times 12\text{N}$, $\bar{B}_{new}$ is $12\text{N} \times 6\text{N}$, $\bar{f}_{new}^{ext}$ is $6\text{N} \times 1$. $\bar{K}_0$ is a $6\text{N} \times 6\text{N}$ matrix incorporating all the initial values of $K_{ij}(t)$.Similar to equation (2.73), the time step $\Delta\tau$ does affect the assembly of $\bar{A}_{new}$, and it also affects the sum of external forces $\bar{f}_{new}^{ext}$.

Equation (2.75) is very similar to equation (1.2) if we ignore the control force f. $\bar{A}_{new}$ and $\bar{B}_{new}$ are corresponding to A and E in equation (1.2). If we consider the feedback force u (use f in the structural control) provided by the DP system for the floating system, the corresponding equation can be written as

$$\dot{Z} = \bar{A}_{new}Z + \bar{B}_{new}\bar{f}_{new}^{ext} + Bu \tag{2.80}$$

where u can be derived from various controllers, e.g., the PID controller or the optimal LQR method. Thus the problem described in Figure 1.1 is to solve the dynamic

responses of a multibody floating system with the feedback force to be determined, similar to the structural control discussed in Chapter I, 1.3.

Finally, we just need to adjust the following matrix $\bar{Y}$ in order to output the desired variables

$$\bar{Y} = \bar{C}_{new} Z \tag{2.81}$$

For a two-body system, if we need to consider the relative heave motion between two bodies, the corresponding matrix $\bar{C}_{new}$ can be written as

$$\bar{C}_{new} = [0 \quad 0 \quad 1 \quad 0 \quad 0 \quad 0 \quad 0 \quad 0 \quad -1 \quad 0 \quad 0 \quad 0] \tag{2.82}$$

The output vector $\bar{Y}$ should be a 1×1 vector.

If we need to consider both the relative sway and heave motions,

$$\bar{C}_{new} = \begin{bmatrix} 0 & 1 & 0 & 0 & 0 & 0 & 0 & -1 & 0 & 0 & 0 & 0 \\ 0 & 0 & 1 & 0 & 0 & 0 & 0 & 0 & -1 & 0 & 0 & 0 \end{bmatrix} \tag{2.83}$$

The output vector $\bar{Y}$ should be a 2×1 vector.

If we need to consider all the horizontal motions, such as the relative surge, sway and heave,

$$\bar{C}_{new} = \begin{bmatrix} 1 & 0 & 0 & 0 & 0 & 0 & -1 & 0 & 0 & 0 & 0 & 0 \\ 0 & 1 & 0 & 0 & 0 & 0 & 0 & -1 & 0 & 0 & 0 & 0 \\ 0 & 0 & 1 & 0 & 0 & 0 & 0 & 0 & -1 & 0 & 0 & 0 \end{bmatrix} \tag{2.84}$$

The output vector $\bar{Y}$ should be a 3×1 vector.

2.5 Random Wave Loads

Sea state is defined in accordance with the North Atlantic Treaty Organization (NATO) standard for the North Atlantic. Both the ship and spar need to continue

operations through Sea State 4 (SS4), with significant wave heights 1.25-2.5 m. Herein, the Bretschneider spectrum (Chakrabarti, 1987) is used

$$S(\omega) = \frac{A}{4} H_s^2 \frac{\omega_s^4}{\omega^5} \exp\left(-A\left(\frac{\omega}{\omega_s}\right)^{-4}\right) \tag{2.85}$$

where A is nondimensional coefficient, H_s is significant wave height and ω_s is significant wave frequency. Herein, $A = 0.675$, and use $H_s = 1.88\,m$ and $\omega_s = 0.5072$ rad/sec to represent SS4.

The irregular sea can be simulated by

$$\eta(x,t) = \sum_{i=1}^{N} A_i \cos(k_i x - \omega_i t + \epsilon_i) \tag{2.86}$$

where $A_i = \sqrt{2S(\omega_i)\Delta\omega_i}$.

2.6 Slow Drift Force

The slow-drift excitation loads F_i^{SV} can be formally written as

$$F_i^{SV} = \sum_{j=1}^{N}\sum_{k=1}^{N} A_j A_k \left[T_{jk}^{ic} \cos\left\{\left(\omega_k - \omega_j\right)t + \left(\epsilon_k - \epsilon_j\right)\right\} + T_{jk}^{is} \sin\left\{\left(\omega_k - \omega_j\right)t + \left(\epsilon_k - \epsilon_j\right)\right\}\right] \tag{2.87}$$

where the wave amplitudes A_j, A_k may be determined by the wave spectrum $S(\omega)$; ω_j and ω_k are the wave frequencies; ϵ_j and ϵ_k are the random phase angles; T_{jk}^{ic} and T_{jk}^{is} are the second-order transfer functions for the difference frequency loads. Newman's approximation implies that

$$T_{jk}^{ic} = T_{kj}^{ic} = 0.5(T_{jj}^{ic} + T_{kk}^{ic}) \tag{2.88}$$

$$T_{jk}^{is} = T_{kj}^{is} = 0 \tag{2.89}$$

It is time-consuming to directly compute the slow drift force based on equation (2.87). Newman (1974) proposed a simplified approach by approximating the double summation by the square of a single series. This implies that N terms should be added together at each time step compared to N^2 terms. This formula can be written as

$$F_i^{SV} = 2\left[\sum_{j=1}^{N} A_j (T_{jj}^{ic})^{1/2} \cos(\omega_j t + \epsilon_j)\right]^2 \tag{2.90}$$

It should be noted that this equation provides forcing at the high frequencies, however, these terms have no influence when studying the slow-drift response. In equation (2.90), T_{jj}^{ic} must be positive (Faltinsen, 1990). Kaasen (1999) showed that a modification to Newman's method can be done in order to eliminate the high frequency noises generated by this method. The Hilbert transformation was applied to the auxiliary process u rather than the wave elevation to eliminate high frequency noise. By not using pre-generation of force time series, filtering out this noise must be done simultaneously with the simulation where there is a significant challenge to avoid a phase lag that may affect the low frequency components.

Pinkster (1980) analyzed the mean and low frequency second order wave drift forces on bodies moored or positioned in waves and compared numerical and experimental measurements of RAOs for a tanker, a semisubmersible and a barge. Chen and Duan (2007) developed a new formulation to compute the QTF using the series expansion of the second-order wave loading with respect to the difference-frequency up to the second order. It provides a novel method to evaluate the low-frequency second-order wave loads in a more accurate way than the zeroth order approximation (often called Newman's approximation) and in a more efficient way compared to the

computation of the complete QTF. Chen and Rezende (2009) further analyzed the time-series reconstruction of excitation loads in the motion simulation of mooring systems and demonstrated that it's a new, efficient and accurate scheme.

2.7 PID Controller

In control theory, the proportional, integral, and derivative terms are summed to calculate the output of the PID controller. Defining $u(t)$ as the controller output, the final form of the PID algorithm is:

$$u(t) = K_p e(t) + K_i \int_0^t e(\tau)d\tau + K_d \frac{d}{dt} e(t) \tag{2.91}$$

where K_p is the proportional gain, K_i is the integral gain, and K_d is the derivative gain. In addition, $e(t)$ is the error function, that is, $e(t) = y(t) - r(t)$; $y(t)$ is the plant output; $r(t)$ is the reference value. Figure 2.1 shows a block diagram of a typical PID controller.

In order to discretize the PID controller in the simulation, approximations for the first-order derivatives are made by backward finite differences. The integral term is discretized with a sampling time Δt, as follows,

$$\int_0^{t_k} e(\tau)d\tau = \sum_{i=1}^{k} e(t_i)\,\Delta t \tag{2.92}$$

The derivative term is approximated as

$$\frac{de(t_k)}{dt} = \frac{e(t_k) - e(t_{k-1})}{\Delta t} \tag{2.93}$$

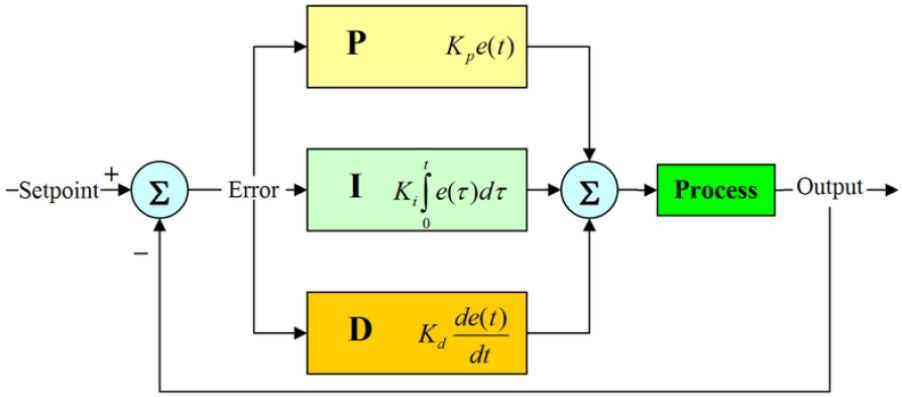

Figure 2.1 A block diagram of a PID controller (PID Controller, 2011)

For more details about the analysis, synthesis and design of a PID controller for continuous and discrete time linear systems, see Chen (1999) and Bhattacharyya, et al. (2009).

2.8 LQR Method

Consider the linear system

$$\dot{x} = Ax + Bu \tag{2.94}$$

If $x(t_0)$ is given at t_0, consider the problem of determining the control function $u(t)$ that minimizes the cost function

$$I = \int_{t_0}^{T_0} [x^T Q x + u^T R u]dt + x^T M x \tag{2.95}$$

where Q, R are weighting factors, both assumed to be symmetric and positive semidefinite and positive definite, respectively. The matrix M is symmetric positive semidefinite.

The following derivation is from Chapter 13 of Bhattacharyya, et al. (2009). Let $V(x,t)$ denote the value function. Then minimization of I requires

$$-\frac{\partial V(x,t)}{\partial t} = \inf_{u(t)}[x^T Q x + u^T R u + \frac{\partial V^T}{\partial x}(Ax + Bu)] \tag{2.96}$$

$$V(x(T_0), T_0) = x^T(T_0) M x(T_0) \tag{2.97}$$

The optimal control $u(t)$ satisfies

$$2Ru + B^T \frac{\partial V}{\partial x} = 0 \tag{2.98}$$

So that

$$u = -\frac{1}{2} R^{-1} B^T \frac{\partial V}{\partial x} \tag{2.99}$$

Substitute equation (2.99) into equation (2.96), we obtain

$$-\frac{\partial V}{\partial t} = x^T Q x + \frac{\partial V^T}{\partial x} A x - \frac{1}{4} \frac{\partial V^T}{\partial x} B R^{-1} B^T \frac{\partial V}{\partial x} \tag{2.100}$$

as the partial differential equation to be satisfied by $V(x,t)$ is subject to the boundary condition

$$V(x(T_0), T_0) = x^T(T_0) M x(T) \tag{2.101}$$

To solve equation (2.100) and equation (2.101), we make the reasonable guess that a V function is quadratic and propose

$$V(x(t), t) = x^T P x \tag{2.102}$$

where P is a symmetric matrix, as a candidate solution. Then equation (2.102) becomes

$$-x^T \dot{P} x = x^T Q x + 2x^T P A x - x^T P B R^{-1} B^T P x \tag{2.103}$$

, and equation (2.101) becomes

$$x^T(T_0) P(T_0) x(T_0) = x^T(T_0) M x(T_0) \tag{2.104}$$

Since

$$2PA = (PA + A^T P) + (PA - A^T P) \tag{2.105}$$

where the terms in the first bracket are symmetric and the second one is antisymmetric and

$$x^T Sx = -x^T Sx \tag{2.106}$$

Since $S(t)$ is antisymmetric, we can write (2.103) as

$$-x^T \dot{P} x = x^T [Q + PA + A^T P - PBR^{-1} B^T P] x \tag{2.107}$$

Thus, we have obtained a solution of equation (2.96) and equation (2.97) if P can be chosen to satisfy

$$-\dot{P} = Q + PA + A^T P - PBR^{-1} B^T P \tag{2.108}$$

for $t \in [t_0, T_0]$ with

$$P(T_0) = M \tag{2.109}$$

If a solution P to equation (2.108) and equation (2.109) can be found, the optimal control is

$$u = -R^{-1} B^T P x = -kx \tag{2.110}$$

where

$$k = R^{-1} B^T P \tag{2.111}$$

Equation (2.110) represents a time-varying state feedback control law. Assuming a very far terminal time $T_0 \to \infty$, the solution of the Ricacati equation (2.108) is expected to approach $\dot{P} = 0$. Then an algebraic Riccati equation can be solved for P

$$0 = A^T P + PA - PBR^{-1} B^T P + Q \tag{2.112}$$

In effect this algorithm therefore finds those controller settings that minimize the undesired deviations - Q , e.g., the deviations from desired altitude or process temperature. Often the magnitude of the control action itself - R is included in this sum so as to keep the energy expended by the control action itself limited.

The LQR controller has several very important properties, including its robustness properties, asymptotic properties, etc. It is important to stress that the properties of LQR designs hinge upon the fact that full-state feedback is used and the specific way that the control gain matrix k is computed from the solution of the Riccati equation. However, the full-state feedback means that every state that appears in the model of the physical system must be measured by a sensor. The other restrictive aspect is the gap between what the LQR controller achieves and the desired control system performance. The last issue is that LQR controller design is an iterative process even though the methodology systematically produces optimal, stabilizing controllers (Levine, 2000).

.

CHAPTER III

EXAMPLE I: MOTIONS OF THE SINGLE BODY

3.1 Hydrodynamic Coefficients of the Single Body

In order to solve the equations of motion, the hydrodynamic coefficients must be calculated in advance by solving the BVP problem. Some postprocessing tools have been developed to assemble the hydrodynamic coefficient matrices obtained from WAMIT.

In this chapter, we will firstly show and discuss some hydrodynamic results of the single spar and the USNS Bob Hope, i.e., the added mass and the radiation damping. Moreover, the impulse response functions for a single body are also obtained and compared with IRFs from the multiple body case.

The mean drift QTF are also solved. For this dynamical system, the optimal LQR controller is selected as the controlling method. Herein, for the purpose of simplicity, it is assumed that the DP system can provide the optimized force calculated from the LQR method, thus it is a full-state feedback case. In other words, it is assumed that the DP system can ideally provide all the 6-DOF feedback forces. Moreover, various time steps $\Delta\tau$, used to evaluate the IRFs, are investigated to study the stability and accuracy of the proposed state-space model as well as the robustness of LQR controller. For the purpose of convenience, the time step Δt in the time-domain simulation is selected as the same as $\Delta\tau$.

Finally, the effects of various weighting parameters (Q, R) on the controlling efficiency are also studied.

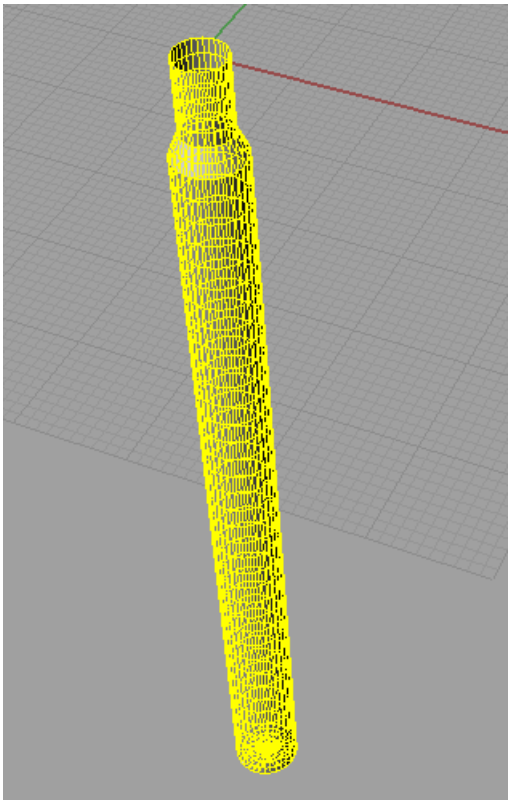

Figure 3.1 Panel model for the spar

As shown in Figure 3.1, the spar consists of three parts with different diameters. The top part is from the Mean Water Level (MWL) to 9 m deep below MWL, with 6.5 m diameter. The bottom part is a 106 m long cylinder with 8 m diameter. There is a 3 m transition area between the top part and the bottom part. The total number of panels for this spar is 1536. Moreover, the principal characteristics of the spar are listed in Table 3.1. The heave natural periods is 30.5 sec, and the angular frequency is 0.206 rad/sec.

The roll and picth natural period is 148.8 sec, and the angular frequency is 0.0422 rad/sec (Selfridge, 2005).

Table 3.1 Principal characteristics of the spar

Total length, L	129.6 m
Draught, T	118.0 m
Lower diameter, D_L	8.5 m
Upper diameter, D_U	6.0 m
Total displacement, Δ	6615.0 t

As shown in Figure 3.2, the total number of panels for the USNS Bob Hope is 1416. In addition, the principle characteristics of the ship are listed in Table 3.2. Obviously the Boh Hope is much bigger than the DWSC spar in the size.

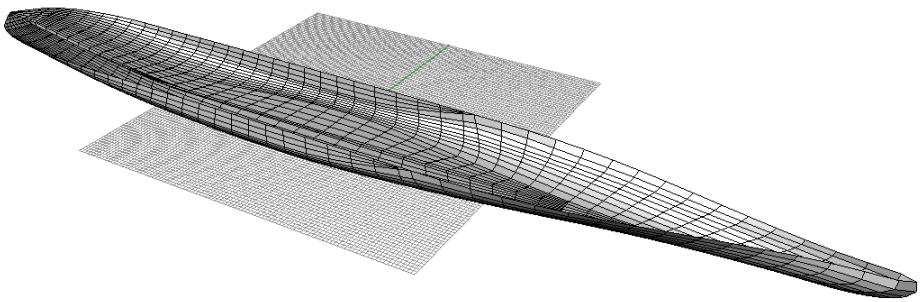

Figure 3.2 Panel model for the Bob Hope

Table 3.2 Principal characteristics of the USNS Bob Hope

Length between perpendiculars, L_{pp}	269.450 m
Breadth molded on waterline, B	32.258 m
Draught, T	8.795 m
Displacement volume molded, ∇	49167.523 m^3

The nondimensional added mass and nondimensional radiation damping are defined in WAMIT (2008) as follows

$$\bar{A}_{ij} = \frac{A_{ij}}{\rho L^k} \tag{3.1}$$

$$\bar{B}_{ij} = \frac{B_{ij}}{\rho L^k \omega} \tag{3.2}$$

where $k = 3$ for $i, j = 1,2,3$; $k = 4$ for $j = 4,5,6$ or $i = 4,5,6$, $j = 1,2,3$ and $k = 5$ for $i, j = 4,5,6$.

For example, Figure 3.3 shows the frequency dependent added mass of the single spar. The selected maximum wave frequency is about 7.0 rad/sec, and such a range is wide enough to estimate the impulse response function. The nondimensional added mass $\bar{A}_{11}$ approaches about 6100 with the increasing wave frequency. The dimensional added mass A_{ij} at the wave frequency 7.0 rad/sec is considered as the added mass at the infinite frequency $a(\infty)$, which will be used in equations (2.51) and (2.53).

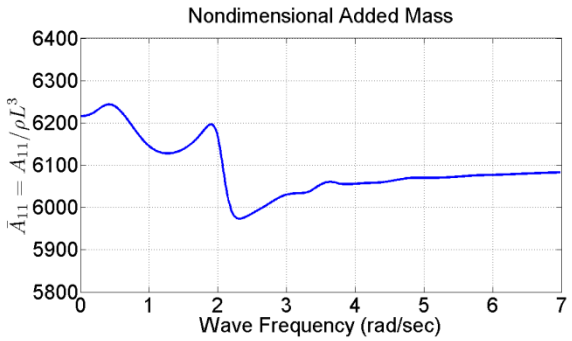

Figure 3.3 Nondimensional added mass $\bar{A}_{11}$ of the single spar

Figure 3.4 shows the frequency dependent radiation damping of the single spar. The nondimensional radiation damping $\bar{B}_{11}$ approaches zero with increasing wave frequency. The dimensional radiation damping B_{ij} at a specific wave frequency is the radiation damping $b(\omega_0)$ in equation (2.66).

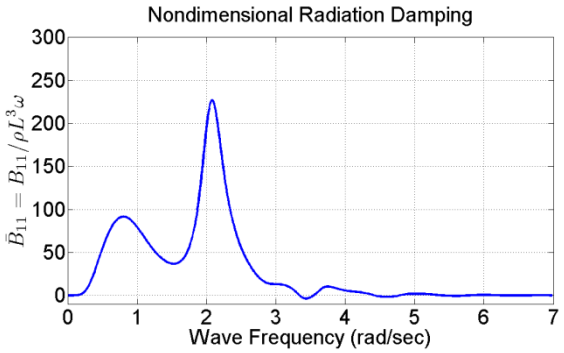

Figure 3.4 Nondimensional radiation damping $\bar{B}_{11}$ of the single spar

3.2 Verification of the Proposed State-space Model

In order to check the accuracy of the code developed based on the state-space modeling technology, several simple cases have been tested as follows. Assume a simple mechanical oscillator

$$M\ddot{x}(t) + b\dot{x}(t) + cx(t) = F(t) \tag{3.3}$$

where M, b, c are the mass matrix, damping matrix and stiffness matrix, respectively; $F(t)$ denotes the sinusoidal exciting fore and $F(t) = F_0 \sin \omega t$.

Equation (3.3) can be reconstructed as

$$\dot{z} = Az + BF^{ext} \tag{3.4}$$

where

$$z(t) = \begin{bmatrix} x(t) \\ \dot{x}(t) \end{bmatrix} = \begin{bmatrix} x \\ - \\ \dot{x} \end{bmatrix} \tag{3.5}$$

$$A = \begin{bmatrix} 0 & I \\ -M^{-1} \cdot c & -M^{-1} \cdot b \end{bmatrix} \tag{3.6}$$

$$B = \begin{bmatrix} 0 \\ M^{-1} \end{bmatrix} \tag{3.7}$$

In this example, M, b and c are all 6×6 unit matrices, and F_0 is a 6×1 unit vector. The excitation frequency ω is 0.7 rad/sec, and the period is around 9 sec. The analytical solution to equation (3.3) is

$$X_A(t) = C \sin 0.7t + D \cos 0.7t \tag{3.8}$$

where $C = 0.6799$ and $D = 0.9332$. Therefore, the amplitude of the steady-state response is

$$|X_A| = \sqrt{C^2 + D^2} = 1.15462 \tag{3.9}$$

Define the deviation between the numerically calculated amplitude $|X_N|$ and the analytical solution $|X_A|$,

$$\Delta D = \frac{|X_A| - |X_N|}{|X_A|} \tag{3.10}$$

Various time steps, e.g., $\Delta t = 0.05$ sec, 0.1 sec, 0.2 sec and 0.5 sec, are tried in the time-domain simulation. The results are given in Table 3.3. Obviously enough numerical accuracy can be guaranteed within a wide range of time steps, from 0.05 sec to 0.2 sec. A relatively large error occurs when the time step is greater than 0.5 sec. The reason may be that the motion response during a large time step cannot be regarded as a constant any more. However, the relative difference ratio between the amplitudes from these cases should be always less than 0.5%.

Therefore, $\Delta t = 0.05$ sec or 0.1 sec is employed herein.

Table 3.3 Comparison of the response amplitudes corresponding to various time steps Δt

Δt (sec)	0.05	0.1	0.2	0.5
$\|X_N\|$	1.1550	1.1545	1.1537	1.1489
ΔD	-0.0329%	0.0104%	0.0797%	0.4954%

It should be noted that the damping coefficient b and the exciting frequency ω may also affect the integration accuracy to some degree. However, the selection of time step Δt is mainly determined by both the accuracy and the total simulation time.

By analog, for the floating systems in ocean waves, we just need to replace the mass M, the damping coefficient b, stiffness terms c with the corresponding terms

$M + a(\omega_0), b(\omega_0)$ and hydrostatic restoring coefficients matrix c, and directly employ the ODE solvers of MATLAB to solve the EOMs.

3.3 Mean Drift Force

The mean drift force of surge, heave and pitch motions are shown in Figures 3.5 - 3.7, respectively. The Newman's approximation is used to obtain the time series of the mean drift force.

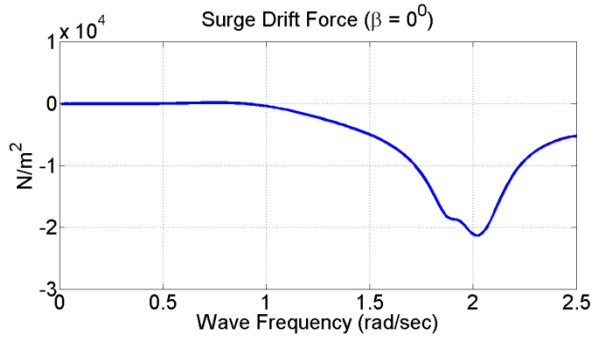

Figure 3.5 Mean drift QTF of surge motion ($\beta = 0^0$)

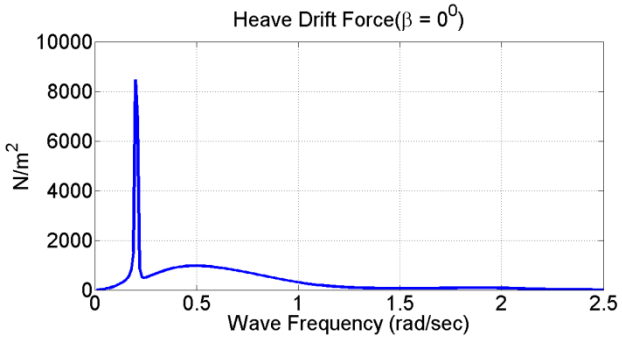

Figure 3.6 Mean drift QTF of heave motion ($\beta = 0^0$)

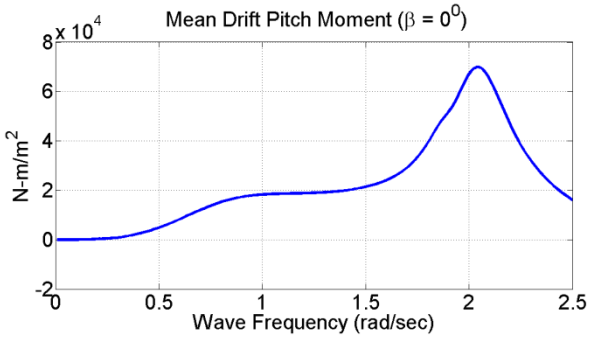

Figure 3.7 Mean drift QTF of pitch motion ($\beta = 0^0$)

3.4 Effects of Δτ and Δt on the Controlling Efficiency Using the LQR Controller

Until now, both the 1st order wave loads and mean drift force are obtained using the equations in Chapter II, 2.5 and 2.6. In this example, the LQR controller is utilized to obtain optimized forces to be applied to this single spar, while assuming that the DP system can provide such an amount of thruster forces. The feedback force is a 12×1 state vector, that is, $z = \begin{bmatrix} x \\ -- \\ \dot{x} \end{bmatrix}$ as defined in equation (2.68). The thruster forces are assumed to be exerted at the origin of the coordinate system in WAMIT. In this example, the origin is at the center point of the water plane of this spar.

As mentioned in Chapter II, how to evaluate the impulse response functions determines the definition of the dynamical system, that is, the modeling of this system depends on how to discretize the IRFs, i.e., $\Delta\tau$. Therefore, various $\Delta\tau$, e.g. 0.05 sec, 0.1 sec and 0.5 sec, have been tried in the simulation tool to study its effects on the controlling efficiency. Moreover, for the purpose of convenience, use the same time step

in the time-domain simulation of motion responses, i.e., $\Delta\tau = \Delta t$. In addition, it should be noted that the wave loads realizations applied in the case $\Delta\tau = \Delta t = 0.1$ sec and $\Delta\tau = \Delta t = 0.05$ sec can be directly derived from the case $\Delta\tau = \Delta t = 0.5$ sec by assuming that the external loads within 0.5 sec is a constant. In other words, the wave exciting force within 0.5 sec can be considered continuously unchanged. This way can further ensure that the realizations for these three cases are the same.

After we have constructed the system matrix A and the input matrix B, we can use equation (2.110) to calculate the feedback force using the LQR method, in order to mitigate the motion responses. In the LQR method, the calculation gain function k is a 2 $\times$ 12 matrix, based on both the six displacements and the six velocity (that is z, a 12 $\times$ 1 vector), thus the feedback force $u = -kz$ is a 6 $\times$ 1 vector. Figures 3.8 - 3.10 indicate that considerable motion mitigation may be achieved for the three cases, i.e., $\Delta\tau = \Delta t =$ 0.05 sec, 0.1 sec and 0.5 sec. Further, LQR controller shows its robustness for a wide range of time steps. In these three cases, the weighting factors (Q, R) are $(1, 1)$.

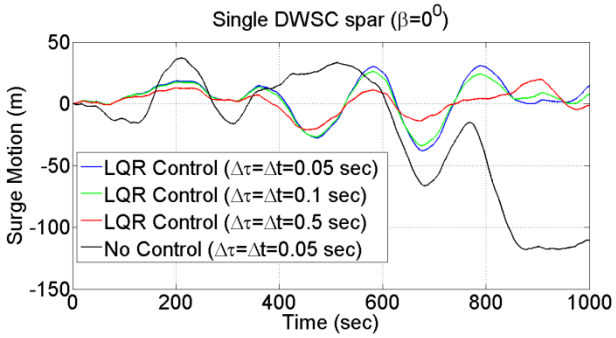

Figure 3.8 Surge motion of the single spar considering various time steps

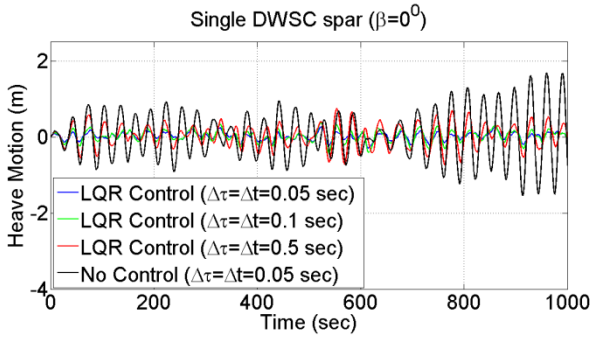

Figure 3.9 Heave motion of the single spar considering various time steps

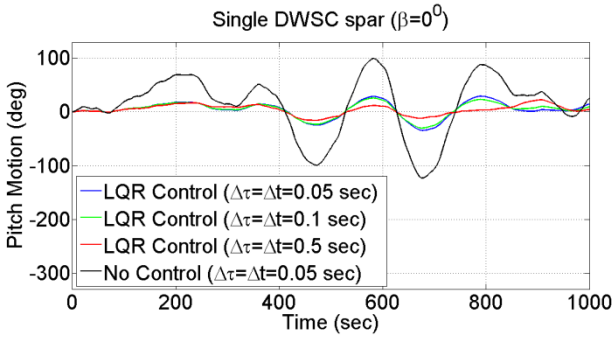

Figure 3.10 Pitch motion of the single spar considering various time steps

However, there is an obvious difference between the case $\Delta\tau = \Delta t = 0.5$ sec and the other two cases with smaller time steps. One of the reasons should be that the definition of the system matrix A depends on $\Delta\tau$, thus the obtained gain function k must be different. Thus the feedback force u calculated from the LQR controller is also different at each time step. Therefore, the mitigated motion responses must be different. Secondly, in accordance with the discussion in Chapter III, 3.2, a larger numerical discrepancy / error is observed when the time step is greater than 0.5 sec.

Table 3.4 Motions of the single spar with and without control

		Min.	Max.	Mean	Std.
Surge (m)	LQR Control($\Delta t = 0.05$ sec)	-37.9770	30.8953	3.511	16.0222
	LQR Control($\Delta t = 0.1$ sec)	-33.9008	26.1866	3.0113	14.2714
	LQR Control($\Delta t = 0.5$ sec)	-21.0984	19.7987	1.7181	9.2451
	No Control ($\Delta t = 0.05$ sec)	-118.0891	37.0682	-21.7803	49.2709
Heave (m)	LQR Control($\Delta t = 0.05$ sec)	-0.2972	0.2795	0.0235	0.0979
	LQR Control($\Delta t = 0.1$ sec)	-0.4112	0.3768	0.0237	0.1466
	LQR Control($\Delta t = 0.5$ sec)	-0.7318	0.751	0.025	0.2972
	No Control ($\Delta t = 0.05$ sec)	-1.5466	1.6863	0.0309	0.6187
Pitch (deg)	LQR Control($\Delta t = 0.05$ sec)	-34.515	29.31825	4.004975	14.87971
	LQR Control($\Delta t = 0.1$ sec)	-30.2374	25.8572	4.081	13.2487
	LQR Control($\Delta t = 0.5$ sec)	-15.7784	22.6316	4.2778	9.0937
	No Control ($\Delta t = 0.05$sec)	-123.2279	99.7561	12.5122	54.0868

Further analysis indicates that the former factor should dominate such difference. For example, we can roughly estimate the relative difference ratios among these cases based on the statistics in Table 3.4, which shows the minimum (Min.), maximum (Max.), mean and standard deviation (Std.) of surge, heave and pitch motions. For the cases $\Delta t = 0.5$ sec and $\Delta t = 0.05$ sec considering LQR control, the difference is around (16.0222 - 9.2451) / 16.02222 = 42.3% for the Std. of surge motion. It is much greater than 0.5% due to the integration error, as discussed in Chapter III, 3.2. Therefore, this

estimation quantitatively indicates that $\Delta\tau$ does affect the construction of state-space model greatly, and this consequently results in different feedback forces, thus different controlling efficiencies.

In sum, the time step 0.05 sec or 0.1 sec is employed in the study, considering various factors, including the numerical accuracy and the desired controlling target.

Therefore, we can briefly summarize the above discussions as follows

- Mathematically the time step $\Delta\tau$ to compute the IRFs does affect the construction of state-space model greatly, as has been indicated in equation (2.73).
- The optimal LQR method shows its robustness for various time steps. For example, for the same weighting factors $(Q, R) = (1,1)$, a wide range of time steps can be chosen to achieve the goal of motion mitigation.
- Thus small time steps can ensure enough numerical accuracy in the simulation, however, a large time step may save more computation time while achieving the goal of motion mitigation if using the LQR controller.

However, the assumptions in this example should be realized as well as the limitations

- Phase lag for the DP system has not been considered, in other words, the DP system is assumed to provide an instantaneous feedback force to the spar.
- It's further assumed that the thrusters can produce the optimized force calculated by LQR controller to counteract the wave forces, and such forces are usually at the same level of the 1st order wave loads.

- Since the LQR method calculates the feedback forces for all the 6-DOF motions, however, the actual DP system can only provide the horizontal forces at most.

Therefore, the DP system employed in the two-body floating system in Chapter IV is assumed to provide horizontal counteracting forces in only x- and y- directions, in order to make the simulation of DP system closer to the real application.

3.5 Various Weighting Factors $(\boldsymbol{Q}, \boldsymbol{R})$ for the LQR Controller

In fact, the LQR algorithm takes care of the tedious work done by the control systems designer in optimizing the controller. However, the designer still needs to specify the weighting factors and compare the results with the specified design goals. Often this means that controller synthesis will still be an iterative process where the system designer judges the produced "optimal" controllers through simulation and then adjusts the weighting factors to get a controller more in line with the specified design goals. In fact, the LQR algorithm is, at its core, just an automated way of finding an appropriate state-feedback controller, i.e., the weighting factors (Q, R).

In all the above cases, we simply set $(Q, R) = (1, 1)$. In order to study the influence of weighting factors on the motion mitigation, we change the value of Q only while maintaining $R = 1$ for the case $\Delta\tau = \Delta t = 0.05\,\text{sec}$. Figure 3.11 shows the robustness of the LQR method.

In order to compare the efficiency of motion mitigation corresponding to the different (Q, R), define the reduction ratio as

$$R_r = \frac{x_{No\ Control} - x_{LQR\ Control}}{x_{No\ Control}} \tag{3.11}$$

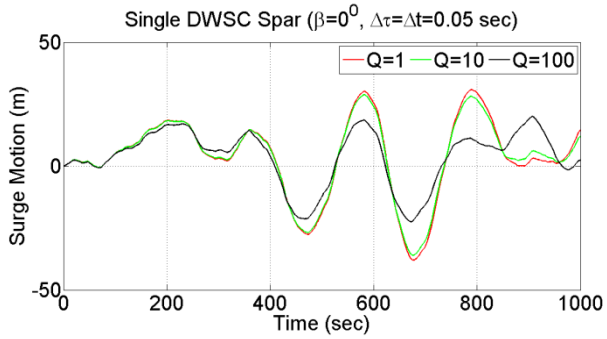

(a)

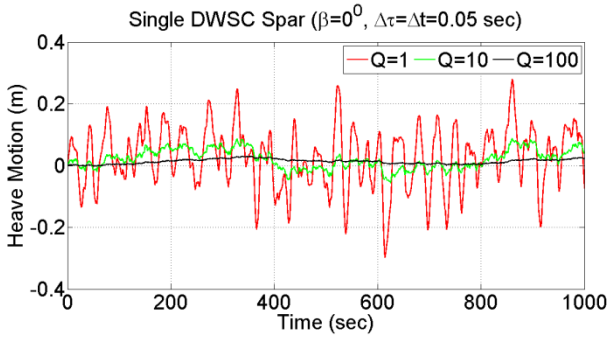

(b)

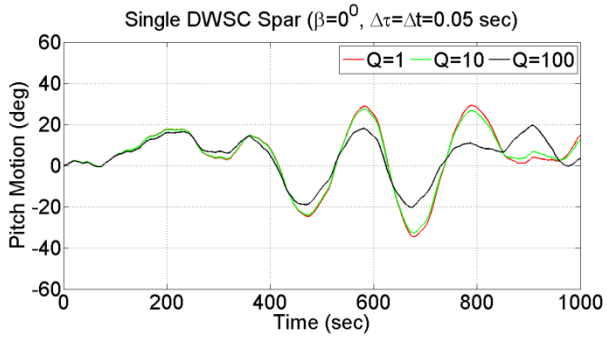

(c)

Figure 3.11 Motion RAOs of the single spar ($\beta = 0^0$). a - surge, b - sway, c - heave.

Table 3.5 Mitigation of motion responses for various weighting factors (Q, R)

(Q, R)		Min.	Max.	Mean	Std.
Surge (m)	(1,1)	-37.9770	30.8953	3.511	16.0222
	(10,1)	-36.0192	28.8501	3.580	15.2341
	(100,1)	-22.5044	20.0646	3.7527	11.1307
Heave (m)	(1,1)	-0.2972	0.2795	0.0235	0.0979
	(10,1)	-0.0562	0.0884	0.0207	0.0314
	(100,1)	-0.0022	0.0301	0.0131	0.0077
Pitch (deg)	(1,1)	-34.515	29.31825	4.004975	14.87971
	(10,1)	-32.7323	27.6702	4.0383	14.1502
	(100,1)	-20.2837	19.6110	4.1394	10.3524

It is obvious that considerable motion mitigation may be achieved for all these various weighting factors (Q, R) if comparing the statistics of each motion listed in Table 3.4 and Table 3.5.

Further, we calculate the reduction ratios defined in equation (3.11), as given in Table 3.6. There are greater than 50% mitigation for all the three motions if Q is within the range of (1,100) while R is 1.

As the weighting factor Q increases while keeping R unchanged, the anticipated feedback forces from the LQR method increase accordingly. We can also understand this result in a simple but more intuitive way. If we increase Q only, the state vector x must be relatively smaller if we hope to keep the term $x^T Q x$ unchanged, assuming that the

integral term - $\int_{t_0}^{T_0}[x^T Qx + u^T Ru]dt$ keeps the same. However, in reality, a smaller state vector requires the larger feedback force provided by the thrusters. Similarly, if we keep Q unchanged, a smaller R means the greater motion mitigation, however, this requires larger thruster forces.

Table 3.6 Comparison of reduction ratios R_r for various weighting factors (Q, R)

(Q, R)		R_r			
		Min.	Max.	Mean	Std.
Surge	(1,1)	67.84%	16.65%	116.12%	67.48%
	(10,1)	69.50%	22.17%	116.44%	69.08%
	(100,1)	80.94%	45.87%	117.23%	77.41%
Heave	(1,1)	80.78%	83.43%	23.95%	84.18%
	(10,1)	96.37%	94.76%	33.01%	94.92%
	(100,1)	99.86%	98.22%	57.61%	98.76%
Pitch	(1,1)	71.99%	70.61%	67.99%	72.49%
	(10,1)	73.44%	72.26%	67.73%	73.84%
	(100,1)	83.54%	80.34%	66.92%	80.86%

CHAPTER IV

EXAMPLE II: A TWO-BODY FLOATING SYSTEM

4.1 Frequency-domain Results

Figure 4.1 shows a schematic view of both the sea base - USNS Bob Hope and the DWSC spar, with a gap *d* between them. Moreover, the origin of the global coordinate system is set at the center of the spar and the corresponding wave heading is defined as shown in Figure 4.1. In this chapter, the gap *d* is 1 m, 3 m and 7 m, respectively. It should be noted that the Bob Hope is much bigger than the spar in size.

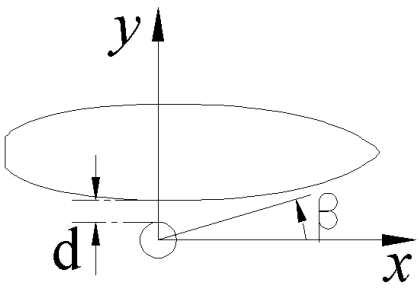

Figure 4.1 Relative positions of the ship and the spar

The BVP problem of this two-body floating system can be solved using WAMIT software. The added mass and radiation damping coefficents can be assembled in 12 × 12 matrix using the developed postprocessing tool, as shown in Appendix D. Moreover, the nondimensional definitions of the body motions in WAMIT (2008) are

$$\bar{\xi}_i = \frac{\xi_i}{A/L^n} \tag{4.1}$$

where $n = 0$ for $i, j = 1,2,3$; $n = 1$ for $j = 4,5,6$.The rotational motions (ξ_4, ξ_5, ξ_6) are measured in radians. In this example, take $L = 1$ m.

For the general purpose, the 6-DOF motion RAOs of spar, corresponding to the wave headings $45°$ and $315°$, are plotted and compared. Figure 4.2 corresponds to surge, sway, heave, roll, pitch and yaw motion of this spar, respectively, when the wave heading is $45°$. Figure 4.3 correspond to surge, sway, heave, roll, pitch and yaw motion of this spar, respectively, when the wave heading is $315°$.

It is observed that there are obvious shielding effects for the surge, sway and pitch motions for the spar. For example, for the surge motion at $\beta = 45^0$, the RAOs of spar in multiple body system are above those for the single spar, especially when the wave frequency is within 0.6 - 1.0 rad/sec. However, the RAOs of surge motion in the two-body system are below those for the single spar within the same wave frequency range. This is because the bigger-size Bob Hope can protect the smaller spar from the incoming wave. A similar conclusion can be found in McTaggart (2003).

On the other hand, the heave RAOs does not change too much with the wave heading, as indicated in Figures 4.2c and 4.3c. In the other words, this spar has a small heave motion at different sea conditions, mainly due to its small water plane area. This is also the reason why the crane is installed on the cylindrical spar to perform the cargo transfer at sea. In addition, the peak point of heave RAOs indicates that the resonant heave motion frequency is around 0.2 rad/sec, as agree well with the estimation of the natural heave period of this spar.

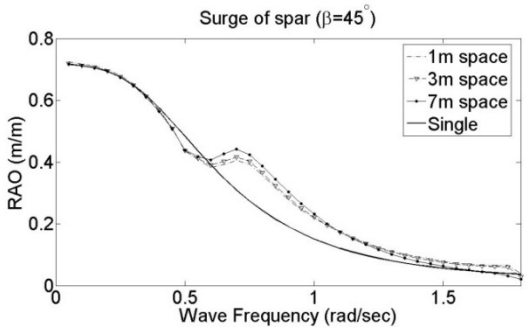

(a)

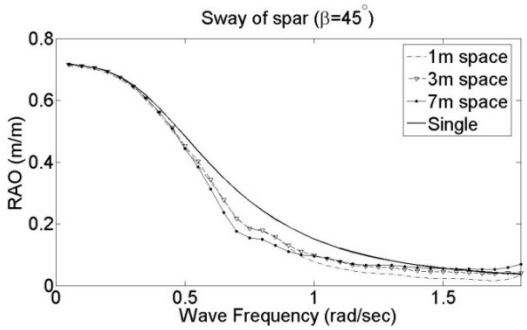

(b)

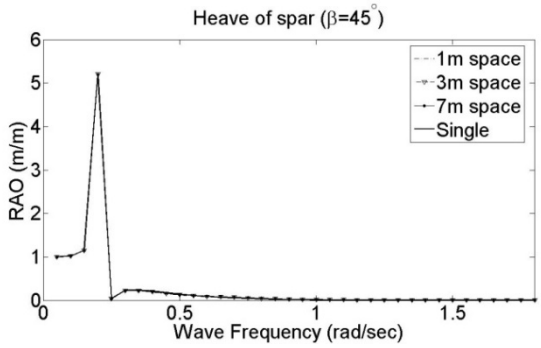

(c)

Figure 4.2 Motion RAOs of the spar in the two-body system ($\beta = 45^0$). a - surge, b - sway, c - heave.

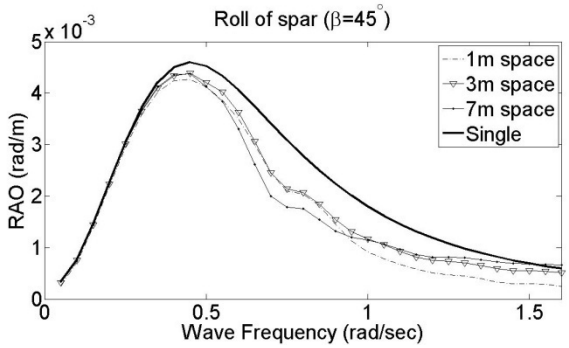

(d)

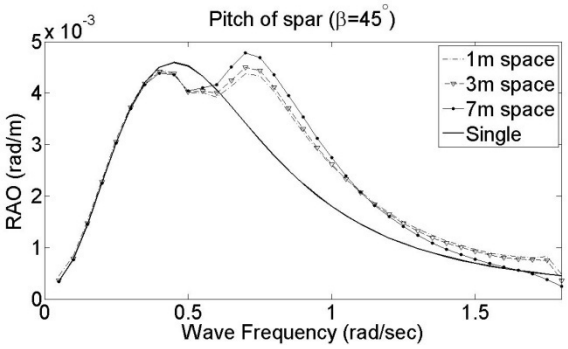

(e)

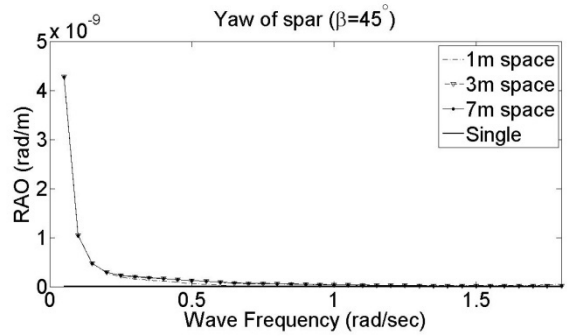

(f)

Figure 4.2 Continued. d - roll, e - pitch, f - yaw.

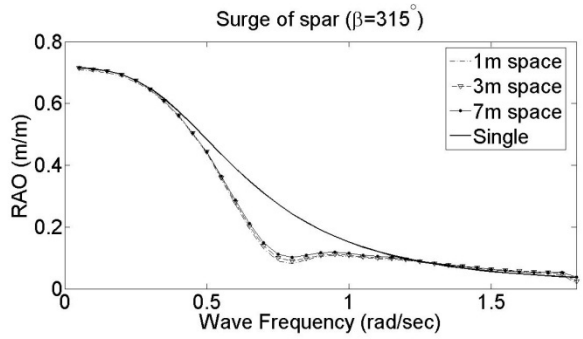

(a)

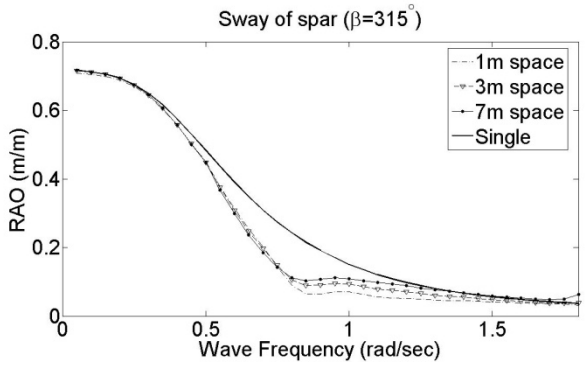

(b)

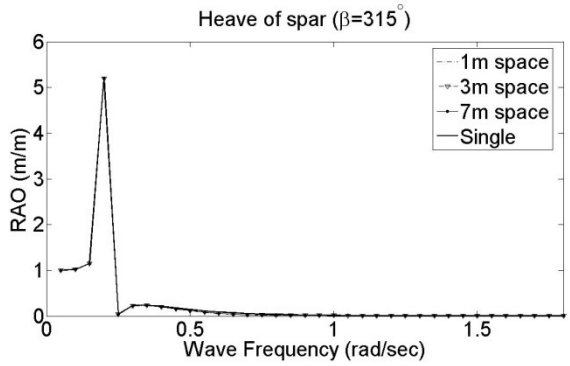

(c)

Figure 4.3 Motion RAOs of the spar in the two-body system ($\beta = 315^0$). a - surge, b - sway, c - heave.

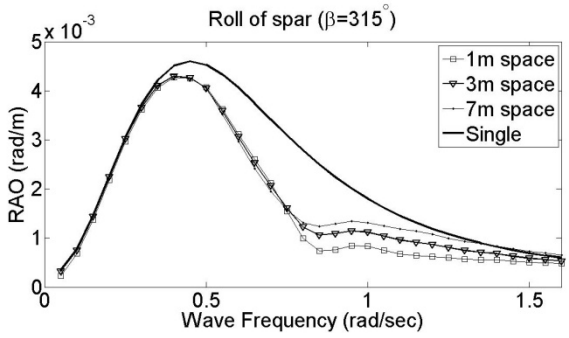

(d)

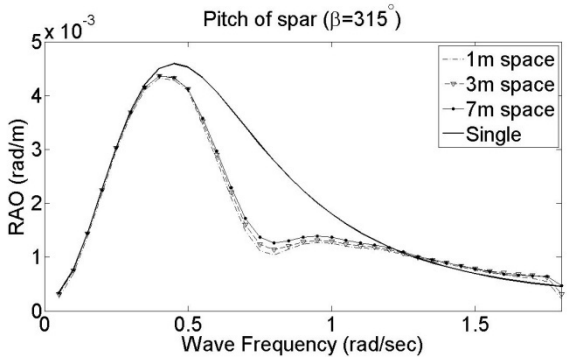

(e)

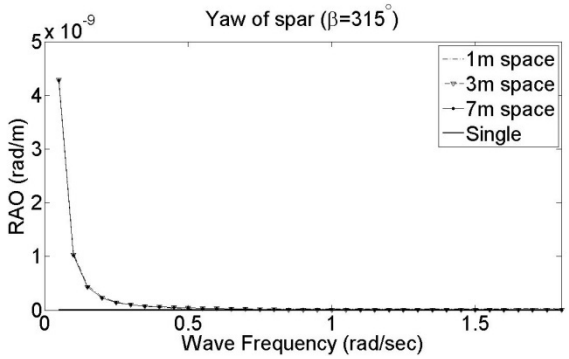

(f)

Figure 4.3 Continued. d - roll, e - pitch, f - yaw.

Further, Figure 4.4 shows the 6-DOF motion RAOs of Bob Hope when the wave heading is 45°.The difference between these RAOs when considering various spacing is so small and can be neglected. Similar observation is for the wave heading $\beta = 315°$, as indicated in Appendix B. This shows that the Bob Hope can provide a good station-keeping capability as the seabase.

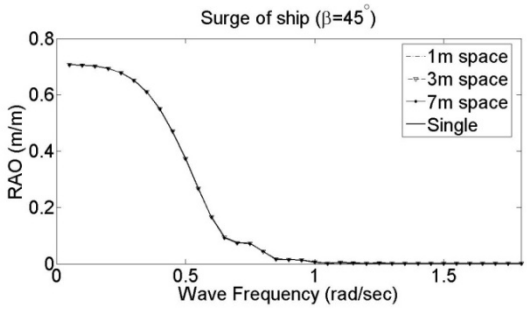

(a)

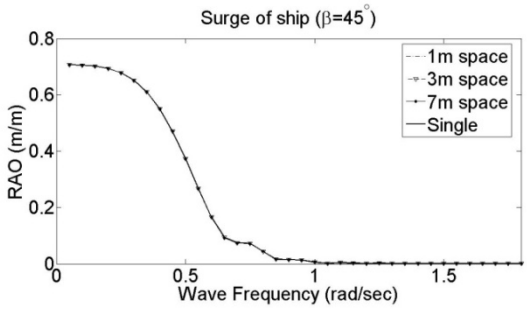

(b)

Figure 4.4 Motion RAOs of the ship in the two-body system ($\beta = 45^0$). a - surge, b - sway.

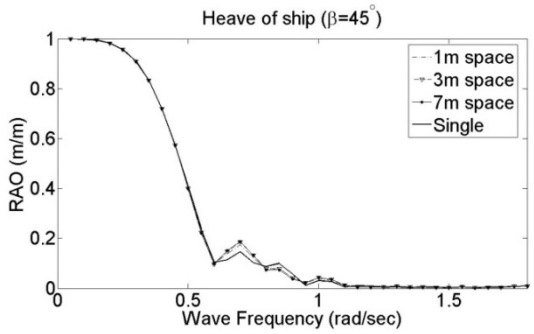

(c)

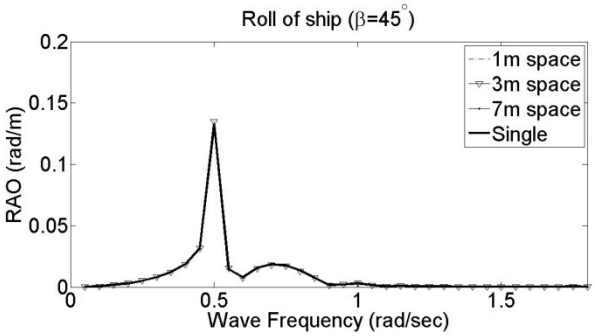

(d)

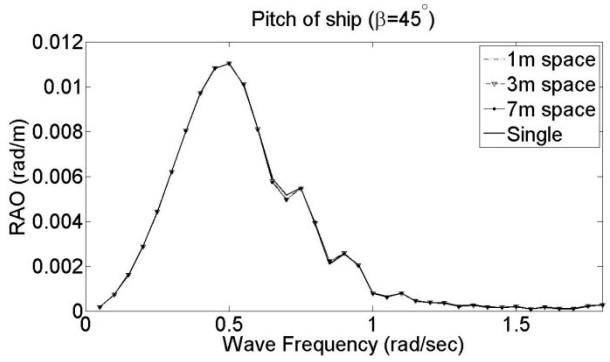

(e)

Figure 4.4 continued ($\beta = 45^0$). c - heave, d - roll, e - pitch.

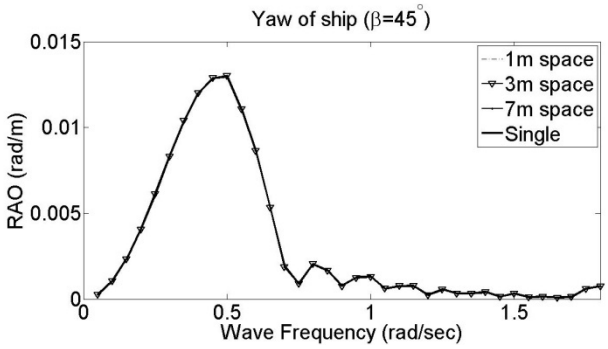

(f)

Figure 4.4 continued ($\beta = 45^0$). f - yaw.

4.2 IRFs of the Single Body and the Multibody System

As plotted in Figures 4.5 - 4.7, obvious oscillation can be observed for the IRFs of this multibody system. This is due to the fluid sloshing between the two bodies, in addition, the memory functions are also lightly damped (Lewandowski, 2008). Thus, the motions of both bodies due to initial values need more time to decay as compared to the single body.

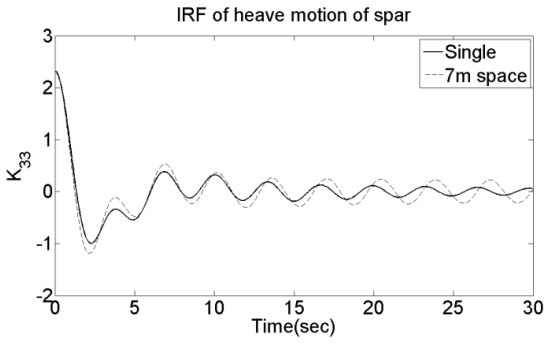

Figure 4.5 IRFs of heave of the spar

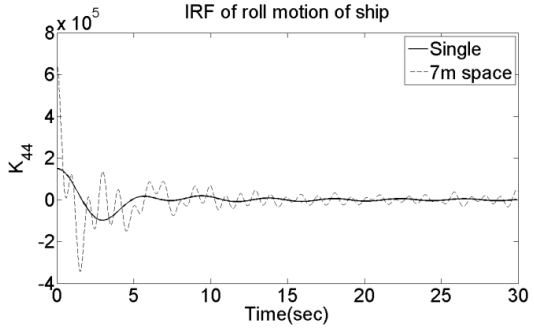

Figure 4.6 IRFs of roll of the ship

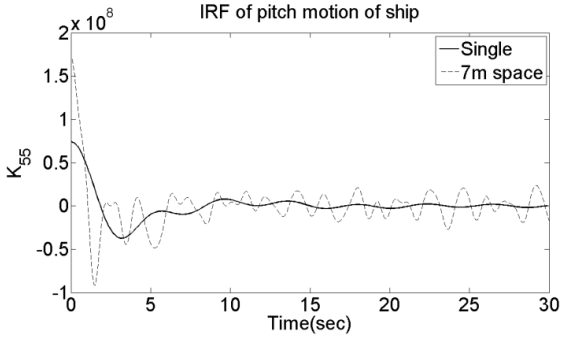

Figure 4.7 IRFs of pitch of the ship

4.3 Time-domain Responses in Regular Waves Based on the IRF Method

In the following sea ($\beta = 0^0$), the roll motion of this single spar is zero theoretically, however, there is an obvious roll motion in the multibody case due to the body-to-body hydrodynamic interaction, especially when the wave frequency is around 0.5 - 0.7 rad/sec, as indicated in Figure 4.8. Therefore, choose this wave frequency $\omega_0 = 0.7$ rad/sec with unit wave height. Then the equations (2.51) and (2.53) based on

IRF are solved to derive the time-domain responses of single body and multiple bodies in the regular wave ω_0. Figure 4.9 is the time-domain roll motion of this spar at this regular wave. It indicates that there is no roll motion for a single spar in the following sea. However, the steady-state amplitude of roll is about 0.002 rad (0.114°) in the multibody system due to the hydrodynamic interaction between the spar and the ship.

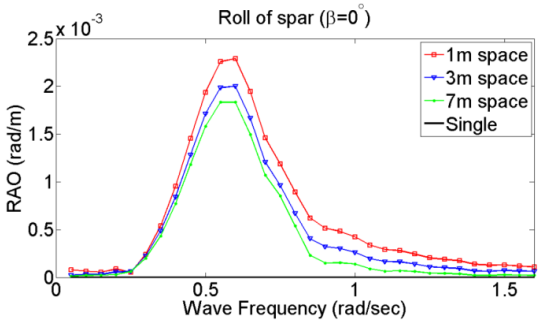

Figure 4.8 Roll RAOs of the spar considering different gaps

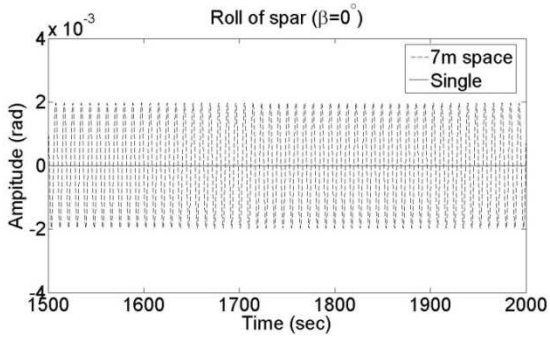

Figure 4.9 Time-domain roll motion of the spar at a regular wave

Further, the pitch RAOs of the spar considering different gaps are plotted in Figure 4.10, and the corresponding time-domain responses of this spar in the regular wave ω_0 are solved and then shown in Figure 4.11. The steady-state amplitude of pitch

in the 7m-space multibody system is about $0.0068\,\text{rad}\,(0.39^{\circ})$, smaller than $0.0105\,\text{rad}\,(0.60^{\circ})$ for the single-body case, as shown in Figure 4.11.

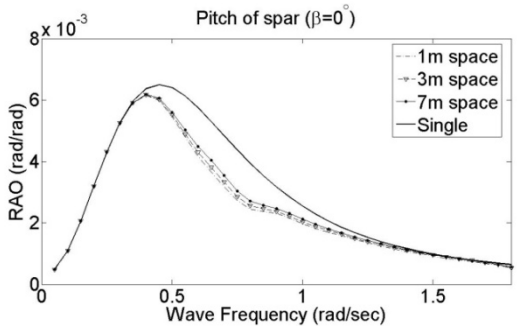

Figure 4.10 Pitch RAOs of the spar considering different gaps

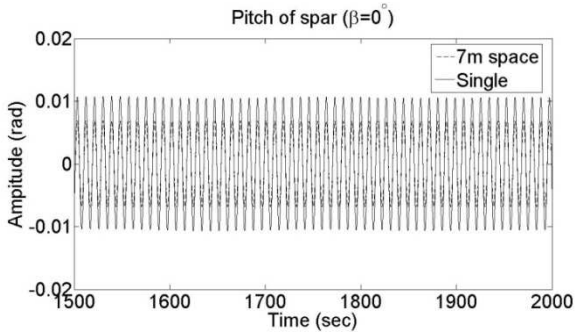

Figure 4.11 Time-domain pitch motion of the spar at a regular wave

4.4 Time-domain Responses in Random Seas

The time-domain responses of the spar in the two-body system in random SS4 are shown in Figure 4.12. Herein, a 7 m gap is assumed. Again the spar shows a very small amplitude response in the following sea, with the heave motion less than 0.3 m during a period of 5000 seconds. Moreover, obvious roll motions are caused by the

hydrodynamic interaction, with the maximum amplitude less than 5^0, the current criteria of ship-based cranes (Selfridge, 2005). The pitch motion of this spar seems a little large, and this may be due to the neglect of some factors, including the restoring effects in y-direction due to the catamaran ship at the free surface, the viscous damping, etc.

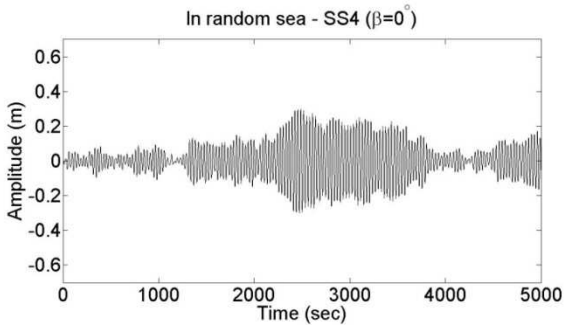

(a)

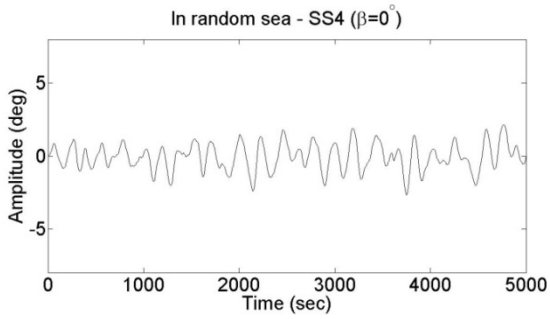

(b)

Figure 4.12 Time-domain simulation of motion responses of the spar in the two-body system at SS4. a - heave, b - roll.

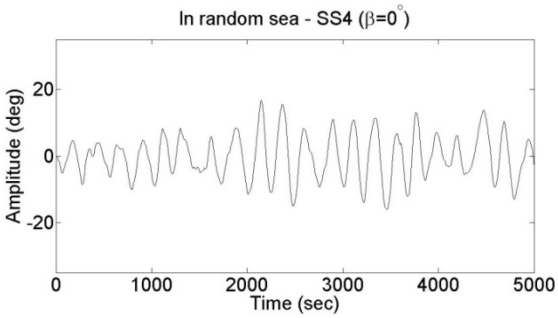

(c)

Figure 4.12 continued. c - pitch.

In order to verify the corresponding code, we can obtain the resonant heave frequency by picking up the summit after the Fast Fourier Transformation (FFT), as shown in Figure 4.13. It's around 0.205 rad/sec, as agree well with the result shown in Figure A.1c in Appendix A, 0.206 rad/sec.

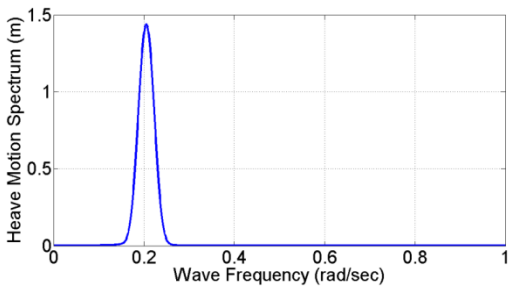

Figure 4.13 Heave spectrum of the spar

As to the ship, generally it has small heave, roll and pitch motions, as indicated in Figure 4.14. That is why it can be utilized as the base when transferring cargo at sea.

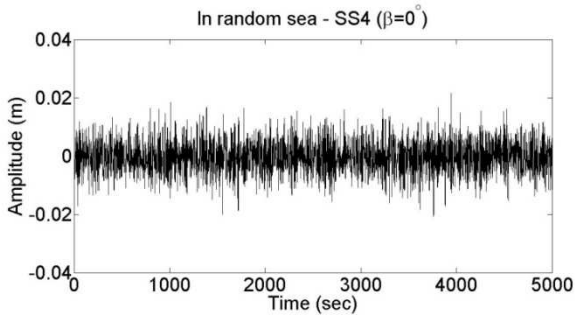

(a)

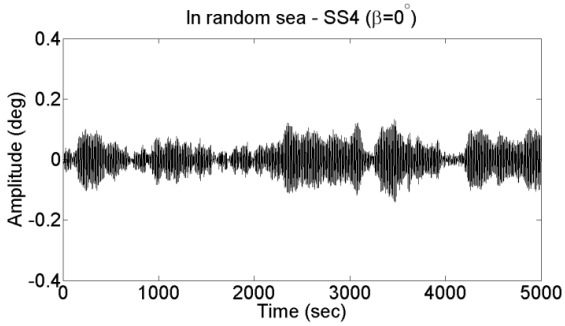

(b)

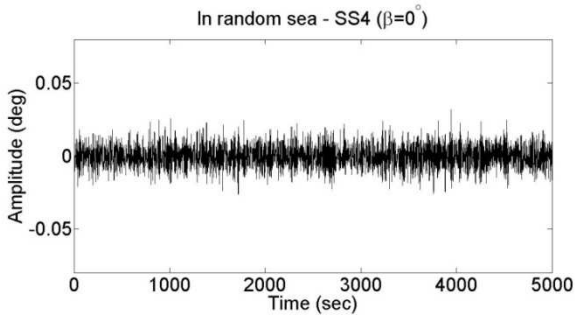

(c)

Figure 4.14 Time-domain simulation of motion responses of the ship in two-body system at SS4. a - heave, b - roll, c - pitch.

In a similar way, we can obtain the resonant roll frequency by picking up the summit after the FFT transformation, as shown in Figure 4.15. It's around 0.514 rad/sec, as is consistent with the result indicated in Figure B.1d in Appendix B.

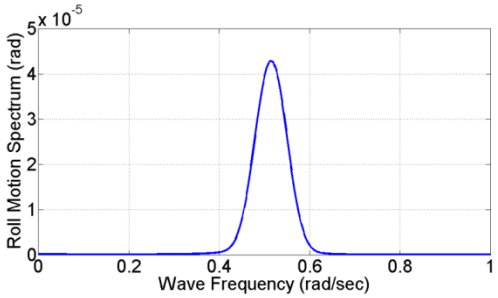

Figure 4.15 Roll spectrum of the ship

4.5 Effects of the Body-to-body Hydrodynamic Interaction Coefficients

The effects of the body-to-body hydrodynamic interaction coefficients on the time-domain responses are considered as follows:

- Not considering the body-to-body hydrodynamic interactions - i.e., the Diagonal Matrix Method (DMM).
- Considering all the hydrodynamic interactions - i.e., the Full Matrix Method (FMM).
- Define the difference ratio $\Delta D_r = (\mathrm{FMM} - \mathrm{DMM}) / \mathrm{FMM}$.
- Take quarter sea ($\beta = 45^0$), for the general purpose.

Table 4.1 Effects of the body-to-body hydrodynamic interaction on the motion responses ($\beta = 45^0$)

Motion	Method	Spar		Ship	
		Std.	ΔD_r	Std.	ΔD_r
Heave (m)	DMM	0.1038	0.0%	0.0053	0.0%
	FMM	0.1038		0.0053	
Roll (deg)	DMM	0.9394	0.25%	0.0418	-1.46%
	FMM	0.9418		0.0412	
Pitch (deg)	DMM	6.0546	0.26%	0.0006	0.0%
	FMM	6.0694		0.0006	
Surge (m)	DMM	67.5432	1.56%	5.0185	-37.28%
	FMM	68.6095		3.6557	
Sway (m)	DMM	14.6033	-0.51%	1.9516	16.71%
	FMM	14.5291		2.3431	
Yaw (deg)	DMM	5.41×10^{-6}	66.91%	0.3126	22.55%
	FMM	1.64×10^{-5}		0.4036	

As indicated in Table 4.1, the body-to-body hydrodynamic interactions have greater effects on the horizontal motions of both the spar and the ship, mainly because there are no hydrostatic restoring coefficients in these modes. Moreover, the difference ratios for the surge, way and yaw motion of the ship are all greater than 15%.

Further, we compare the time-domain series of yaw motion of the ship using FMM and DMM, as given in Figure 4.16. There is a considerable difference between the two ways to estimate the time-domain responses. However, in the side-by-side offshore operations, such discrepancy may result in potential dangers. Therefore, the body-to-body hydrodynamic interactions coefficients should be considered in the time-domain simulations of multiples bodies in close proximity.

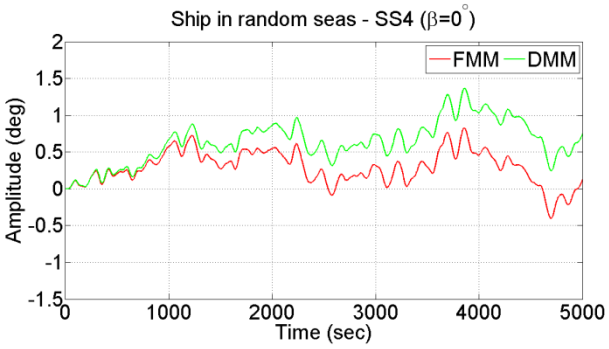

Figure 4.16 Time-domain yaw motion of the ship based on FMM and DMM at SS4

4.6 Mean Drift Force of the Two-body System

Figure 4.17 shows the QTF curves of both the spar and the ship. Newman's approximation is used to create the time series of mean drift force, which is plotted together with 1st order wave loads, as shown in Figure 4.18. The slow drift force is approximately 1% - 10% of the 1st order wave loads.

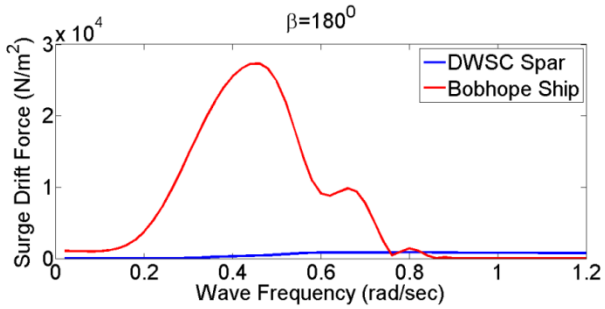

(a)

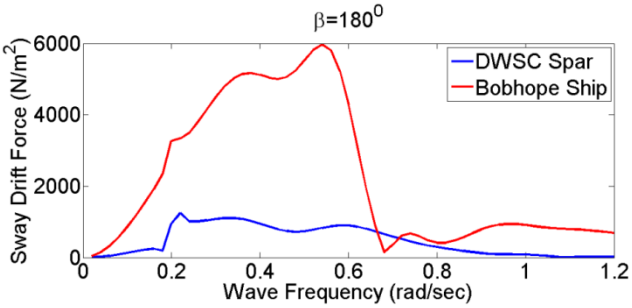

(b)

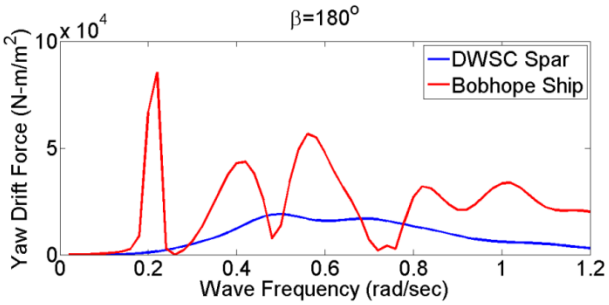

(c)

Figure 4.17 Force and moment QTFs of the two bodies at the heading sea. a - surge, b - sway, c - yaw.

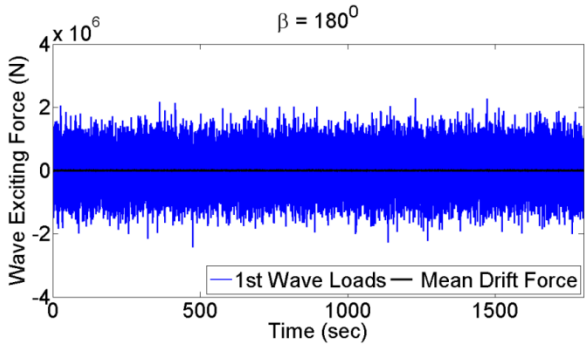

Figure 4.18 Time series of 1st-order wave loads and mean drift force

4.7 No Control vs. Optimal LQR Control

The LQR method is utilized in this example. It can provide the spar with an appropriate feedback force to counteract the other external forces and moments. However, we need to assume that the DP system can ideally produce such optimized forces. It is easy to simulate the DP system using the state-space model. It is especially convenient to incorporate various modern controllers and different controlling parameters can be adjusted in the simulation.

In this example, the weighting parameters (Q, R) are $(1,1)$, the simulation time-step is 0.05 sec, and we assume that the DP system can only provide the horizontal feedback force in the x- and y- directions, and this is different from the motion control of the single spar in Chapter III. As indicated in equations (2.110) and (2.111), the feedback forces for the two-body system are the 24×1 state vectors, as expressed in equation (2.69). Herein, $N = 2$, and this 24×1 state vector consists two parts: one is the 12×1 displacement vector of the two bodies, and the other one is the 12×1 velocity

vector. In addition, as shown in equation (2.95), the minimization of index I is based on the absolute responses of each body in this example, instead of the relative motions.

It should be noted that the state-space modeling of a two-body system requires a 24×24 matrix to represent the internal system, so more computation time is needed for such models with a high dimension. In addition, the calculation of the gain function k using the LQR method also becomes more time-consuming.

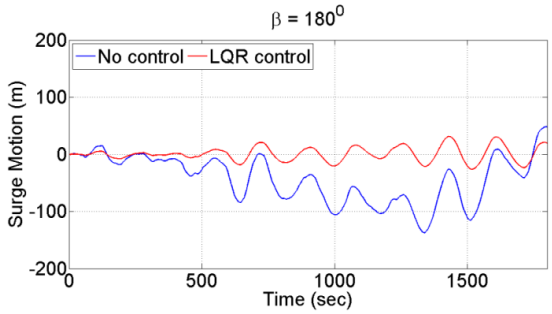

(a)

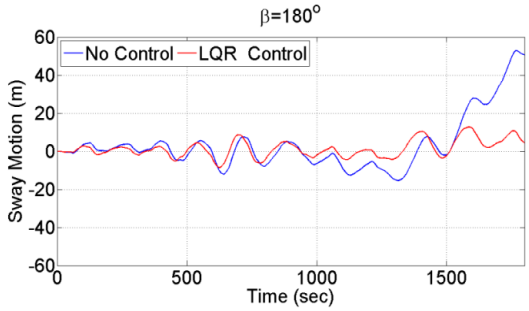

(b)

Figure 4.19 Motion responses of the spar at the heading sea (SS4) - No control vs. LQR control. a - surge, b - sway.

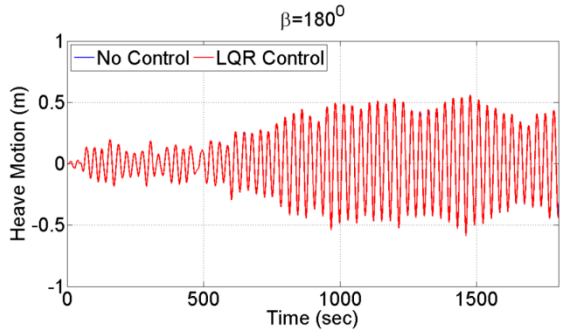

(c)

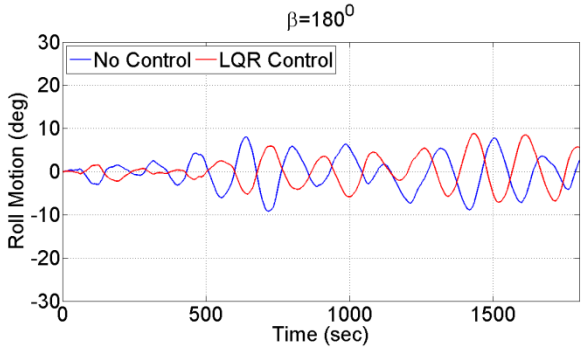

(d)

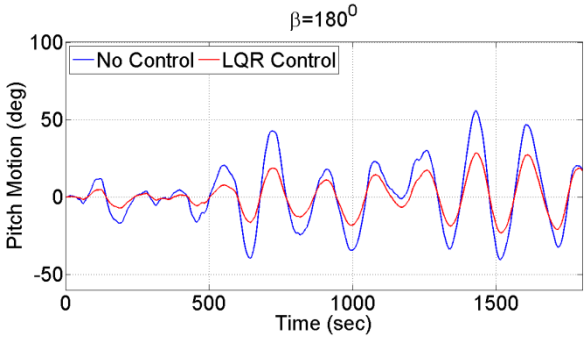

(e)

Figure 4.19 continued. c - heave, d - roll, e - pitch.

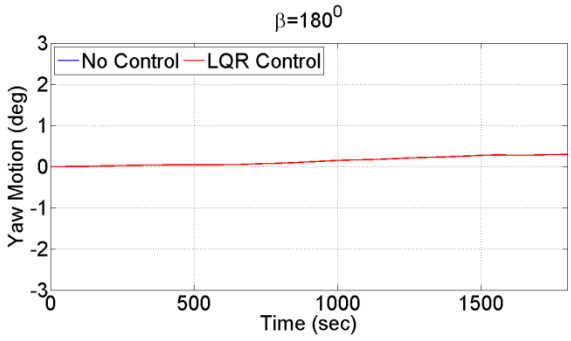

(f)

Figure 4.19 continued. f - yaw.

As shown in Figures 4.19a - 4.19b, the surge and sway motions of the spar can be mitigated to a considerable degree by assuming the DP system can produce optimized horizontal thruster forces in both the x- and y- directions. However, the thruster forces almost do not affect the heave motion of the spar, as indicated in Figure 4.19c.

The FFT is used to obtain the response spectra and plot them in Figures 4.20a - 4.20f. The summit in Figure 4.20c shows again that the natural frequency is around 0.206 rad/sec. Figures 4.20c - 4.20d indicate that the resonance roll and pitch frequency is around 0.04909 rad/sec, close to the natural frequency 0.0422 rad/sec. In accordance to the time-domain responses, this DP system can reduce the energy distribution of the surge and sway motions, as indicated in Figures 4.20a - 4.20b. Moreover, this DP system can also help to reduce the energy distribution of the roll and pitch motions as indicated in Figures 4.20d - 4.20e, because the thruster forces exerted at the origin of the global coordinate system can result in the restoring roll and pitch moments. In this case, these moments can help to reduce the roll and pitch in the time-domain. Figure 4.20c shows

almost no difference for the heave motion between the two cases, as is also consistent with the time-domain response given in Figure 4.19c.

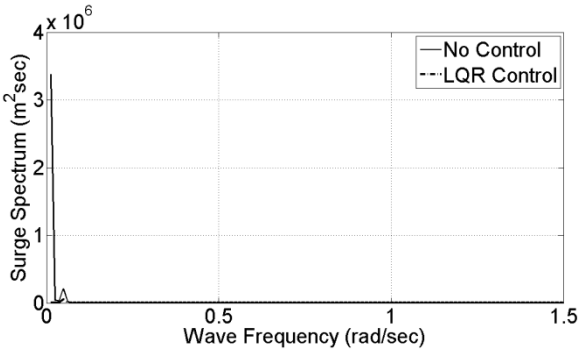

(a)

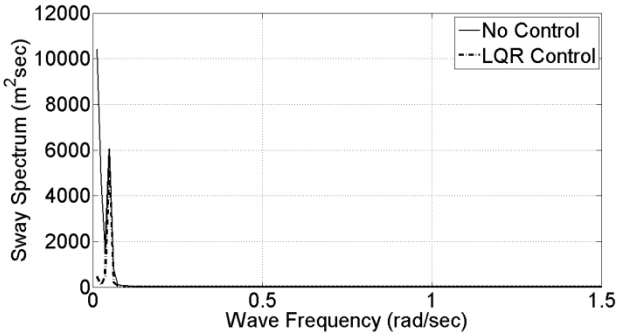

(b)

Figure 4.20 Motion responses spectrum of the spar at the heading sea (SS4) - No control vs. LQR control. a - surge, b - sway.

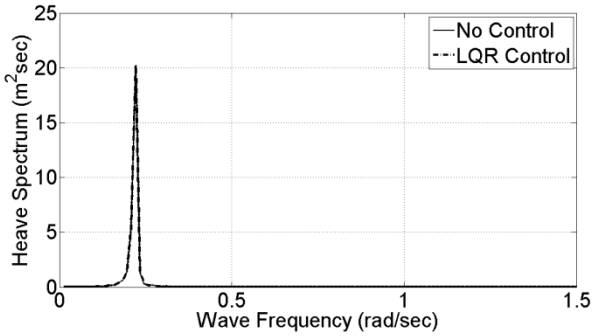

(c)

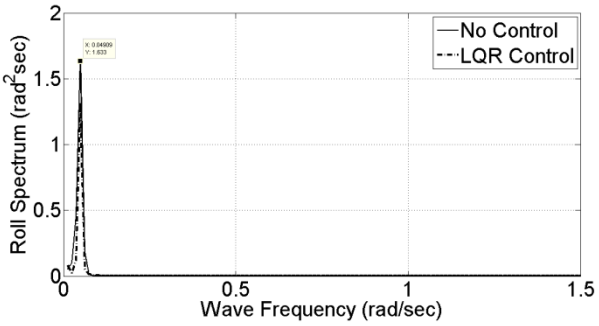

(d)

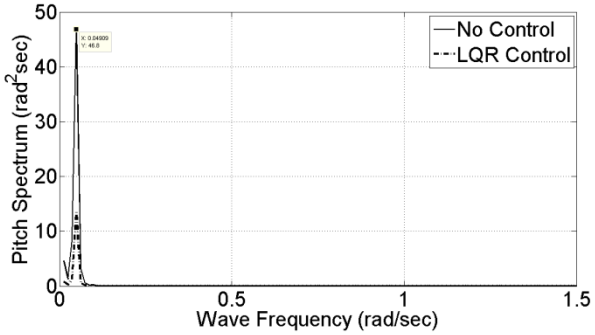

(e)

Figure 4.20 continued. c - heave, d - roll, e - pitch.

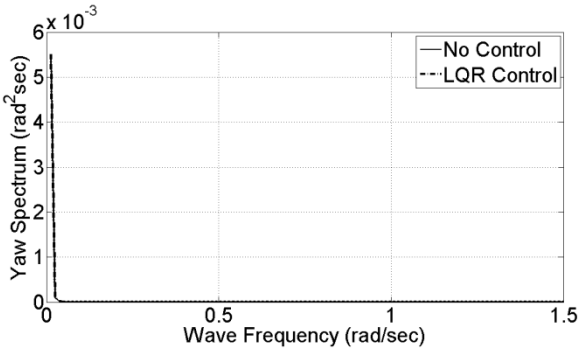

(f)

Figure 4.20 continued. f - yaw.

Finally, the time-domain simulations of the heave of spar and the roll of ship are transformed into motion spectra, and then they are further divided by the corresponding wave spectrum. The square root of the quotient is the corresponding RAO value. Thus the RAOs derived from the simulations are compared with the results from WAMIT. As shown in Figure 4.21, the heave resonance frequency of the spar from the simulation result is close to the result from WAMIT, around 0.20 rad/sec. Moreover, the roll motion RAO of the ship derived from the simulation is roughly consistent with the RAO from WAMIT, as indicated in Figure 4.22.

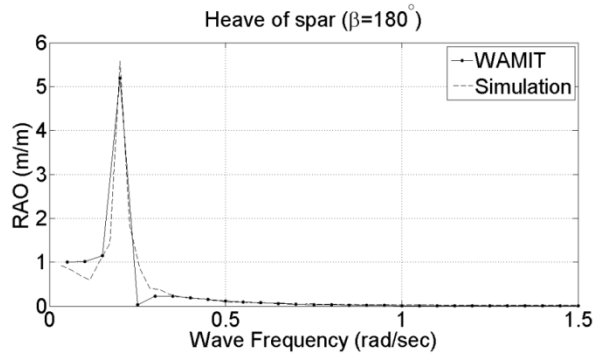

Figure 4.21 Comparison of the heave RAO of spar from WAMIT and the simulation

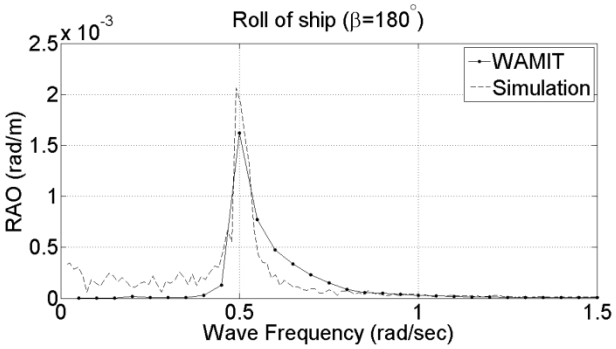

Figure 4.22 Comparison of the roll RAO of ship from WAMIT and the simulation

CHAPTER V

EXAMPLE III: A THREE-BODY FLOATING SYSTEM

5.1 Principal Characteristics of the T-craft

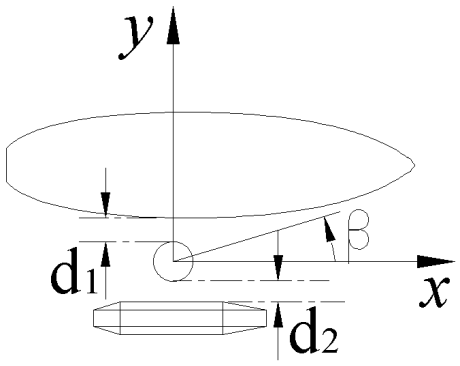

Figure 5.1 Arrangement of the three-body floating system

Figure 5.1 shows the relative positions of the three bodies, and they are the Bob Hope, the spar and the T-craft, from the top to the bottom. The gap between the ship and spar is defined as d_1, and it is 3 m in this example. The gap between the spar and the T-craft is d_2, and it is assumed to be 1 m, 3 m and 5 m. The grid of this T-craft is plotted in Figure 5.2, totally 914 panels, and herein the air cushion effect is not considered. The principal characteristics of this T-craft are given in Table 5.1.

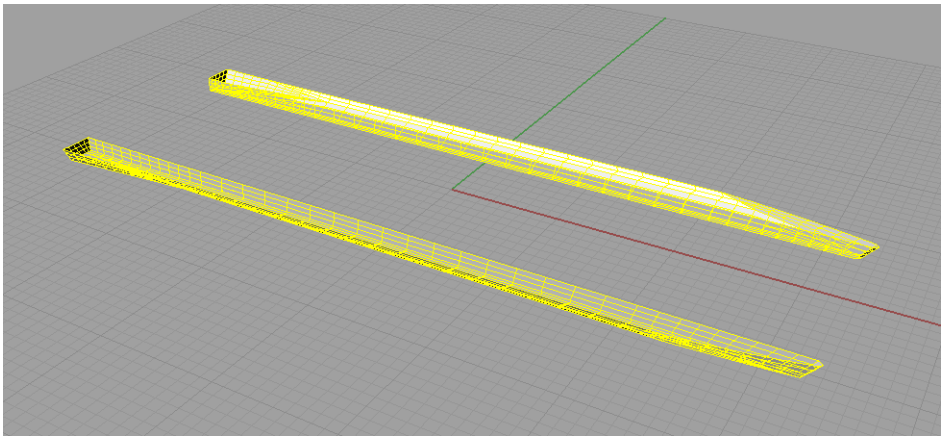

Figure 5.2 Panel model for the T-craft

Table 5.1 Principal characteristics of the T-craft

Length between perpendiculars, L_{pp}	76.35 m
Breadth molded on waterline, B	21.73 m
Draught, T	1.366 m
Displacement volume molded, ∇	1529.86 m^3

5.2 RAOs of the T-craft

WAMIT is used to solve the three-body BVP problem as shown in Figure 5.1, and then postprocess the obtained hydrodynamic coefficients to output the corresponding added mass, radiation damping and IRFs in the 18×18 matrix. The RAOs of the single T-craft and those for the three-body floating system are plotted in the same figure for comparison.

In the cargo transfer operations, the crane that is located on the spar transfers the cargo from the Bob Hope to the T-craft. When the wave heading is 45^0, the T-craft is exposed directly to the disturbance from the ocean waves, resulting in a relatively larger RAO if compared with the single T-craft, as shown in Figures 5.3a - 5.3f. Similarly, when the wave heading is 315^0, the Bob Hope protects the T-craft from the excitation of the ocean waves, resulting in smaller amplitude RAOs, as shown in Figures 5.4a - 5.4f.

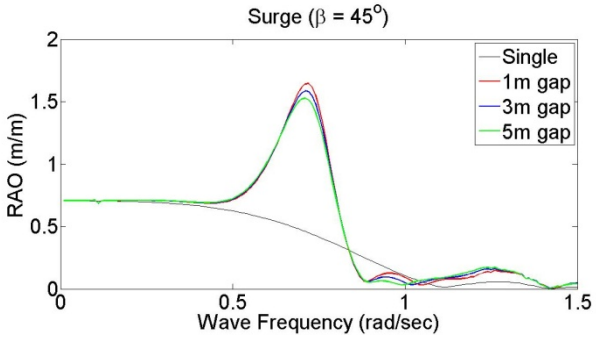

(a)

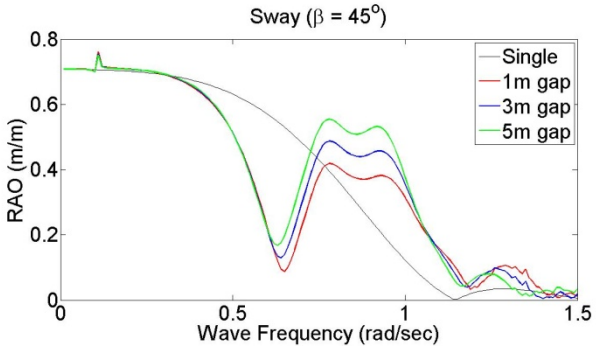

(b)

Figure 5.3 Motion RAOs of the T-craft ($\beta = 45^0$). a - surge, b - sway

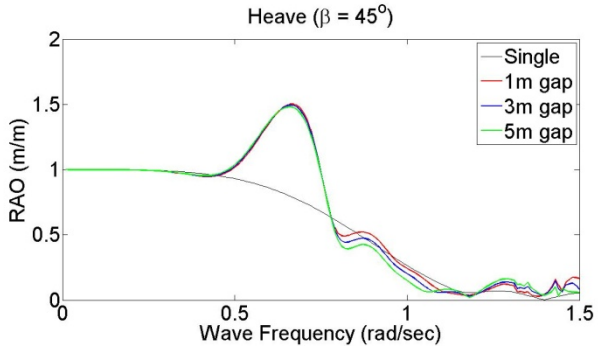

(c)

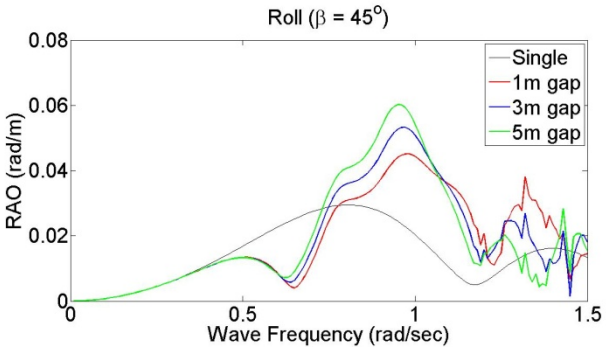

(d)

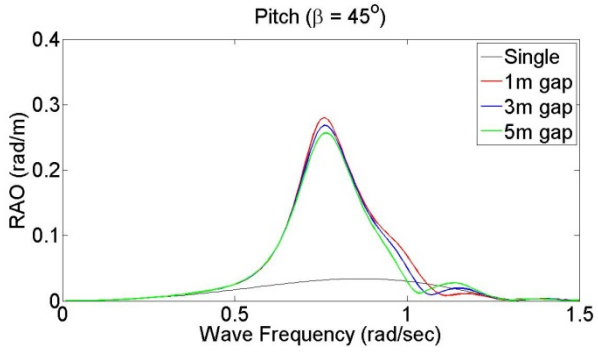

(e)

Figure 5.3 continued. c - heave, d - roll, e - pitch.

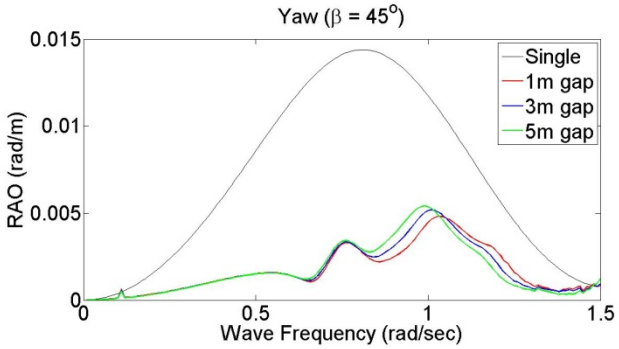

(f)

Figure 5.3 continued. f - yaw.

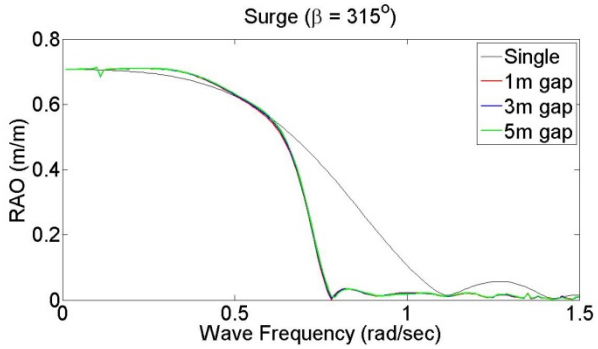

(a)

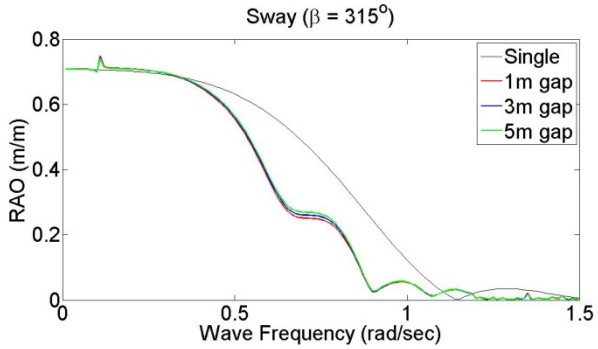

(b)

Figure 5.4 Motion RAOs of the T-craft ($\beta = 315^0$). a - surge, b - sway

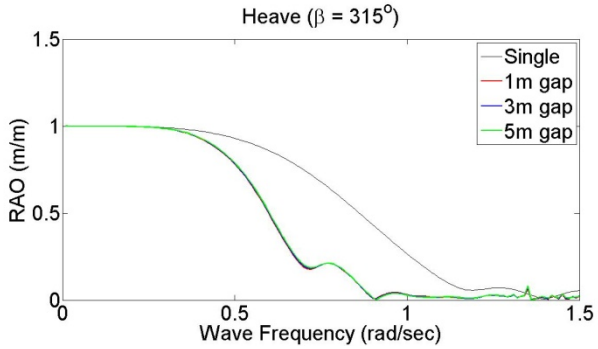

(c)

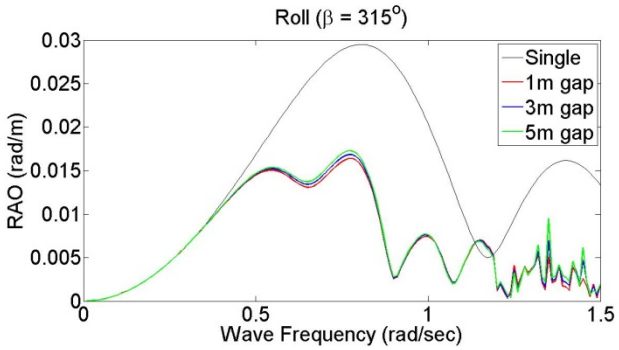

(d)

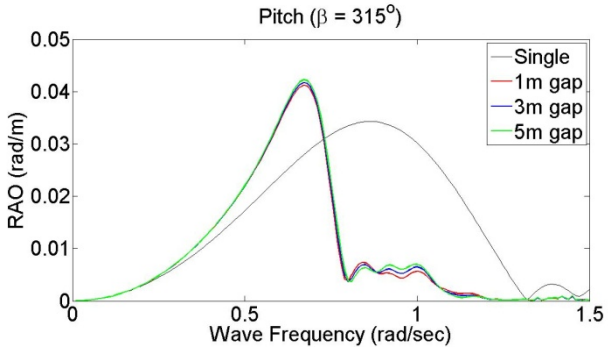

(e)

Figure 5.4 continued. c - heave, d - roll, e - pitch.

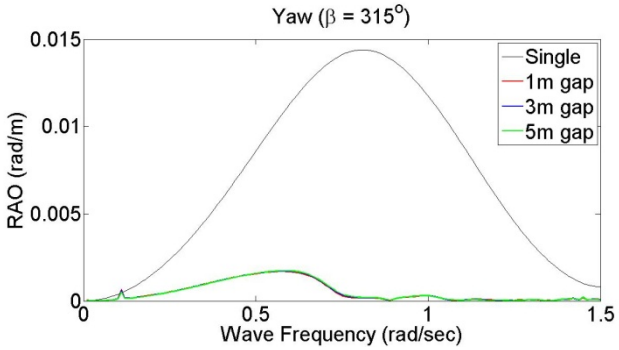

(f)

Figure 5.4 continued. f - yaw.

5.3 Time-domain Responses of the Three-body Floating System

In this example, the simulation code for the two-body floating system is extended to the three-body case. All the 12 × 12 mass matrix, convolution terms and hydrostatic matrix for the two-body system are expanded to 18 × 18. Especially much more computation time is required to evaluate the 18 × 18 convolution terms. However, it is easy to output the relative motions between the three bodies after solving all the 18 × 1 state vectors.

After we have solved the time-domain responses of all the three bodies at each time step, it is easy to obtain the relative motions between them. Since the relative vertical motions between the three bodies are most concerned in the cargo transfer, Table 5.2 gives a comparison of absolute vertical motions and relative vertical motions. In fact, the relative motions are critically important in the safety evaluations of offshore

operations. It is obvious that the relative motion $x_3 - x_{15}$ is smaller than $x_3 - x_9$. This is most probably because the displacement of the T-craft is much smaller than the Bob Hope.

Table 5.2 Statistics of vertical motions at SS4 during a 5000-sec simulation

	Min.	Max.	Std.
x_3 (m)	-0.1177	0.1163	0.0513
$x_3 - x_9$ (m)	-0.1438	0.1476	0.0528
$x_3 - x_{15}$ (m)	-0.1911	0.1802	0.0555

NOTE: x_3, x_9 and x_{15} are the heave motion of the spar, the Bob Hope and the T-craft, respectively.

Further, plot the relative vertical motions between the multiple bodies from 200-sec to 1200-sec, as shown in Figures 5.5 and 5.6. Since the heave period of the T-craft is very small, there appear many spikes for relative vertical motions.

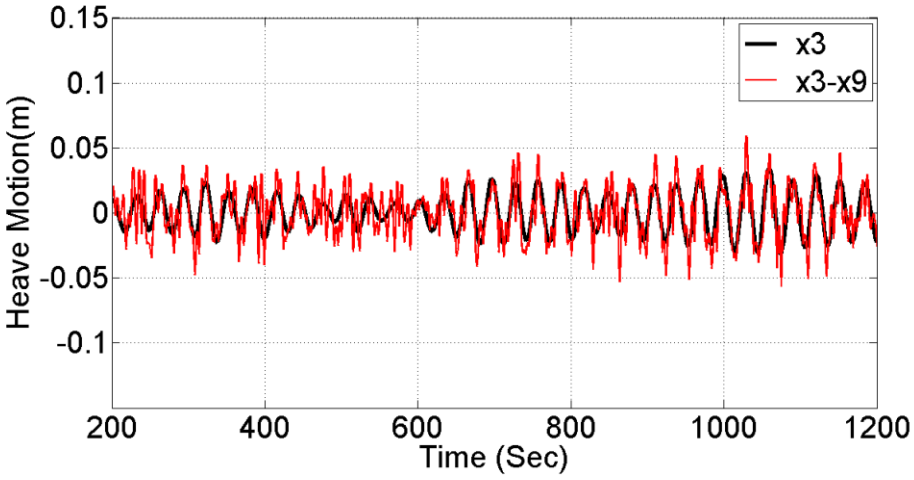

Figure 5.5 Relative vertical motions between the spar and the ship at the heading sea

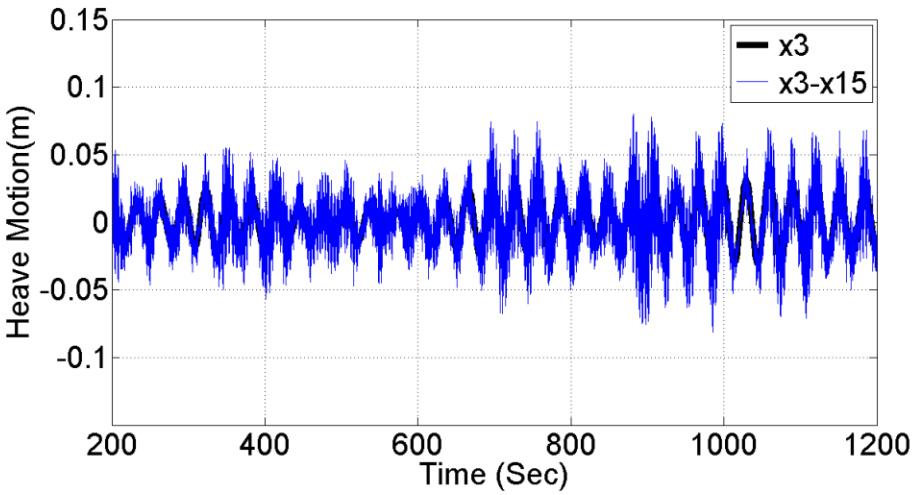

Figure 5.6 Relative vertical motions between the spar and the T-craft at the heading sea

It should be noted that the DP system has not been considered, and this part is very similar to the work for the two-body system in Chapter IV. However, it can be predicted that more computation time is needed to obtain the gain function k if using the optimal LQR controller, since the dimension of internal system A will be 36×36 and the input matrix B will be 36×1.

CHAPTER VI

CONCLUSIONS AND FUTURE WORK

In this study, a new numerical scheme to simulate time-domain motion responses of multibody floating systems has been successfully proposed, with hydrodynamic coefficients obtained from the hydrodynamic software - WAMIT by solving the BVP problem. The fourth-order Runge-Kutta method is employed. The way of transforming the EOM into the state-space model makes it possible and convenient to directly utilize the ODE45 solver of MATLAB. All the other nonlinear external forces can be conveniently included in the right hand side of the state-space model at each time step, including the thruster forces from DP system. The frequency- and time-domain results of multibody floating systems show:

- The large size ship affects the relative smaller spar more, from the comparison of RAOs in the frequency domain.
- The IRFs of the two-body system show more obvious oscillation than those of the single body, due to the fluid sloshing between the two bodies in close proximity and the light radiation damping.
- The body-to-body hydrodynamic coefficients have more effect on the horizontal motions that have no restoring terms, such as surge, sway and yaw.

The developed time-domain simulation tool based on this proposed scheme has been verified for the single body case and the two-body case. Finally, it is extended to the three-body case.

Since the EOMs of the multibody floating systems have been written in standard state-space format, thus it is easy to numerically simulate the DP system in MATLAB, for the purpose of simulating the motion response control in ship-to-ship operations. The memory effects have been considered while assembling the state-space models for the multibody floating system. Thus it can also be used as a new station-keeping model for the multibody floating system, with the fluid memory effects incorporated.

The modern LQR controller has been applied in the numerical simulation. It shows its robustness for the single body case for various time steps $\Delta\tau$ and Δt. In addition, the study of weighting factors (Q, R) on the effectiveness and controlling efficiency of motion mitigations also demonstrates LQR's robustness. It is further successfully applied to a two-body floating system considering the feedback forces only in x- and y-directions. In sum, the numerical study shows that the optimal LQR method can help to mitigate the motion responses of both single-body and two-body floating system at sea.

However, the LQR method requires the full-state measure and this is difficult to achieve in reality. In addition, though this numerical scheme can be used to perform time-domain simulations for the single body and two-body system, the calculation of feedback forces using LQR method requires too much computation time for the multiple-body case.

In sum, the proposed state-space modeling technologies can be used to simulate the dynamics of multiple floating bodies in close proximity, with the thruster forces considered as the feedback signal. As an approximate but efficient and effective way, it can be improved in several aspects. Firstly, how to calculate the second-order wave loads in a more accurate way is important to the design of a DP system. Secondly, the phase lag is ignored in the current simulations, thus how and when to command the thrusters is a critical issue. Thirdly, the incorporation of the DP system in the three-body system should be also an interesting but challenging work. Finally, some techniques to improve the computing speed and reduce the simulation time are also in the scope of future work, e.g., mode reduction of the proposed state-space models and the replacement of convolution terms.

REFERENCES

Aamo, O.M., Fossen, T.I., 1999. Controlling line tension in thruster assisted mooring systems. In: Proceedings of IEEE – International Conference on Control Application, HI, USA.

API Recommended Practice 2SK, 2005. Design and Analysis of Stationkeeping Systems for Floating Structures. American Petroleum Institute, Washington D.C., USA.

Balchen, J.N., Jenssen, N.A., Mathisen, E., Saelid, S., 1980. A dynamic positioning system based on Kalman filtering and optimal control. Modeling, Identification and Control 1(3), 135-163.

Bhattacharyya, S.P., Datta, A., Keel, L.H., 2009. Linear Control Theory - Structure, Robustness, and Optimization. CRC Press, Boca Raton, FL, USA.

Buncher, B., Van, Dijk A., Wilde J. de, 2001. Numerical multiple-body simulation of side-by-side mooring to an FPSO. In: Proceedings of the 21th International Offshore and Polar Engineering Conference – ISOPE2001, Stavanger, Norway.

Chakrabarti, S.K., 1987. Hydrodynamics of Offshore Structures. WIT Press, London, UK.

Chakrabarti, S.K., 2000. Hydrodynamic interaction forces on multi-moduled structures. Ocean Engineering 27, 1037-1063.

Chen, C.T., 1999. Linear System Theory and Design. Oxford University Press, New York, USA.

Chen X., 2002. Studies on Dynamic Interaction between Deep-water Floating Structures and Their Mooring/Tendon Systems. Ph.D. Dissertation, Texas A&M University, USA.

Chen, X.B., 2007. Middle-field formulation for the computation of wave-drift loads. Journal of Engineering Mechanics 59, 61-82.

Chen, X.B., Duan, W.Y., 2007. Formulation of low frequency QTF by $O(\Delta_\omega)$ approximation. In: Proceedings of the 22nd International Workshop on Water Waves and Floating Bodies (IWWWFB), Plitvice , Croatia.

Chen, X.B., Rezende, F., 2009. Efficient computations of second-order low-frequency wave loads. In: Proceedings of 28th International Conference on Offshore Mechanics and Arctic Engineering - OMAE2009, Honolulu, USA.

Cummins, W.E., 1962. The impulse response function and ship motions. Schiffstechnik, 101-109.

Driscoll, F.R., Venezia, A., Alsenas, G., Galvan, F., Radanovic, B., Selfridge, M., 2006. A scale model rapidly deployable stable craneship for seabased cargo transfer. In: Proceedings of the 16th International Offshore and Polar Engineering Conference – ISOPE 2006, San Francisco, California, USA.

El-Hawary, F., Raton, B., 2000. The Ocean Engineering Handbook. CRC Press, Boca Raton, FL, USA.

Faltinsen, O.M., 1990. Sea Loads on Ships and Offshore Structures. Cambridge University Press, UK.

Faÿ, H., 1990. Dynamic Positioning Systems: Principles, Design and Applications. Technip, Paris, France.

Greenhow, M., 1986. High- and low-frequency asymptotic consequences of the Kramers-Kronig relations, Journal of Engineering Mechanics 20, 293-306.

Grimble, M.J., Patton, R.J., 1980. The design of dynamic ship positioning control systems using stochastic optimal control theory. Optimal Control Application & Methods 1, 167-202.

Grimble, M.J., Sen, A.F.I.M.A., Patton, R.J., Wise, D.A., 1980. Use of Kalman filtering techniques in dynamic ship-positioning systems. In: Proceedings of IEEE 127(3), 93-102.

Hong, S.Y., Kim, J.H., Cho,S.K., Kim. Y.S., 2005. Numerical and experimental study on hydrodynamic interaction of side-by-side moored multiple vessels. Ocean Engineering 32, 783-801.

Hughes, G., Harris R., Quadvlieg, I.F., Hawallmann I.R. 2009. Close-in precision DP using wave feed forward: STLVAST phase 2 & 3. In: Proceedings of Dynamic Positioning Conference, Houston, USA.

Hughes, G., Quadvlieg, I.F., Hawallmann I.R. 2010. DP advances in the USN seabase: STLVAST sea trial and completion. In: Proceedings of Dynamic Positioning Conference, Houston, USA.

Jacobsen, K., Clauss, G.F., 2006. Time-domain simulations of multi-body systems in deterministic wave trains. In: Proceedings of the 25th International Conference on Offshore and Arctic Engineering - OMAE2006, Hamburg, Germany.

Kaasen, K.E., 1999. An improvement to Newman's method for approximate calculation of slow-drift wave force eliminating the high frequency noise. In: Proceedings of the 18th International Conference on Offshore and Arctic Engineering - OMAE1999, St. John's, Newfoundland, Canada.

Kagemoto, H., Yue, D.K.P., 1986. Interactions among multiple three-dimensional bodies in water waves: an exact algebraic method. Journal of Fluid Mechanics 166, 189-209.

Kashiwagi, M., Endo, K., Yamaguchi, H., 2005. Wave drift forces and moments on two ships arranged side by side in waves. Ocean Engineering 32, 529-555.

Kim, C.H. 2008. Nonlinear Waves and Offshore Structures. World Scientific Publishing Co. Pte. Ltd., Singapore.

Kim, Y.B., 2003.Dynamic Analysis of Multiple-body Floating Platforms Coupled with Mooring Lines and Risers, Ph.D. Dissertation, Texas A&M University, USA.

Koo, B. J., Kim, M. H., 2005. Hydrodynamic interactions and relative motions of two floating platforms with mooring lines in side-by-side offloading operation. Applied Ocean Research 27, 292-310.

Kristansen, E., Egeland, O., 2003. Frequency dependent added mass in models for controller design for wave motion ship damping. In: Proceedings of 6th IFAC Conference on Maneuvering and Control of Marine Craft MCMC'03, Girona, Spain.

Lee, C.H., 1995. WAMIT Theory Manual, Department of Ocean Engineering, MIT, Boston, USA.

Levine, W.S., 2000. Control System Fundamentals. CRC Press, Boca Raton, FL, USA.

Lewandowski, E.M., 2008. Multi-vessel seakeeping computations with linear potential theory. Ocean Engineering, 35, 1121-1131.

Liang, C.C., Cheng, W.H., 2004. The optimum control of thruster system for dynamically positioned vessels. Ocean Engineering, 31, 97-110.

Marikle S.P., 2009. Dynamic Positioning and Motion Mitigation of a Scaled Sea Basing, Master Thesis, Florida Atlantic University, FL, USA.

MARIN, 2010. Website: http://www.marin.nl/web/Issues/Mooring-offloading/sidebyside-offloading.htm.

McAllister, K.R., 1997. Mobile offshore bases – an overview of recent research, Journal of Marine Science and Technology, 2, 172-181.

McTaggart, K., Cumming, D., Hsiung C.C., Li, L., 2003. Seakeeping of two ships in close proximity. Ocean Engineering, 30, 1051-1063.

Mercier, S., 2009. Class notes for OCEN 676 – Dynamics of Offshore Structures, Texas A&M University, USA.

Moler, C., 2004. Numerical Computing with MATLAB. Website: http://www.mathworks.com/moler.

Naciri, M., Waals, O., Wilde, J.D., 2007. Time domain simulations of side-by-side moored vessels lessons learnt from a benchmark test. In: Proceedings of the 26th International Conference on Offshore Mechanics and Arctic Engineering - OMAE2007, San Diego, USA.

Newman, J.N., 1974. Second-order slowly-varying forces on vessels in irregular waves. In: Proceedings of the Symposium on the Dynamics of Marine Vehicles and Structures in Waves, London, UK.

Newman, J.N., 2001. Wave effects on multiple bodies. In: Proceedings of Hydrodynamics in Ship and Ocean Engineering, RIAM, Kyushu University, Japan.

Nienhuis, I.U., 1986. Simulations of low frequency motions of dynamically positioned offshore structures. Royal Institution of Naval Architects Transactions 129, 127-145.

Ogilvie, T., 1964. Recent progress towards the understanding and prediction of ship motions. In: Proceedings of 6th Symposium on Naval Hydrodynamics.

Ohkusu, M., 1969. On the Heaving Motion of Two Circular Cylinders on the Surface of a Fluid. Reports of Research Institute for Applied Mechanics, XVII, 58, 167-185.

OTRC, 2010. Website: http://otrc.tamu.edu/Current%20Projects/FSPOStatus.html

Pauw, W.H., Huijsmans, R.H.M., Voogt, A., 2007. Advances in the hydrodynamics of side-by-side moored vessels. In: Proceedings of the 27th International Conference on Offshore and Arctic Engineering - OMAE2007, San Diego, California, USA.

Perez, T., 2005. Ship Motion Control - Course Keeping and Roll Stabilization Using Rudder and Fins. Springer, London, UK.

Perez, T., Fossen, T.I., Sørensen, A.J., 2004. A Discussion about Seakeeping and Maneuvering Models for Surface Vessels. Technical report MSS-TR- 001,

Centre for Ships and Ocean Structures (CESOS), Norwegian University of Science and Technology NTNU, Trondheim, Norway.

PID Controller, 2011. Website: http://en.wikipedia.org/wiki/PID_controller.

Pinkster, J.A., 1980. Low Frequency Second Order Wave Excitation Forces on Floating Structures. Ph.D. Dissertation, Delft University, The Netherlands.

Press, W.H., Teukolsky, S.A., Vetterling, W.T., Flannery. B.P., 2001. Numerical Recipes in Fortran 77: The Art of Scientific Computing. Cambridge University Press, UK.

Ran, Z., 2000. Coupled Dynamic Analysis of Floating Structures in Waves and Currents. Ph.D. Dissertation, Texas A&M University, USA.

Ryu, S., Kim, M. H., 2003. Coupled dynamic analysis of thruster-assisted turret-moored FPSO. In: Proceedings of OCEANS 2003 MTS/IEEE, San Diego, California.

Saelid S., Jenssen, N.A., Balchen, J.B., 1983. Design of analysis of a dynamic positioning system based on Kalman filtering and optimal control. IEEE Transactions on Automatic Control AC-28(3), 331-339.

Selfridge, M., 2005. Spar Technology as a Seabasing Enabler.Center for Innovation in Ship Design / Naval Surface Warfare Center Carderock Division, West Bethesda, Maryland, USA.

Sørensen, A.J., Sagatun, S.I., Fossen, T.I., 1996. Design of a dynamic positioning system using model-based control. Control Engineering Practice, 4 (3), 359-368.

Srinvasan, N., Sen, D., 2002. Time-domain simulation of DP semisubmersibles in numerical wave-tank for large nonlinear random waves. Dynamic Positioning Conference, USA.

Strand, J.P., Sørensen, A.J., Ronæss, M., Fossen, T.F., 2001. In: The Ocean Engineering Handbook - Chapter 3. CRC Press, Boca Raton, FL.

Tannuri, E.A., Morishita, H.M., 2006. Experimental and numerical evaluation of a typical dynamic positioning system. Applied Ocean Research 28, 133-146.

WAMIT, 2008. WAMIT Inc., MA USA verstion 6.3.

Xiang, X., Miao, Q.-M., Chen, X.B. Kuang, X., 2007. Study on coupled motion response and relative motion between two side-by-side ships in Waves. In: Proceedings of the Asialink-EAMARNET International Conference on Ship Design, Production and Operation, Harbin Engineering University, Harbin, China.

Yamamoto, M., Morooka, C.K., 2005. Dynamic positioning system of semi-submersible platform using fuzzy control. Journal of Brazil Society of Mechanical Sciences and Engineering. XXVII(4), 449-455

Yu, X., Falzarano, J.M., 2011. Time-domain simulation of multibody floating systems based on state-space modeling technology. In: Proceedings of the 30th International Conference on Offshore Mechanics and Arctic Engineering - OMAE2011, Rotterdam, The Netherlands.

Yu, X., Falzarano, J.M., Su, Z., 2010a. Time-domain simulation of multibody floating systems in waves. In: Proceedings of the 29th International Conference on Offshore Mechanics and Arctic Engineering - OMAE2010, Shanghai, China.

Yu, X., Kang H., Huang, L., Xie, Y., Zhai, Q., Chen, G., 2011. Dynamic response control of a jacket platform using MR dampers based on an inverse dynamic model. In: Proceedings of the 21st International Offshore and Polar Engineering Conference – ISOPE 2011, Maui, USA.

Yu, X., Lakhotia, C., Falzarano, J.M., 2009. Development of a multibody vessel dynamics simulation tool. In: Proceedings of the 28th International Conference on Offshore Mechanics and Arctic Engineering - OMAE2009, HI, USA.

Yu, X., Ma, T., Falzarano, J.M., 2010b. Application of a new semi-active control strategy to dynamic response control of an offshore platform using MR dampers. In: Proceedings of the 29th International Conference on Offshore Mechanics and Arctic Engineering - OMAE2010, Shanghai, China.

APPENDIX A

RAOs of the Spar in the Two-body System

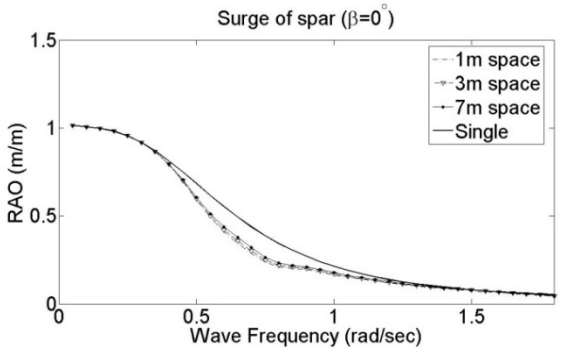

(a)

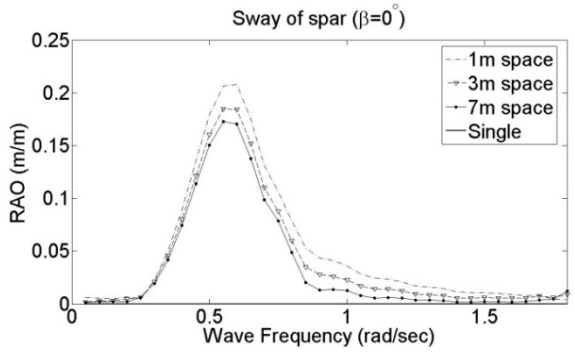

(b)

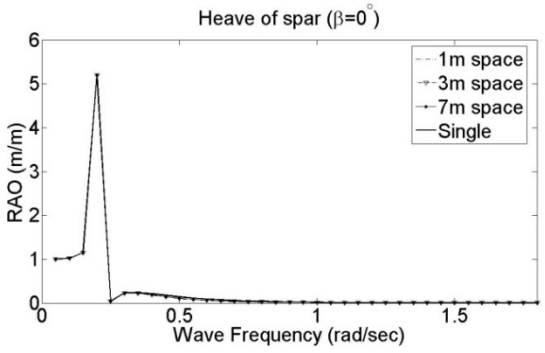

(c)

Figure A.1 Motion RAOs of the spar ($\beta = 0^0$). a - surge, b - sway, c - heave.

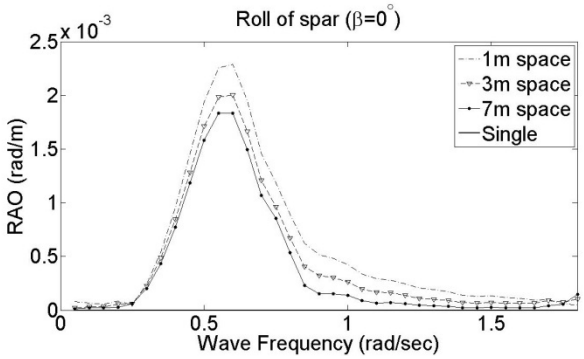

(d)

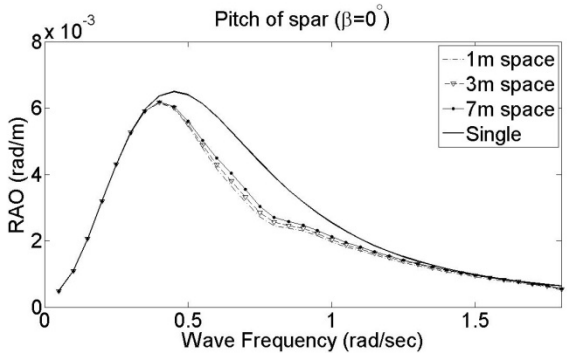

(e)

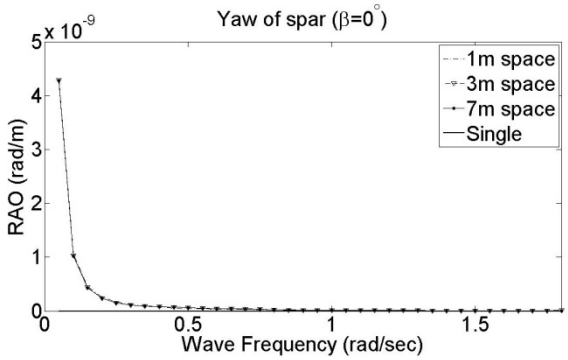

(f)

Figure A.1 continued. d - roll, e - pitch, f - yaw.

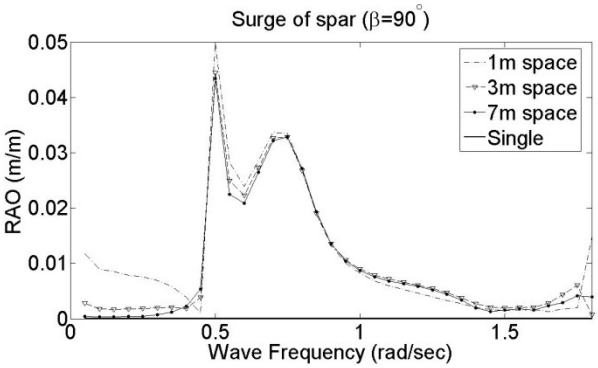

(a)

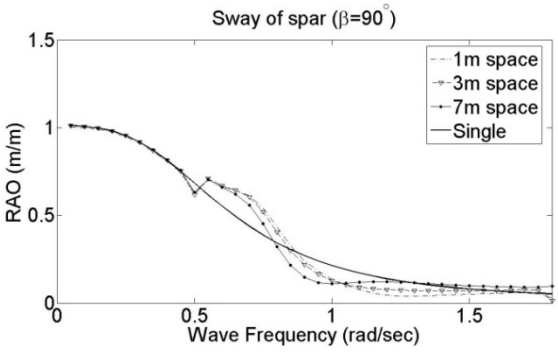

(b)

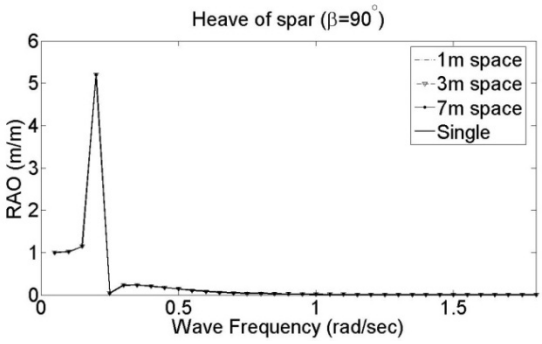

(c)

Figure A.2 Motion RAOs of the spar ($\beta = 90^0$). a - surge, b - sway, c - heave.

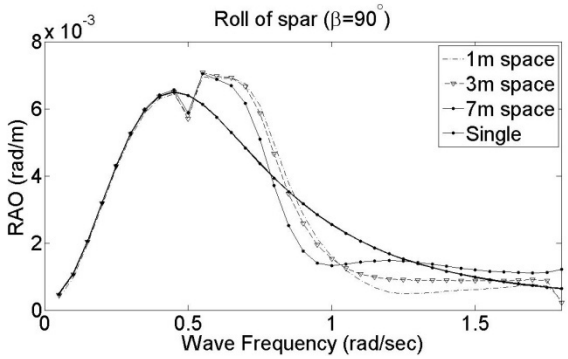

(d)

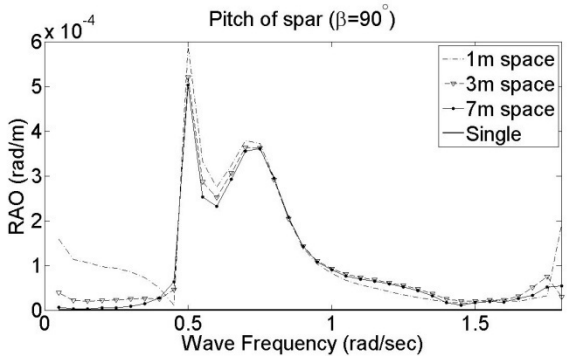

(e)

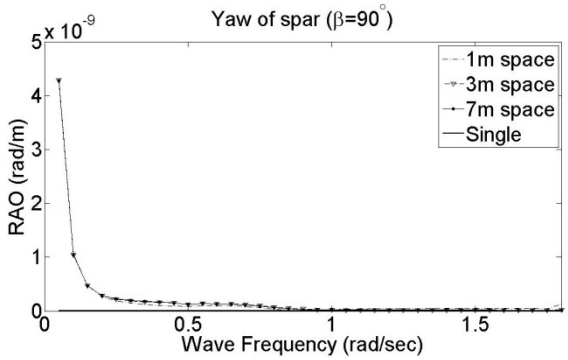

(f)

Figure A.2 continued. d - roll, e - pitch, f - yaw.

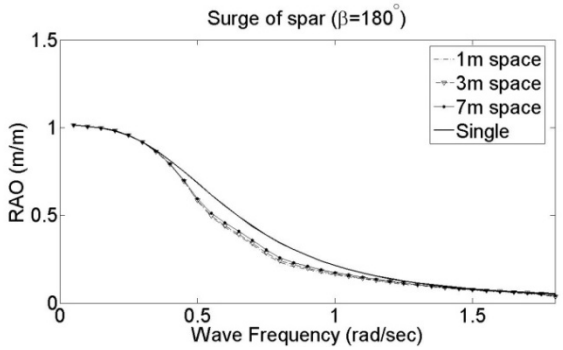

(a)

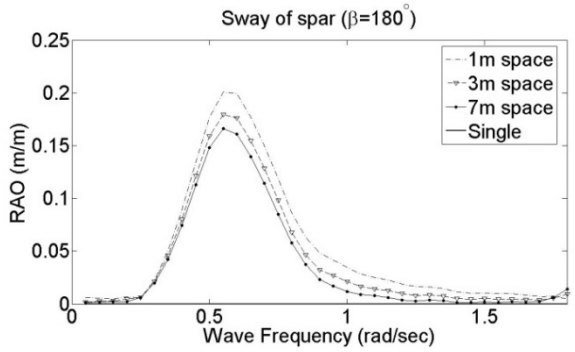

(b)

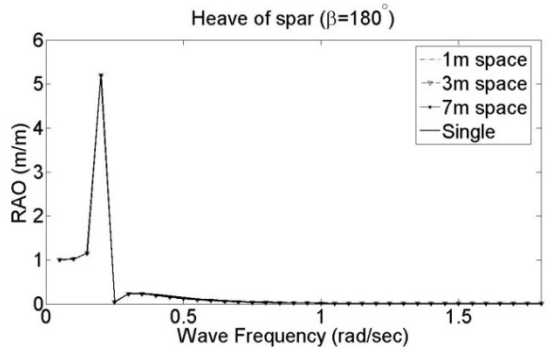

(c)

Figure A.3 Motion RAOs of the spar ($\beta = 180^0$). a - surge, b - sway, c - heave.

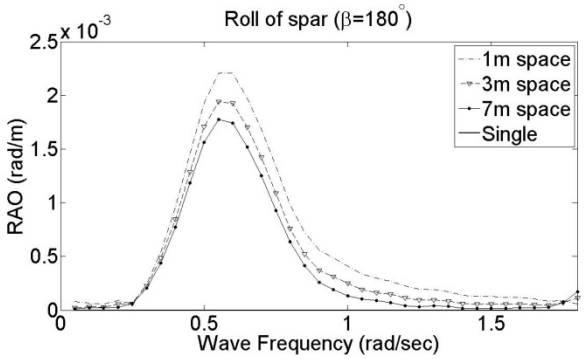

(d)

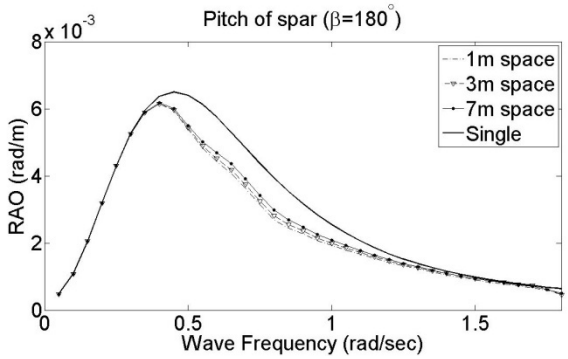

(e)

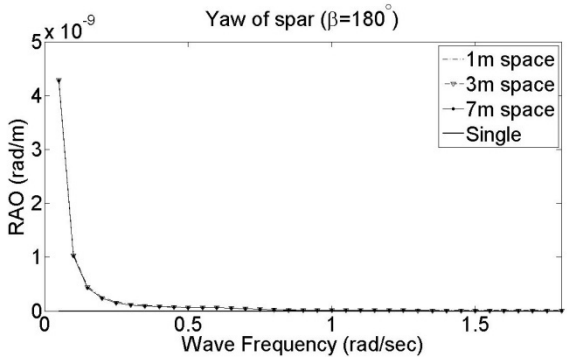

(f)

Figure A.3 continued. d - roll, e - pitch, f - yaw.

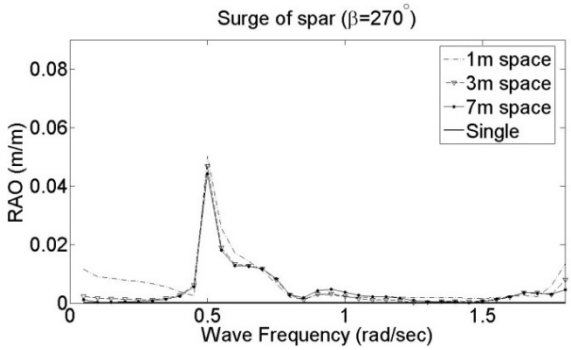

(a)

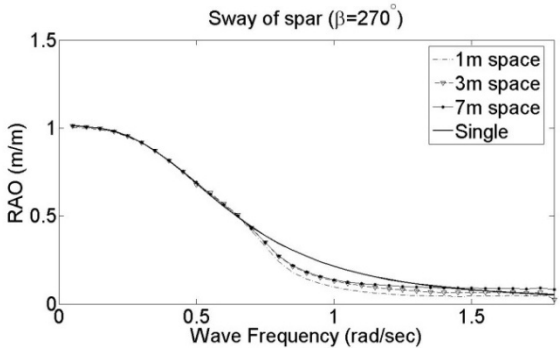

(b)

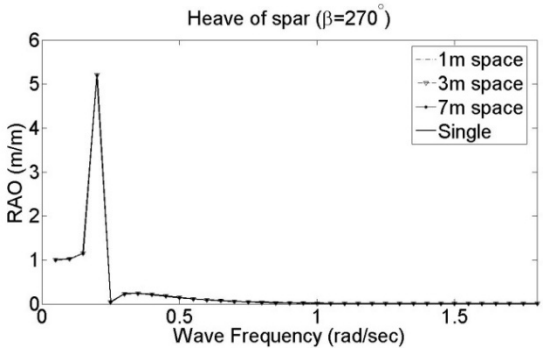

(c)

Figure A.4 Motion RAOs of the spar ($\beta = 270^0$). a - surge, b - sway, c - heave.

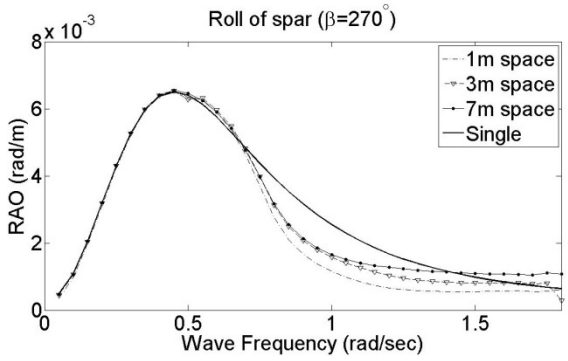

(d)

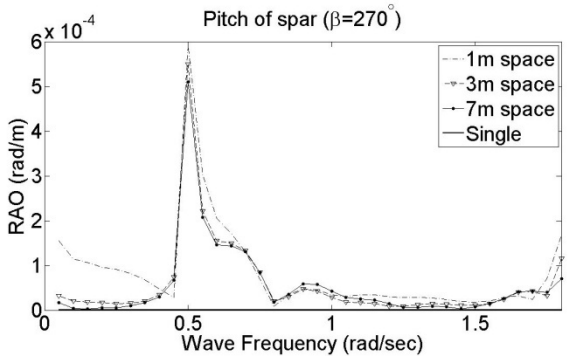

(e)

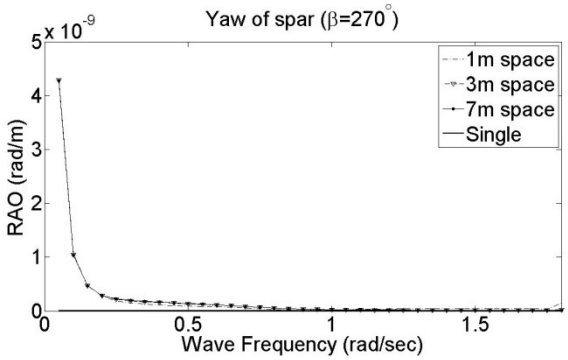

(f)

Figure A.4 continued. d – roll, e – pitch, f - yaw.

APPENDIX B

RAOs of the Bob Hope in the Two-body System

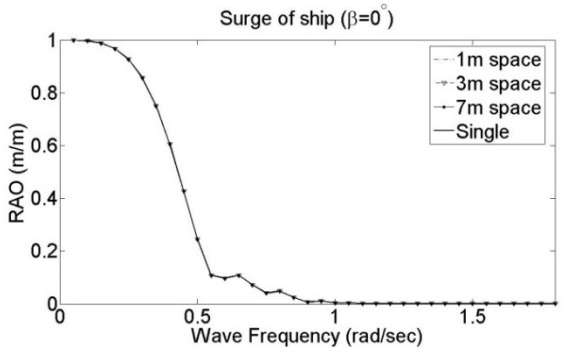

(a)

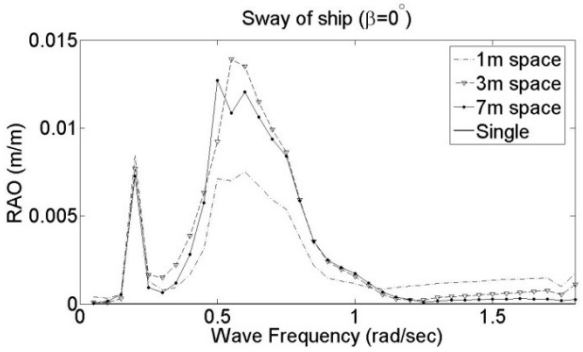

(b)

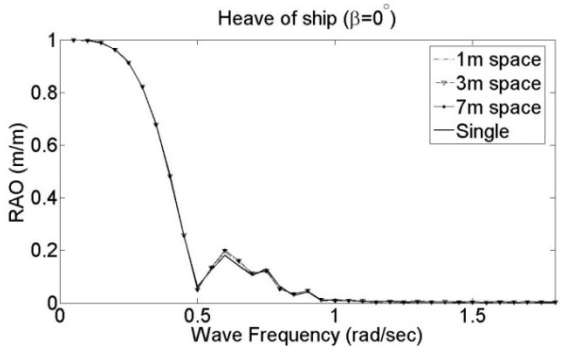

(c)

Figure B.1 Motion RAOs of the ship ($\beta = 0^0$). a - surge, b - sway, c - heave.

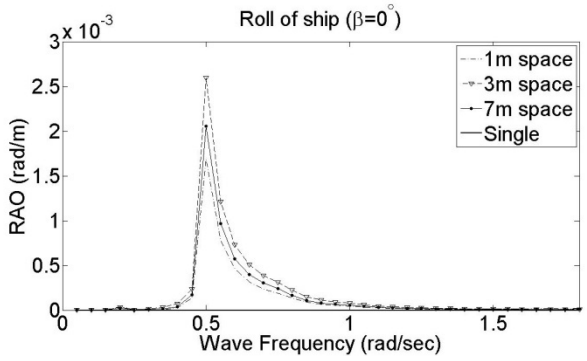

(d)

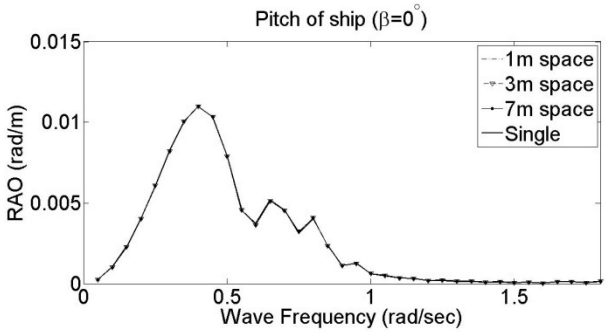

(e)

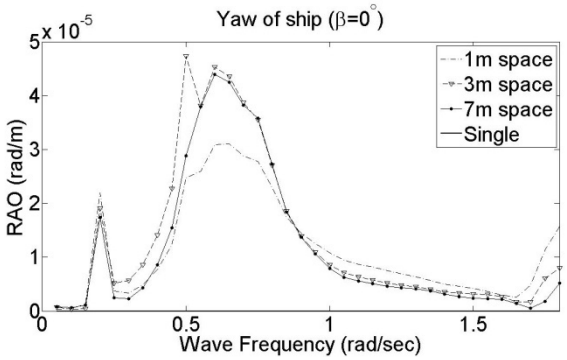

(f)

Figure B.1 continued. d - roll, e - pitch, f - yaw.

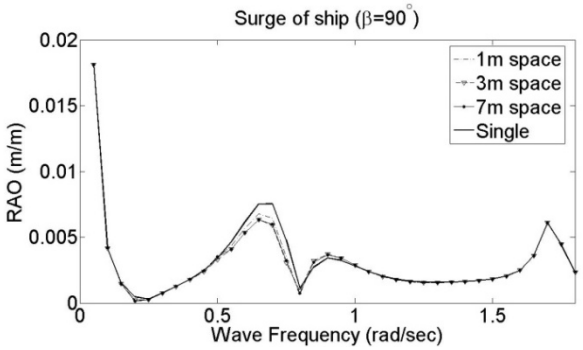

(a)

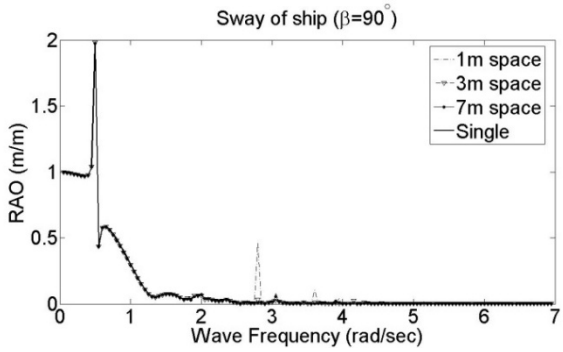

(b)

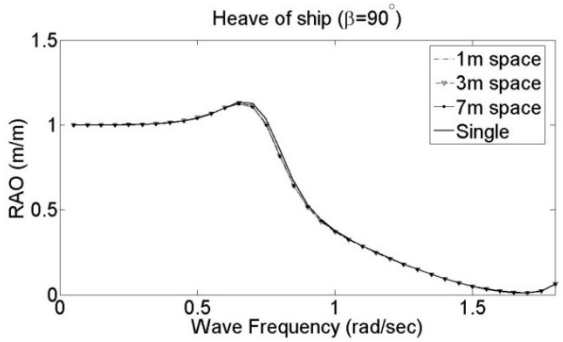

(c)

Figure B.2 Motion RAOs of the ship ($\beta = 90^0$). a - surge, b - sway, c - heave.

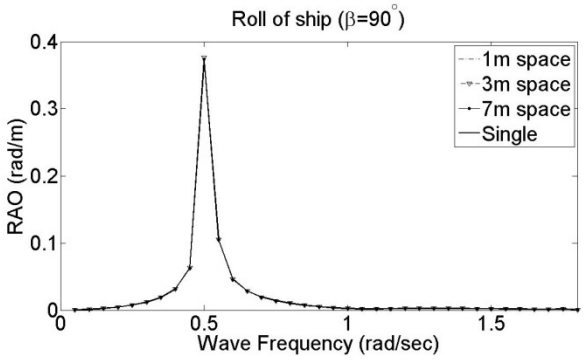

(d)

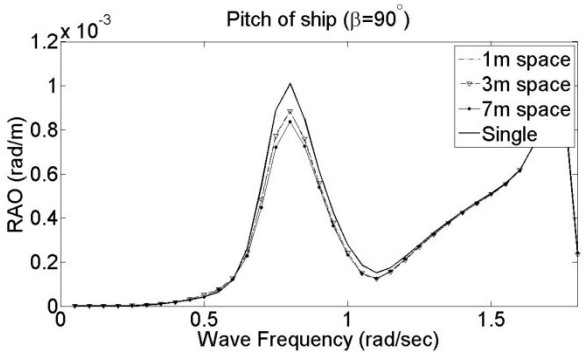

(e)

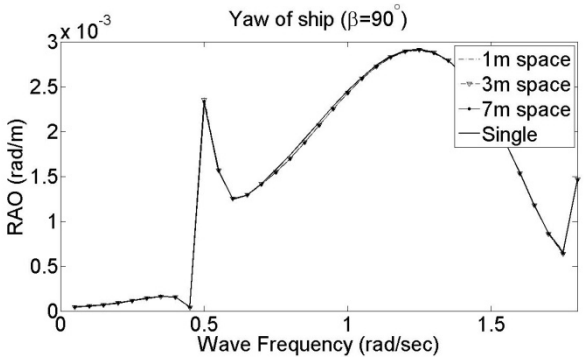

(f)

Figure B.2 continued. d - roll, e - pitch, f - yaw.

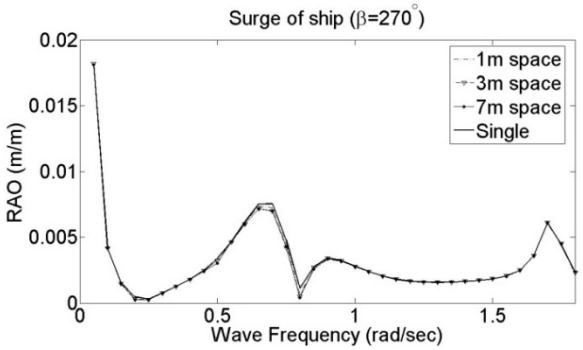

(a)

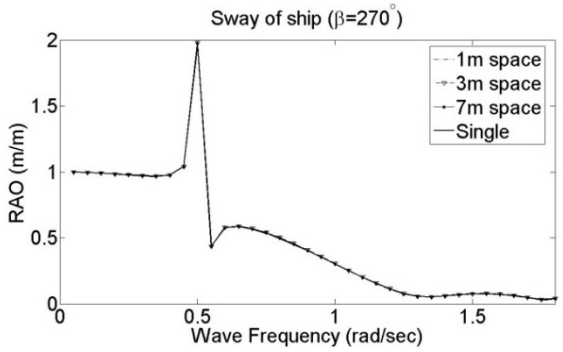

(b)

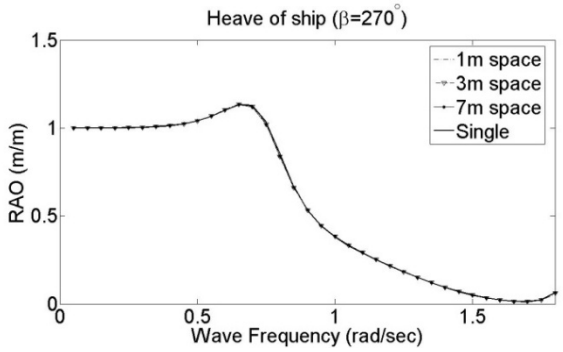

(c)

Figure B.3 Motion RAOs of the ship ($\beta = 270^0$). a - surge, b - sway, c - heave.

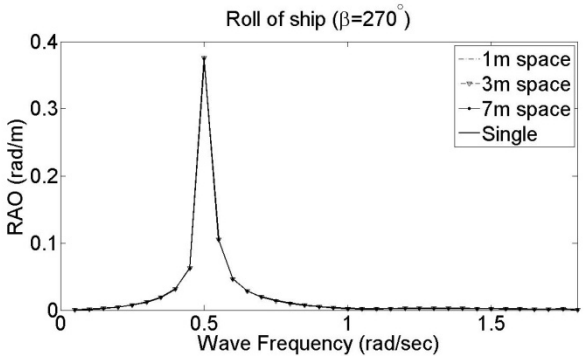

(d)

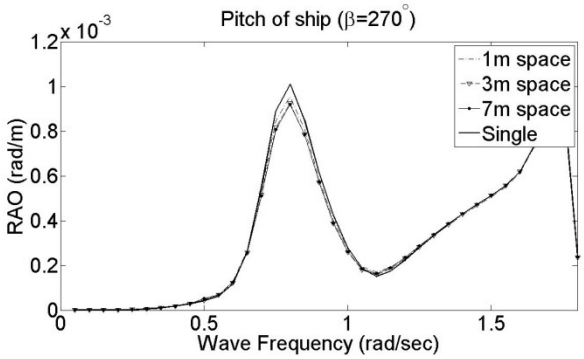

(e)

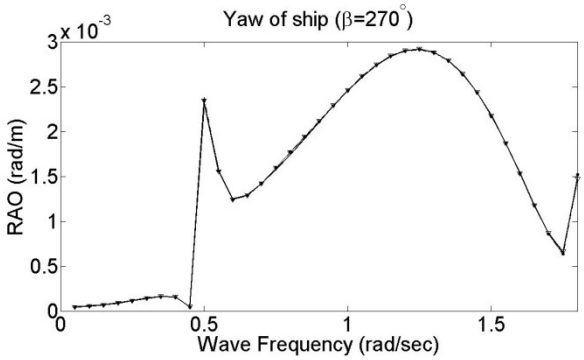

(f)

Figure B.3 continued. d - roll, e - pitch, f - yaw.

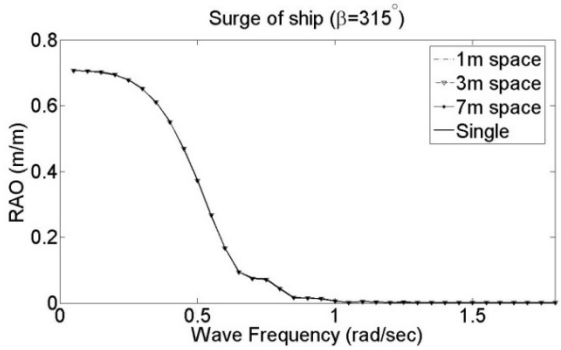

(a)

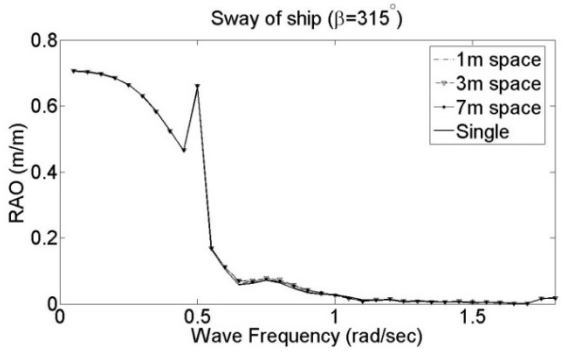

(b)

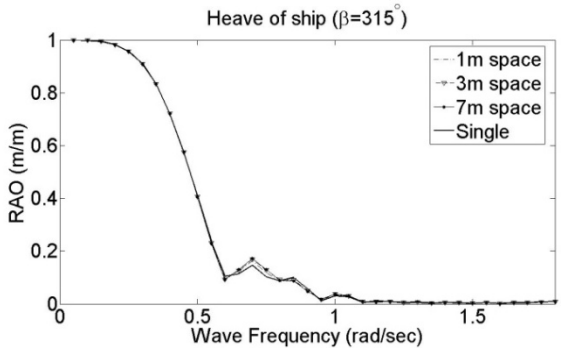

(c)

Figure B.4 Motion RAOs of the ship ($\beta = 315^0$). a - surge, b - sway, c - heave.

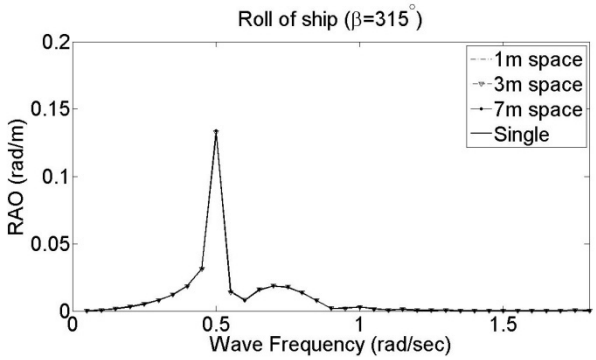

(d)

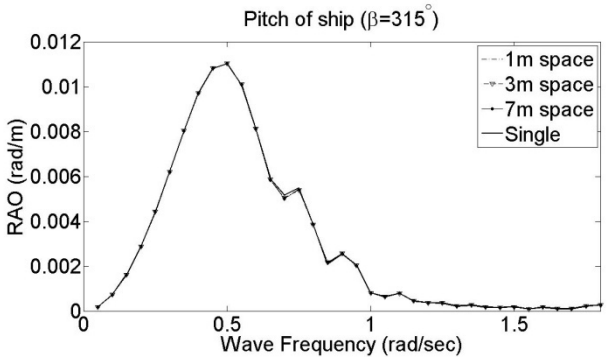

(e)

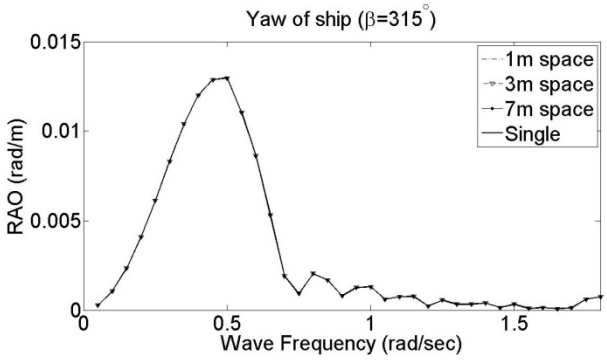

(f)

Figure B.4 continued. d - roll, e - pitch, f - yaw.

APPENDIX C

Classical Fourth-order Runge-Kutta Formula

Single-step methods are often called Runge-Kutta methods. The classical Runge-Kutta Method uses four function evaluations per step (Press, et al., 2001):

$k_1 = hf(x_n, y_n)$

$k_2 = hf(x_n + \frac{h}{2}, y_n + \frac{k_1}{2})$

$k_3 = hf(x_n + \frac{h}{2}, y_n + \frac{k_2}{2})$

$k_4 = hf(x_n + h, y_n + k_3)$

$y_{n+1} = y_n + \frac{k_1}{6} + \frac{k_2}{3} + \frac{k_3}{3} + \frac{k_4}{6} + O(h^5)$

A more general single-step formula is characterized by a number of parameters,$\alpha_i, \beta_{i,j}, \gamma_i$ and δ_i,

$k_i = hf(x_n + \alpha_i h, y_n + h\sum_{j=1}^{i-1} \beta_{i,j} k_j)$, i $= 1, \ldots\ldots,$ k

The parameters are determined by matching terms in Taylor series expansions of the slopes. The order of a method is the exponent of the smallest power of h that cannot be matched. The fourth-order Runge-Kutta method requires four evaluations of the right hand side per step h and is fourth-order.

The names of the MATLAB ODE solvers are all of the form *ode***xx** with digits **nn** indicating the order of the underlying method and a possibly empty **xx** indicating some special characteristic of the method (Moler, 2004).

APPENDIX D

Postprocessing Tool for the Two-body System

Note: The following codes are written in MATLAB. This tool can be used to output all the added mass (AM) and radiation damping (AD) coefficients from the result files of WAMIT. The corresponding matrices at the specific wave frequency can also be written out in the 12 x 12 matrix for both bodies and in the 6 x 6 matrix for each independent body. Further, the anticipated exciting force RAO can be output as a 12 x 1 vector.

```
%%%%%%%%%%%%%%%%%%%%%%%%%%%%%%%%%%%%%%%%%%%%%%%%%%%%%%%%%%%%%%%%%%%%%%%%
% This code can be used to generate the AM & AD of two bodies and each
% body.
%%%%%%%%%%%%%%%%%%%%%%%%%%%%%%%%%%%%%%%%%%%%%%%%%%%%%%%%%%%%%%%%%%%%%%%%

clear all;
Filename1=input('Please input the full name of file(AD&AM): ','s');
disp(sprintf('The file to be postprocessed is(AD&AM): %s',Filename1));
OPTN1 = importdata(Filename1);
NPER=length(OPTN1.data(:,1))/(12*12);
for i=1:1:NPER
   tempID=(i-1)*12*12;
   PER(i,1)=OPTN1.data(tempID+1,1);
   Freq(i,1)=2*pi/PER(i,1);
end

%%%%%%---START: 1st Body (AD & AM)---%%%%%%
for k=1:1:NPER
    tempID=(k-1)*12*12;
    for i=1:1:6
        AM1st(k).data(i,:)=OPTN1.data(tempID+(i-1)*12+1:tempID+(i-
1)*12+6,4);
        AD1st(k).data(i,:)=OPTN1.data(tempID+(i-1)*12+1:tempID+(i-
1)*12+6,5);
    end
    AM1st(k).PER=PER(k);AD1st(k).PER=PER(k);
end
%%%%%%---END: 1st BODY (AD & AM)---%%%%%%
```

```
%%%%%%---START: 2nd BODY (AD & AM)---%%%%%%
for k=1:1:NPER
    tempID=(k-1)*12*12+6*12;
    for i=1:1:6
        AM2nd(k).data(i,:)=OPTN1.data(tempID+(i-1)*12+7:tempID+(i-
1)*12+12,4);
        AD2nd(k).data(i,:)=OPTN1.data(tempID+(i-1)*12+7:tempID+(i-
1)*12+12,5);
    end
    AM2nd(k).PER=PER(k);AD2nd(k).PER=PER(k);
end
%%%%%%---END: 2nd BODY (AD & AM)---%%%%%%

%%%%%%---START: Full matrix of both bodies (AD & AM)---%%%%%%
for k=1:1:NPER
    tempID=(k-1)*12*12;
    for i=1:1:12
        AMmulti(k).data(i,:)=OPTN1.data(tempID+(i-1)*12+1:tempID+(i-
1)*12+12,4);
        ADmulti(k).data(i,:)=OPTN1.data(tempID+(i-1)*12+1:tempID+(i-
1)*12+12,5);
    end
    AMmulti(k).PER=PER(k);AD_multi(k).PER=PER(k);
End
%%%%%%---END: Full matrix of both bodies (AD & AM)---%%%%%%

disp(sprintf('The available PER are: %d ','' ));
disp(sprintf('%8.4f',PER(:)));

%---> Input the period we need to study:
PER1=input('Please input a specific PER : ');
disp(sprintf('The selected PER is: ',PER1));
PER            for i=1:1:NPER
 if abs(AM1st(i).PER-PER1)<=10^(-4)
     PERID=i;
     abs(AM1st(1,i).PER-PER1);
     break;
 end
end

%%%%%%---START: Output the AM & AD---%%%%%%
AM1st_OPTN1=fopen('AM1st.txt','wt'); AM1st_ok=AM1st(1,PERID).data;
fprintf(AM1st_OPTN1,'%10.10f %10.10f %10.10f %10.10f %10.10f %10.10f \n
',AM1st_ok' );
AD1st_OPTN1=fopen('AD1st.txt','wt'); AD1st_ok=AD1st(1,PERID).data;
fprintf(AD1st_OPTN1,'%10.10f %10.10f %10.10f %10.10f %10.10f %10.10f \n
',AD1st_ok' );
AM2nd_OPTN1=fopen('AM2nd.txt','wt'); AM2nd_ok=AM2nd(1,PERID).data;
fprintf(AM2nd_OPTN1,'%10.10f %10.10f %10.10f %10.10f %10.10f %10.10f \n
',AM2nd_ok' );
AD2nd_OPTN1=fopen('AD2nd.txt','wt'); AD2nd_ok=AD2nd(1,PERID).data;
fprintf(AD2nd_OPTN1,'%10.10f %10.10f %10.10f %10.10f %10.10f %10.10f \n
',AD2nd_ok' );
```

```
AMmulti_OPTN1=fopen('AMmulti.txt','wt');
AMmulti_ok=AMmulti(1,PERID).data;
fprintf(AMmulti_OPTN1,'%10.10f %10.10f %10.10f %10.10f %10.10f %10.10f
%10.10f %10.10f %10.10f %10.10f %10.10f %10.10f \n ',AMmulti_ok' );
ADmulti_OPTN1=fopen('ADmulti.txt','wt');
ADmulti_ok=ADmulti(1,PERID).data;
fprintf(ADmulti_OPTN1,'%10.10f %10.10f %10.10f %10.10f %10.10f %10.10f
%10.10f %10.10f %10.10f %10.10f %10.10f %10.10f \n ',ADmulti_ok' );
%%%%%%---END: Output the AM & AD---%%%%%%

%%%%%%%%%%%%%%%%%%%%%%%%%%%%%%%%%%%%%%%%%%%%%%%%%%%%%%%%%%%%%%%%%%%%%%%%%%%
% Postprocess the exciting force.
%%%%%%%%%%%%%%%%%%%%%%%%%%%%%%%%%%%%%%%%%%%%%%%%%%%%%%%%%%%%%%%%%%%%%%%%%%%

Filename3=input('Please input the full name of file(Exciting force):
','s');
disp(sprintf('The file to be postprocessed is(Exciting
force): %s',Filename3));
OPTN3 = importdata(Filename3);
NBETA=length(OPTN3.data(:,2))/(12*NPER);
for i=1:1:NBETA
BETA(i)=OPTN3.data((i-1)*12+1,2);
End

%%%%%%---START: Output all the exciting force - Fext---%%%%%%
  for i=1:1:NPER
      for j=1:1:NBETA
      temp_ID=12*NBETA*(i-1)+12*(j-1);
      Fext(i,j).PER=OPTN3.data(temp_ID+1,1);
      Fext(i,j).BETA=OPTN3.data(temp_ID+1,2);
      Fext(i,j).data=OPTN3.data(temp_ID+1:temp_ID+12,4);
      end
  end
%%%%%%---END: Output all the exciting force - Fext---%%%%%%

PER3=PERID;
disp(sprintf('The available BETA are: %d ','' ));
disp(sprintf('%8.2f',BETA(:) ));
BETA3=input('Please input a specific BETA : ');
disp(sprintf('The selected BETA is: ',BETA3));
BETA3
for i=1:1:NBETA
 if abs(BETA(i)-BETA3)<=10^(-4)
     BETAID=i;
     break;
 end
end

%%%%%%---START: Output the exciting force---%%%%%%
Fext1st_OPTN3=fopen('Fext1st.txt','wt');
Fext1st_ok=Fext(PERID,BETAID).data(1:6);
```

```
fprintf(Fext1st_OPTN3,'%10.6f \n ',Fext1st_ok );
Fext2nd_OPTN3=fopen('Fext2nd.txt','wt');
Fext2nd_ok=Fext(PERID,BETAID).data(7:12);
fprintf(Fext2nd_OPTN3,'%10.6f \n ',Fext2nd_ok );
Fextmulti_OPTN3=fopen('Fextmulti.txt','wt');
Fextmulti_ok=Fext(PERID,BETAID).data(1:12);
fprintf(Fextmulti_OPTN3,'%10.6f \n ',Fextmulti_ok );

%%%%%%%%%%%%%%%%%%%%%%%%%%%%%%%%%%%%%%%%%%%%%%%%
% Postprocess the motion RAOs.
%%%%%%%%%%%%%%%%%%%%%%%%%%%%%%%%%%%%%%%%%%%%%%%%
Filename4=input('Please input the full name of file( RAO): ','s'); %
disp(sprintf('The file to be postprocessed is(RAOs): %s',Filename4));
OPTN4 = importdata(Filename4);
NBETA=length(OPTN4.data(:,2))/(12*NPER);   % Num of wave headings(BETA)
for i=1:1:NBETA
BETA(i)=OPTN3.data((i-1)*12+1,2);
end

%%%%%%---START: Output all the motion RAOs---%%%%%%
  for i=1:1:NPER
      for j=1:1:NBETA
      temp_ID=12*NBETA*(i-1)+12*(j-1);
      RAOs(i,j).PER=OPTN4.data(temp_ID+1,1);
      RAOs(i,j).BETA=OPTN4.data(temp_ID+1,2);
      RAOs(i,j).data=OPTN4.data(temp_ID+1:temp_ID+12,4);
      end
  end
  for j=1:1:length(BETA)
      for ii=1:1:length(PER)
      motionRAO1(ii,j)=RAOs(ii,j).data(1,1);
      motionRAO2(ii,j)=RAOs(ii,j).data(2,1);
      motionRAO3(ii,j)=RAOs(ii,j).data(3,1);
      motionRAO4(ii,j)=RAOs(ii,j).data(4,1);
      motionRAO5(ii,j)=RAOs(ii,j).data(5,1);
      motionRAO6(ii,j)=RAOs(ii,j).data(6,1);
      motionRAO7(ii,j)=RAOs(ii,j).data(7,1);
      motionRAO8(ii,j)=RAOs(ii,j).data(8,1);
      motionRAO9(ii,j)=RAOs(ii,j).data(9,1);
      motionRAO10(ii,j)=RAOs(ii,j).data(10,1);
      motionRAO11(ii,j)=RAOs(ii,j).data(11,1);
      motionRAO12(ii,j)=RAOs(ii,j).data(12,1);
      end
  end
%%%%%%---START: Output all the motion RAOs---%%%%%%

%%%%%%---START: Output the frequency dependent FDAM(w) & FDAD(w) of
each body---%%%%%%
for i=1:1:length(Freq)
FDAM1st_11(i)=AM1st(1,i).data(1,1);FDAM1st_12(i)=AM1st(1,i).data(1,2);
FDAM1st_13(i)=AM1st(1,i).data(1,3);FDAM1st_14(i)=AM1st(1,i).data(1,4);
FDAM1st_15(i)=AM1st(1,i).data(1,5);FDAM1st_16(i)=AM1st(1,i).data(1,6);
FDAM1st_21(i)=AM1st(1,i).data(2,1);FDAM1st_22(i)=AM1st(1,i).data(2,2);
```

```
FDAM1st_23(i)=AM1st(1,i).data(2,3);FDAM1st_24(i)=AM1st(1,i).data(2,4);
FDAM1st_25(i)=AM1st(1,i).data(2,5);FDAM1st_26(i)=AM1st(1,i).data(2,6);
FDAM1st_31(i)=AM1st(1,i).data(3,1);FDAM1st_32(i)=AM1st(1,i).data(3,2);
FDAM1st_33(i)=AM1st(1,i).data(3,3);FDAM1st_34(i)=AM1st(1,i).data(3,4);
FDAM1st_35(i)=AM1st(1,i).data(3,5);FDAM1st_36(i)=AM1st(1,i).data(3,6);
FDAM1st_41(i)=AM1st(1,i).data(4,1);FDAM1st_42(i)=AM1st(1,i).data(4,2);
FDAM1st_43(i)=AM1st(1,i).data(4,3);FDAM1st_44(i)=AM1st(1,i).data(4,4);
FDAM1st_45(i)=AM1st(1,i).data(4,5);FDAM1st_46(i)=AM1st(1,i).data(4,6);
FDAM1st_51(i)=AM1st(1,i).data(5,1);FDAM1st_52(i)=AM1st(1,i).data(5,2);
FDAM1st_53(i)=AM1st(1,i).data(5,3);FDAM1st_54(i)=AM1st(1,i).data(5,4);
FDAM1st_55(i)=AM1st(1,i).data(5,5);FDAM1st_56(i)=AM1st(1,i).data(5,6);
FDAM1st_61(i)=AM1st(1,i).data(6,1);FDAM1st_62(i)=AM1st(1,i).data(6,2);
FDAM1st_63(i)=AM1st(1,i).data(6,3);FDAM1st_64(i)=AM1st(1,i).data(6,4);
FDAM1st_65(i)=AM1st(1,i).data(6,5);FDAM1st_66(i)=AM1st(1,i).data(6,6);
End
for i=1:1:length(Freq)
FDAD1st_11(i)=AD1st(1,i).data(1,1);FDAD1st_12(i)=AD1st(1,i).data(1,2);
FDAD1st_13(i)=AD1st(1,i).data(1,3);FDAD1st_14(i)=AD1st(1,i).data(1,4);
FDAD1st_15(i)=AD1st(1,i).data(1,5);FDAD1st_16(i)=AD1st(1,i).data(1,6);
FDAD1st_21(i)=AD1st(1,i).data(2,1);FDAD1st_22(i)=AD1st(1,i).data(2,2);
FDAD1st_23(i)=AD1st(1,i).data(2,3);FDAD1st_24(i)=AD1st(1,i).data(2,4);
FDAD1st_25(i)=AD1st(1,i).data(2,5);FDAD1st_26(i)=AD1st(1,i).data(2,6);
FDAD1st_31(i)=AD1st(1,i).data(3,1);FDAD1st_32(i)=AD1st(1,i).data(3,2);
FDAD1st_33(i)=AD1st(1,i).data(3,3);FDAD1st_34(i)=AD1st(1,i).data(3,4);
FDAD1st_35(i)=AD1st(1,i).data(3,5);FDAD1st_36(i)=AD1st(1,i).data(3,6);
FDAD1st_41(i)=AD1st(1,i).data(4,1);FDAD1st_42(i)=AD1st(1,i).data(4,2);
FDAD1st_43(i)=AD1st(1,i).data(4,3);FDAD1st_44(i)=AD1st(1,i).data(4,4);
FDAD1st_45(i)=AD1st(1,i).data(4,5);FDAD1st_46(i)=AD1st(1,i).data(4,6);
FDAD1st_51(i)=AD1st(1,i).data(5,1);FDAD1st_52(i)=AD1st(1,i).data(5,2);
FDAD1st_53(i)=AD1st(1,i).data(5,3);FDAD1st_54(i)=AD1st(1,i).data(5,4);
FDAD1st_55(i)=AD1st(1,i).data(5,5);FDAD1st_56(i)=AD1st(1,i).data(5,6);
FDAD1st_61(i)=AD1st(1,i).data(6,1);FDAD1st_62(i)=AD1st(1,i).data(6,2);
FDAD1st_63(i)=AD1st(1,i).data(6,3);FDAD1st_64(i)=AD1st(1,i).data(6,4);
FDAD1st_65(i)=AD1st(1,i).data(6,5);FDAD1st_66(i)=AD1st(1,i).data(6,6);
end
for i=1:1:length(Freq)
FDAM2nd_11(i)=AM2nd(1,i).data(1,1);FDAM2nd_12(i)=AM2nd(1,i).data(1,2);
FDAM2nd_13(i)=AM2nd(1,i).data(1,3);FDAM2nd_14(i)=AM2nd(1,i).data(1,4);
FDAM2nd_15(i)=AM2nd(1,i).data(1,5);FDAM2nd_16(i)=AM2nd(1,i).data(1,6);
FDAM2nd_21(i)=AM2nd(1,i).data(2,1);FDAM2nd_22(i)=AM2nd(1,i).data(2,2);
FDAM2nd_23(i)=AM2nd(1,i).data(2,3);FDAM2nd_24(i)=AM2nd(1,i).data(2,4);
FDAM2nd_25(i)=AM2nd(1,i).data(2,5);FDAM2nd_26(i)=AM2nd(1,i).data(2,6);
FDAM2nd_31(i)=AM2nd(1,i).data(3,1);FDAM2nd_32(i)=AM2nd(1,i).data(3,2);
FDAM2nd_33(i)=AM2nd(1,i).data(3,3);FDAM2nd_34(i)=AM2nd(1,i).data(3,4);
FDAM2nd_35(i)=AM2nd(1,i).data(3,5);FDAM2nd_36(i)=AM2nd(1,i).data(3,6);
FDAM2nd_41(i)=AM2nd(1,i).data(4,1);FDAM2nd_42(i)=AM2nd(1,i).data(4,2);
FDAM2nd_43(i)=AM2nd(1,i).data(4,3);FDAM2nd_44(i)=AM2nd(1,i).data(4,4);
FDAM2nd_45(i)=AM2nd(1,i).data(4,5);FDAM2nd_46(i)=AM2nd(1,i).data(4,6);
FDAM2nd_51(i)=AM2nd(1,i).data(5,1);FDAM2nd_52(i)=AM2nd(1,i).data(5,2);
FDAM2nd_53(i)=AM2nd(1,i).data(5,3);FDAM2nd_54(i)=AM2nd(1,i).data(5,4);
FDAM2nd_55(i)=AM2nd(1,i).data(5,5);FDAM2nd_56(i)=AM2nd(1,i).data(5,6);
FDAM2nd_61(i)=AM2nd(1,i).data(6,1);FDAM2nd_62(i)=AM2nd(1,i).data(6,2);
FDAM2nd_63(i)=AM2nd(1,i).data(6,3);FDAM2nd_64(i)=AM2nd(1,i).data(6,4);
FDAM2nd_65(i)=AM2nd(1,i).data(6,5);FDAM2nd_66(i)=AM2nd(1,i).data(6,6);
```

```
end
for i=1:1:length(Freq)
FDAD2nd_11(i)=AD2nd(1,i).data(1,1);FDAD2nd_12(i)=AD2nd(1,i).data(1,2);
FDAD2nd_13(i)=AD2nd(1,i).data(1,3);FDAD2nd_14(i)=AD2nd(1,i).data(1,4);
FDAD2nd_15(i)=AD2nd(1,i).data(1,5);FDAD2nd_16(i)=AD2nd(1,i).data(1,6);
FDAD2nd_21(i)=AD2nd(1,i).data(2,1);FDAD2nd_22(i)=AD2nd(1,i).data(2,2);
FDAD2nd_23(i)=AD2nd(1,i).data(2,3);FDAD2nd_24(i)=AD2nd(1,i).data(2,4);
FDAD2nd_25(i)=AD2nd(1,i).data(2,5);FDAD2nd_26(i)=AD2nd(1,i).data(2,6);
FDAD2nd_31(i)=AD2nd(1,i).data(3,1);FDAD2nd_32(i)=AD2nd(1,i).data(3,2);
FDAD2nd_33(i)=AD2nd(1,i).data(3,3);FDAD2nd_34(i)=AD2nd(1,i).data(3,4);
FDAD2nd_35(i)=AD2nd(1,i).data(3,5);FDAD2nd_36(i)=AD2nd(1,i).data(3,6);
FDAD2nd_41(i)=AD2nd(1,i).data(4,1);FDAD2nd_42(i)=AD2nd(1,i).data(4,2);
FDAD2nd_43(i)=AD2nd(1,i).data(4,3);FDAD2nd_44(i)=AD2nd(1,i).data(4,4);
FDAD2nd_45(i)=AD2nd(1,i).data(4,5);FDAD2nd_46(i)=AD2nd(1,i).data(4,6);
FDAD2nd_51(i)=AD2nd(1,i).data(5,1);FDAD2nd_52(i)=AD2nd(1,i).data(5,2);
FDAD2nd_53(i)=AD2nd(1,i).data(5,3);FDAD2nd_54(i)=AD2nd(1,i).data(5,4);
FDAD2nd_55(i)=AD2nd(1,i).data(5,5);FDAD2nd_56(i)=AD2nd(1,i).data(5,6);
FDAD2nd_61(i)=AD2nd(1,i).data(6,1);FDAD2nd_62(i)=AD2nd(1,i).data(6,2);
FDAD2nd_63(i)=AD2nd(1,i).data(6,3);FDAD2nd_64(i)=AD2nd(1,i).data(6,4);
FDAD2nd_65(i)=AD2nd(1,i).data(6,5);FDAD2nd_66(i)=AD2nd(1,i).data(6,6);
end
```

APPENDIX E

Motion Responses Spectrum of the Bob Hope of the Two-body System at Heading Sea (SS4) -No control vs. LQR control

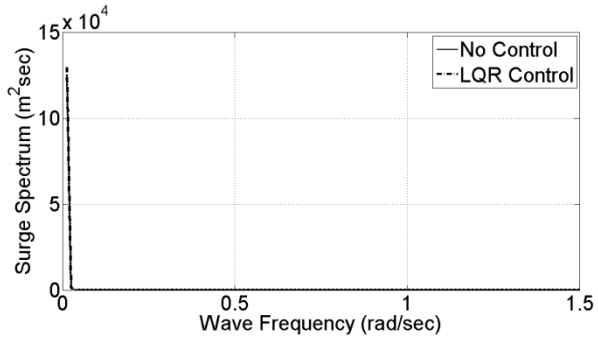

(a)

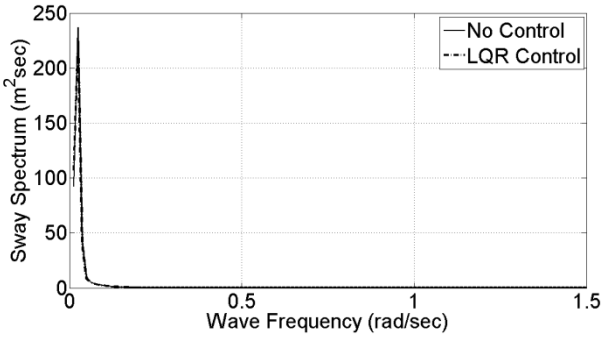

(b)

Figure E.1 Motion responses spectrum of the ship at the heading sea (SS4) - No control vs. LQR control. a - surge, b - sway.

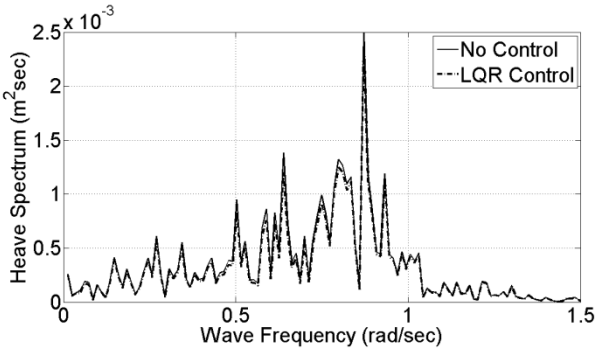

(c)

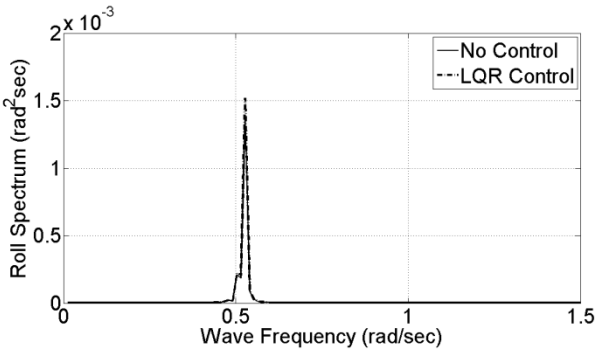

(d)

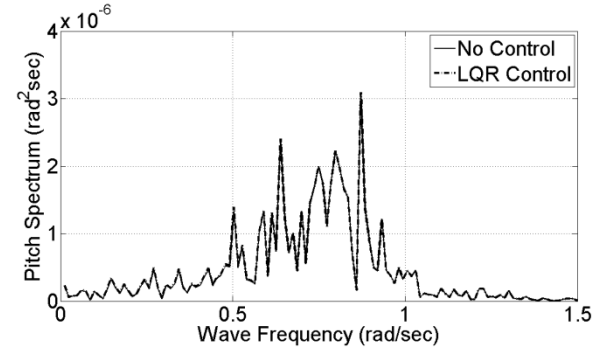

(e)

Figure E.1 continued. c - heave, d - roll, e - pitch.

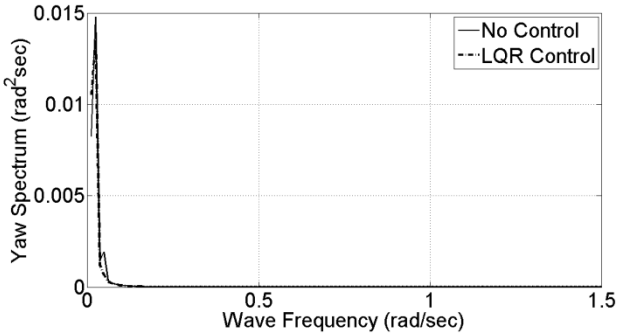

(f)

Figure E.1 continued. f - yaw.

VITA

Name: Xiaochuan Yu

Address: Technip USA Inc.

11700 Katy Freeway, Suite 150

Houston, Texas 77079, USA

Email Address: xcyu66@gmail.com

Education: B.S., Naval Architecture, Shanghai Jiao Tong University, 2000

B.S., Management Engineering, Shanghai Jiao Tong University, 2001

M.S., Naval Architecture and Ocean Engineering, Shanghai Jiao Tong University, 2004

M.S., Civil Engineering, University of Hawaii at Manoa, 2008

Ph.D., Ocean Engineering, Texas A&M University, 2011